

STOCHASTIC PROCESSES UNDER LINEAR DIFFERENTIAL CONSTRAINTS : APPLICATION TO GAUSSIAN PROCESS REGRESSION FOR THE 3 DIMENSIONAL FREE SPACE WAVE EQUATION

IAIN HENDERSON, PASCAL NOBLE, AND OLIVIER ROUSTANT

ABSTRACT. Let P be a linear differential operator over $\mathcal{D} \subset \mathbb{R}^d$ and $U = (U_x)_{x \in \mathcal{D}}$ a second order stochastic process. In the first part of this article, we prove a new necessary and sufficient condition for all the trajectories of U to verify the partial differential equation (PDE) $T(U) = 0$. This condition is formulated in terms of the covariance kernel of U . When compared to previous similar results, the novelty lies in that the equality $T(U) = 0$ is understood in the *sense of distributions*, which is a relevant framework for PDEs. This theorem provides precious insights during the second part of this article, devoted to performing “physically informed” machine learning for the homogeneous 3 dimensional free space wave equation. We perform Gaussian process regression (GPR) on pointwise observations of a solution of this PDE. To do so, we propagate Gaussian processes (GP) priors over its initial conditions through the wave equation. We obtain explicit formulas for the covariance kernel of the propagated GP, which can then be used for GPR. We then explore the particular cases of radial symmetry and point source. For the former, we derive convolution-free GPR formulas; for the latter, we show a direct link between GPR and the classical triangulation method for point source localization used in GPS systems. Additionally, this Bayesian framework provides a new answer for the ill-posed inverse problem of reconstructing initial conditions for the wave equation with a limited number of sensors, and simultaneously enables the inference of physical parameters from these data. Finally, we illustrate this physically informed GPR on a number of practical examples.

1. INTRODUCTION

Machine learning techniques have proved countless times that they can provide efficient solutions to difficult problems when field data are available. One key element to a great part of this success is the incorporation of “expert knowledge” in the corresponding statistical models. In a good deal of practical applications, this knowledge takes the form of mathematical models which, at times, are already well understood. This is very common when dealing with problems coming from physics such as thermodynamics, continuum mechanics or fluid mechanics to name a few. In these examples, the mathematical models take the form of Partial Differential

2020 *Mathematics Subject Classification.* Primary 60G12 60G17 62F15 65M32; Secondary 35L15 60G15 46E22.

Key words and phrases. Gaussian Process Regression, Partial Derivative Equations, Wave equation, Physical Parameter Estimation, Initial Value Inverse Problems.

©XXXX American Mathematical Society

Equations (PDEs). The zoology of PDEs is incredibly vast [27] and their applications are ubiquitous. As such, tremendous efforts have been devoted to solving them, both theoretically [27] and numerically [5]. These equations impose very specific structures on the observed data which can be extremely difficult to capture or mimic with general machine learning models. Therefore, given the available knowledge of the underlying PDEs, one may try incorporating these structures in machine learning models. How can this be done? Gaussian Process Regression (GPR) [60], which is a type of Bayesian framework for machine learning, provides a possible answer when the PDE is *linear*. Indeed, Gaussian processes (GPs) are the most “linear” of all random processes : they are stable under (finite) linear combinations of their elements [60]. Although they are very simple mathematical objects when compared to non linear ones, linear PDEs are central in general PDE theory and remain physically relevant in a number of applications such as acoustics, electromagnetics or quantum mechanics. In this paper, we focus on the 3D wave equation which in fact plays a fundamental role in all three of the aforementioned domains.

1.1. State of the Art. GPR is a “kernel based” machine learning method, which means that it is built around a positive definite function (see equation (2.1)) called kernel. Solving or “learning” linear ODEs and PDEs thanks to GPR is not a very new idea. The first initiative in that direction may go back to [32] and has been re-explored ever since. It has been developed in the context of latent forces ([46], [4], [63], [45]) and was then applied to certain wave equations ([3], [53]). Latent forces are interested in linear PDEs of the form

$$(1.1) \quad Lu = f$$

where both u and f are defined on the same domain $\mathcal{D} \subset \mathbb{R}^d$, and L is a linear differential operator. Latent forces put a GP prior on the driving source term f . Explicit resolution of (1.1), thanks to Green’s function [23], translates this prior as a GP distribution over the solution u . Conversely, a second approach ([58], [59]) rather puts a GP prior on the *solution* u and straightforwardly translates (1.1) as a GP distribution on the driving term f , avoiding the need for Green’s functions and convolutions. Though both of these approaches are “physically informed”, they may not account for strict linear equality constraints in the interior domain \mathcal{D} , i.e. when f is known and should not be seen as random. In this case, this knowledge could be exploited for dimension reduction. Actually, a number of famous PDEs can be studied with no interior source term ($f \equiv 0$), in which case initial conditions or more general boundary source terms are provided. Such PDEs fall in the category of initial value or boundary problems (IVP/BP). This is frequent in the evolution equation literature, which for instance gives rise to the elegant semi-group theory for PDEs ([54] or [27], section 7.4). Equation (1.1) then writes $Lu = 0$ and while u may be modelled as a random object, 0 should be strictly 0 and not just a centered stochastic process, as would be the case if using any of the two frameworks described above. A first step towards enforcing strict linear constraints in the approximation space probably dates back to [49] where in a deterministic context, divergence-free interpolation spaces were first built. This idea was pursued in [65] where an interpolation space comprised of solutions to Laplace’s equation was constructed. In both cases, these spaces are built upon positive definite kernels (see equation (2.1)), which makes them easy to transpose in a GPR framework. As such, the

kernel from [65] was then used in [48] for performing GPR on Laplace's equation. Likewise for [67], where GPs are built so that their trajectories are systematically divergence/curl free. This was then taken a step further in [79], [38], [37] and [41] in the more general context of Maxwell's stationary equations. Finally, [2] applies this framework to the 1D heat equation, Laplace's and Helmholtz' 2D equations. The matter of enforcing strict homogeneous boundary conditions in the context of GPR has also been addressed in [33], [42]. Enforcing these constraints provides another way of lowering the dimension of the initial problem. Following [71], [33] builds a PDE-tailored covariance kernel thanks to a spectral decomposition of the differential operator L . Note that [52] tackles the matter of defining a unifying GPR framework in which all the above approaches can fit, in the context of numerical Bayesian homogenization. As in many of the references above, the central tool in [52] is the PDE's Green's function (and the chosen example is elliptic); in applications, the philosophy of [52] is more or less that of latent forces [46]. Actually, [15] and [16] reformulate the approach exposed in [52] and term it probabilistic meshless method (PMM). They also consider putting the prior directly over the solution u , as in [58]; they then expose a convergence result of PMM in a probability framework. GP priors can also be used to quantify uncertainty w.r.t. ODE and PDE discretization in numerical solvers ([17]). Interestingly, [42] raises the question of rigorous proofs and regularity issues regarding the derivations and applications of GPR for PDEs, and resorts to algebraic techniques to justify the different steps of their approach. We raise the same questions here, though we rather make use of a functional analysis framework adapted to PDEs. All of the aforementioned approaches as well as the one presented in this article can be formulated using the theory of stochastic partial differential equations (SPDE), which are PDEs whose source term is a random function. The general matter of applying physically informed GPR to linear PDEs thanks to an SPDE formulation is tackled in [64], without addressing regularity questions. [72] reformulates GPR as an SPDE problem, enabling the use of Kalman filter theory for computational efficiency. In [50], the variational formulation (see [27], section 6.1.2 for a definition) of certain linear PDEs has been incorporated into a GPR framework thanks to a SPDE reformulation. This approach requires the use of Gaussian generalized stochastic processes (see [9], section 2.2.1.1), or "functional Gaussian processes" following [50]. In [51], covariance kernels on graphs are obtained thanks to an adaptation of SPDEs on graphs. Finally, [77] focuses on the study of stationary stochastic processes that are solutions of a wide class of linear SPDEs, outside the context of GPR. In particular, [77] provides a description of all the second order stationary stochastic processes that are solutions to the 3D wave equation, a central equation in the present article; this description is done in terms of the covariance kernel of the corresponding stochastic process. Note that as in this article, [77] also makes use of the theory of generalized functions. On a side note, an in-depth theoretical study of a stochastic 3D wave equation (central in this paper) and the regularity of the associated random paths is exposed in [19]. In a much wider framework, general linearly constrained stochastic processes and GPs in particular are thoroughly explored in [31]. Though [31] deals with many different types of linear operators, the application of the corresponding results to linear PDEs are not straightforward, see section 3. Indeed, these results are not phrased using generalized functions, which are especially convenient to study differential equations. This is why we prove in Proposition 2 a theorem which is

reminiscent of [31], but specifically adapted to linear PDEs. A recent survey on linearly constrained GPs presents most of these different approaches [74]. Finally, a recent article [13] extended the use of GPR to nonlinear PDEs by imposing nonlinear interpolation constraints, thus setting the way forward for many possible applications of GPR to nonlinear realistic PDE models, as found e.g. in biology of fluid mechanics.

Very closely related approaches are the kernal-based methods for solving PDEs ([80], section 16.3), which make extensive use of the theory of reproducing kernel Hilbert spaces (RKHS, [9]). These spaces are also built upon positive definite kernels (equation (2.1)) and kernal based methods naturally generalize collocation methods with radial basis functions (RBF, [80], [28]); those are actually not a new tool for solving PDEs ([12], section 2.4 and the references therein). The RKHS point of view can be seen as a deterministic counterpart of GPR (section 2.3.3); in particular the final function approximation formula (2.3) is the same. Kernel based methods can also be used to tackle linear SPDEs : in this case, one can go back and forth between the RKHS and GPR points of view ([14]). Interestingly, [29] and [30] also build positive definite kernels thanks to the PDE's Green's function when it exhibits sufficient Sobolev regularity.

In this article, we focus on the so-called (3 dimensional, free space, time dependent) wave equation. As a time-dependent PDE, we show that performing GPR on wave equation data amounts to reconstructing the corresponding initial conditions of the wave equation from incomplete scattered data. This immediately echoes with questions arising from the inverse problem community ([75], [6]); the solution we provide in this article falls in the domain of Photo Acoustic Tomography (PAT), which aims at recovering the initial conditions of wave propagation problems similar to equation (4.1). We refer [40] and the many references therein for PAT. Closely related is [56] (and the references within), where a GPR framework based on linear Radon transforms are described to solve x-ray tomography problems. Also, Bayesian approaches for inverse problems involving PDEs are in fact standard ([75], [73], [18], [20]) and have been set up a number of times for equations from fluid mechanics in particular (see e.g. [73], [18] and the related references therein). However, these approaches never entirely follow the GPR methodology presented in this article when it comes down to reconstructing some initial conditions, see the contributions section for a more detailed discussion. Additionally, the questions at hand in [73], [18] and [20] differ from those that are targeted in the present article, as these works rather study general theoretical questions such as well-posedness and stability in the Bayesian inversion framework. The general work-flow of Bayesian inversion is the following : a probability prior is set on the model's parameter space. This prior is then conditioned on field data thanks to Bayes' theorem, in order to estimate the model's true parameters. See [75], sections 5.6 to 5.8 for practical examples, or [25] for an inversion of a non uniform propagation speed $c(x)$.

1.2. Contribution. We consider the general problem of applying GPR on scattered observations of solutions of the wave equation using “physically informed” GPs. We explore both the theoretical and applied aspects of this task.

In Proposition 2, we prove a general result that provides a simple necessary and sufficient condition for the trajectories of any second order stochastic process to be solutions to a given linear PDE in the distributional sense (section 3). This

condition is formulated in terms of its covariance function. The hypotheses are minimal and the displayed result is concise. This theorem is phrased in a functional analysis framework, using the permissive language of generalized functions.

We describe a general Gaussian process model for the homogeneous 3D wave equation, with the corresponding proofs (section 4). This model is obtained by putting GP priors over the initial conditions of the wave equation, which comes naturally if considering those to be unknown. In particular we derive the corresponding covariance kernel which we will directly use for GPR. For short, we denote WIGPR the use of this kernel to perform GPR, as in “Wave Informed GPR”. Our approach enforces strict linear homogeneous PDE constraints in the interior domain, similarly to what was observed in [79], [38] and [41] among others for different PDEs (see the state of the art section for more details). More precisely, we get from Proposition 2 that the trajectories of the corresponding GP all verify the wave equation, as well as the predictions provided by WIGPR. Here, these linear constraints are understood in light of our result from section 2, i.e. in the sense of distributions. The key difference with the kernels presented in [77] is that here, no stationarity assumptions are made on the underlying stochastic process. In particular the spectral measure provided by Bochner’s theorem [60], which is the key tool used in [77], is not available anymore. We thus resort to more general integration techniques in the proofs.

We then provide an inverse problem interpretation of the use of WIGPR on wave equation data, as the prediction from WIGPR evaluated at $t = 0$ provides a finite dimensional reconstruction of the real initial conditions corresponding to the observed data. This is a natural thing to do because here, the uncertainty (randomness) was initially set on the initial conditions. The resulting posterior distribution then enables the estimation of said initial conditions. Note that this approach differs from the Bayesian approach to PDE inverse problems described e.g. in [73] and [18] because here, the forward linear problem is completely solved inside the GPR kernel *before* conditioning the GP prior on the field data. When compared to equation (2.6) from [73], we use a wave equation-tailored GP prior π_0 for the full space-time solution : the forward model is already solved in the prior π_0 and doesn’t appear in the noise term ρ . It is only after choosing this tailored prior that the corresponding initial conditions are estimated by evaluating the Kriging mean at $t = 0$. Among other things, the solution to the corresponding inverse problem provided by our approach is implementable in practice.

We investigate the two particular cases of radial symmetry and point source. When the initial conditions exhibit radial symmetry, we derive convolution-free covariance formulas and discuss them when the initial conditions are compactly supported. Indeed, these formulas can be directly linked to the finite speed propagation principle for the 3D wave equation, also known as the strong Huygens principle. In the point source case, we show numerically (Figure 1) and theoretically that the parameter fitting step from WIGPR naturally reduces to the classic triangulation approach for point source localization, used for instance in GPS systems. Indeed, as in [58], WIGPR can be used to jointly estimate physical parameters such as wave speed, source localization or source size.

Note that the wave equation differs from most of the PDEs mentioned in the introduction, such as the heat equation or Laplace’s equation, because these are either parabolic or elliptic. There are known regularization effects for such PDEs

([27], sections 6.3 and 7.1.3) which somewhat mitigate the need for overly prudent mathematical argumentation w.r.t. the derivations of GPR for PDEs. Such regularization effects disappear for hyperbolic PDEs such as the wave equation ([27], section 7.2.4) and careful derivations now become critical ([27], section 3.4.1). Equivalently, such derivations require special care because the wave equation's Green's function is singular, see equation (4.4). This is also why we cannot directly refer to [52], [15] or [14] for an adapted theoretical framework. This is the reason why throughout this section, effort is done to formulate the arguments necessary for the derivations that lead to the exposed formulas.

We illustrate WIGPR on a few numerical experiments (section 5). They are performed on simulated wave equation data, with radially symmetric compactly supported initial conditions. This data takes the form of a number of noise polluted time series, each of them corresponding to an “artificial” sensor placed in the numerical simulation. We thus use the fast-to-compute covariance expressions derived in the previous section. The tackled questions concern (i) the quality of the joint estimation of the wave speed, source position and size and the quality of the resulting initial condition reconstruction and (ii) the sensibility of the reconstruction step w.r.t. the sensor location. We display initial condition reconstruction images, in light of the inverse problem interpretation described in the previous section. In appendix A are presented more complete numerical results, showing for each example the quality of the physical parameter estimation as well as L^2 , L^1 and L^∞ relative error estimates in terms of the number of sensors used.

1.2.1. Organization of the paper. The paper is organized as follow. For self-containment, section 2 is dedicated to reminders on GPs, GPR and generalized functions. This section and all the proofs are detailed enough so that this article is accessible both to the analyst and the statistician. In section 3, we state and prove our new necessary and sufficient condition on stochastic processes that are subject to linear differential constraints. Section 4 is dedicated to the study of the wave equation thanks to Gaussian processes and Gaussian process regression. In section 5, we showcase some numerical applications of the previous section on wave equation data. We conclude in section 6.

2. NOTATIONS AND BACKGROUND

2.1. Notations. Let m be a scalar function defined on an open set $\mathcal{D} \subset \mathbb{R}^d$ and k a scalar function defined on $\mathcal{D} \times \mathcal{D}$. Let $X = (x_1, \dots, x_n)^T$ be a column vector in \mathcal{D}^n . Let $(\Omega, \mathcal{F}, \mathbb{P})$ be a probability space, over which all the random objects of this article will be defined.

- N.1** Note $m(X)$ the column vector such that $m(X)_i = m(x_i)$, $k(X, X)$ the square matrix such that $k(X, X)_{ij} = k(x_i, x_j)$ and given $x \in \mathcal{D}$, $k(X, x)$ the column vector such that $k(X, x)_i = k(x_i, x)$.
- N.2** for any positive definite kernel k (see equation (2.1)), \mathcal{H}_k denotes the associated Reproducing Kernel Hilbert Space (RKHS) as defined in [9].
- N.3** Note $L^2(\mathbb{P})$ the Hilbert space of real-valued random variables defined on Ω with finite second order moment endowed with the inner product $\langle X, Y \rangle = \mathbb{E}[XY]$. For a GP $(U(x))_{x \in \mathcal{D}}$, the trajectory of U at point $\omega \in \Omega$ is the deterministic function $x \mapsto U(x)(\omega)$ and is noted U_ω . $\mathcal{L}(U) := \overline{\text{Span}(U(x), x \in \mathcal{D})} \subset L^2(\mathbb{P})$ denotes the Hilbert subspace of $L^2(\mathbb{P})$ induced

by U . Since $L^2(\mathbb{P})$ -limits of Gaussian random variables drawn from the same GP remain Gaussian ([36], section 1.3), $\mathcal{L}(U)$ only encompasses Gaussian random variables.

- N.4** If X is a random variable, then “ $X \in A$ a.s.” means “ $X \in A$ almost surely”, or equivalently $\mathbb{P}(X \in A) = 1$. Likewise, if f is a function defined on $\mathcal{D} \subset \mathbb{R}^d$, then “ $f(x) \in A$ a.e.” means “ $f(x) \in A$ almost everywhere” or equivalently, $\lambda_d(\{x \in \mathcal{D} : f(x) \notin A\}) = 0$ where λ_d is the Lebesgue measure on \mathbb{R}^d .
- N.5** $L_{loc}^1(\mathcal{D})$ denotes the space of measurable scalar functions f defined on \mathcal{D} that are locally integrable, i.e. such that $\int_K |f| < +\infty$ for all compact sets $K \subset \mathcal{D}$. $\mathcal{D}(\mathcal{D})$ denotes the space of compactly supported infinitely differentiable functions supported on \mathcal{D} .
- N.6** for a multi-index $k = (k_1, \dots, k_d) \in \mathbb{N}^d$, we use the usual notation $|k| = k_1 + \dots + k_d$ and $\partial^k := \partial_{x_1}^{k_1} \dots \partial_{x_d}^{k_d}$ where $\partial_{x_i}^{k_i}$ is the k_i^{th} derivative w.r.t the i^{th} coordinate x_i .
- N.7** The variables (r, θ, ϕ) will always denote spherical coordinates; $S(0, 1)$ denotes the unit sphere of \mathbb{R}^3 and we will always write $d\Omega = \sin \theta d\theta d\phi$ its surface differential element; $\gamma = (\sin \theta \cos \phi, \sin \theta \sin \phi, \cos \theta)^T \in S(0, 1)$ denotes the unit length vector parametrized by (θ, ϕ) .

2.2. Gaussian Processes. We refer to [60] for further details on Gaussian processes.

2.2.1. Definition. Let $(\Omega, \mathcal{F}, \mathbb{P})$ be a probability space and $\mathcal{D} \subset \mathbb{R}^d$ an open set. A Gaussian process $(U(x))_{x \in \mathcal{D}}$ is a collection of normally distributed random variables defined on Ω and indexed by \mathcal{D} such that for any $(x_1, \dots, x_n) \in \mathcal{D}^n$, the law of $(U(x_1), \dots, U(x_n))^T$ is a multivariate normal distribution. The law of a GP is characterized by its mean and covariance functions ([36], section 8), defined by

- $m(x) := \mathbb{E}[U(x)]$
- $k(x, x') = \text{Cov}(U(x), U(x')) = \mathbb{E}[(U(x) - m(x))(U(x') - m(x')))]$

We write $(U(x))_{x \in \mathcal{D}} \sim GP(m, k)$.

2.2.2. Covariance kernels. The mean function m can be any function, and is actually often set to zero. On the other hand, the function k has to be positive definite (PD) :

$$(2.1) \quad \sum_{i,j=1}^n a_i a_j k(x_i, x_j) \geq 0 \quad \forall (x_1, \dots, x_n) \in \mathcal{D}^n, \quad \forall (a_1, \dots, a_n) \in \mathbb{R}^n$$

PD functions verify the Cauchy-Schwarz inequality [60] :

$$(2.2) \quad \forall x, x' \in \mathcal{D}, \quad |k(x, x')| \leq \sqrt{k(x, x)} \sqrt{k(x', x')}$$

The covariance kernel k is the core element that encodes the mathematical properties of the GP. Furthermore, there is a one-to-one correspondence between positive definite kernels and (covariance kernels of) centered GPs [22]. Thus we will focus on the design of positive definite kernels.

Among all covariance kernels, some are said to be *stationary*, in which case the value at (x, x') only depends on the increment $x - x'$: $k(x, x') = k_S(x - x')$. Common examples are the squared exponential and Matérn kernels [60]; see equation (5.1) for an example.

2.2.3. Bayesian inference of functions. A Gaussian process $U = (U(x))_{x \in \mathcal{D}}$ can also be seen as a random variable that is valued in a space of functions through the mapping $T : \omega \mapsto U_\omega$, i.e. a random function. This in turn defines a probability distribution over functions [60] through the pushforward measure of \mathbb{P} through T . Suppose a function u is unknown, one can model it as a GP $U \sim GP(m, k)$ just as one would model an unknown scalar y as a normally distributed random variable $Y \sim \mathcal{N}(\mu, \sigma^2)$. We then say that we put a Gaussian process prior over u . Thanks to Bayes' theorem, the prior GP distribution of U can then be updated through probability conditioning when data on u is available. The resulting conditioned GP distribution is called the posterior. Statistical indicators can then be derived from the posterior, such as expectation and standard deviation, to estimate the unknown function u over which the prior was initially set. Bayesian inference is one way of understanding Gaussian process regression.

2.3. Gaussian Process Regression. We refer to [60] for further details on GPR.

2.3.1. Kriging equations. GPs can be used for function interpolation. Let u be a function defined on \mathcal{D} for which we know a dataset of values $B = \{u(x_1), \dots, u(x_n)\}$. Conditioning the law of a GP $(U(x))_{x \in \mathcal{D}} \sim GP(m, k)$ on the database B yields a second GP \tilde{U} with $\tilde{U}(x) := (U(x) | U(x_i) = u(x_i), i = 1, \dots, n)$. The law of \tilde{U} is known : $(\tilde{U}(x))_{x \in \mathcal{D}} \sim GP(\tilde{m}, \tilde{k})$. \tilde{m} and \tilde{k} are given by the so-called *Kriging* equations (2.3) and (2.4). Note $X = (x_1, \dots, x_n)^T$ and suppose that $K(X, X)$ is invertible, then [60]

$$(2.3) \quad \begin{cases} \tilde{m}(x) &= m(x) + k(X, x)^T k(X, X)^{-1} (u(X) - m(X)) \end{cases}$$

$$(2.4) \quad \begin{cases} \tilde{k}(x, x') &= k(x, x') - k(X, x)^T k(X, X)^{-1} k(X, x') \end{cases}$$

In a Bayesian framework, the initial GP $(U(x))_{x \in \mathcal{D}}$ is the prior and the conditioned GP $(\tilde{U}(x))_{x \in \mathcal{D}}$ is the posterior; the Kriging mean \tilde{m} and covariance \tilde{k} are simply the mean and covariance of the posterior. At location x , $\tilde{m}(x)$ is the prediction of $u(x)$. By construction, for all $i \in \{1, \dots, n\}$, we have that $\tilde{m}(x_i) = u(x_i)$ and $\tilde{k}(x_i, x_i) = 0$. If observing noisy data $U_i = U(x_i) + \varepsilon_i$ with $(\varepsilon_1, \dots, \varepsilon_n)^T \sim \mathcal{N}(0, \sigma^2 I_n)$ independent from U , one replaces $K(X, X)$ with $K(X, X) + \sigma^2 I$ above and leaves the terms $k(X, x)$ unchanged. This amounts to applying Tikhonov regularization on $k(X, X)$ and may also be used to approximate (2.3) and (2.4) when $k(X, X)$ is ill-conditioned.

2.3.2. Tuning covariance kernels. For discussions on general kernel construction and selection, we refer to [60], chapter 5. Usually, a family of kernels k_θ indexed by $\theta \in \Theta \subset \mathbb{R}^q$ is first selected. The elements of θ are the *hyperparameters* of k_θ . One may then try to find the value θ^* that fits the best the observations, which corresponds to maximizing the *marginal likelihood*. It is the probability density of the Gaussian random vector $(U(x_1), \dots, U(x_n))^T$ at point $(u(x_1), \dots, u(x_n))^T$, see equation (2.6). Note $u_{obs} = (u(x_1), \dots, u(x_n))^T$ the vector of observations at locations $X = (x_1, \dots, x_n)$ and $p(u_{obs} | \theta)$ the associated marginal likelihood at point θ , we search for θ^* such that

$$(2.5) \quad \theta^* = \arg \max_{\theta \in \Theta} p(u_{obs} | \theta)$$

Explicitly, assuming that $m \equiv 0$, then $(U(x_1), \dots, U(x_n))^T \sim \mathcal{N}(0, k_\theta(X, X))$ and

$$(2.6) \quad p(u_{\text{obs}}|\theta) = \frac{1}{(2\pi)^{n/2} \det k_\theta(X, X)^{1/2}} e^{-\frac{1}{2} u_{\text{obs}}^T k_\theta(X, X)^{-1} u_{\text{obs}}}$$

Set $\mathcal{L}(\theta) := -2 \log p(u_{\text{obs}}|\theta) - n \log 2\pi$, then (2.5) is equivalent to

$$(2.7) \quad \theta^* = \arg \min_{\theta \in \Theta} \mathcal{L}(\theta)$$

Problem (2.7) is better behaved numerically. From now on, we call $\mathcal{L}(\theta)$ the negative log marginal likelihood and we have, for noiseless observations,

$$(2.8) \quad \mathcal{L}(\theta) = u_{\text{obs}}^T k_\theta(X, X)^{-1} u_{\text{obs}} + \log \det k_\theta(X, X)$$

and for noisy observations with noise standard deviation σ ,

$$(2.9) \quad \mathcal{L}(\theta, \sigma^2) = u_{\text{obs}}^T (k_\theta(X, X) + \sigma^2 I_n)^{-1} u_{\text{obs}} + \log \det (k_\theta(X, X) + \sigma^2 I_n)$$

σ can be interpreted as an additional hyperparameter and estimated through (2.7).

2.3.3. Scattered Data interpolation and the RKHS point of view. Kriging equations (2.3) and (2.4) can be encountered without resorting to GPs. Given a positive definite kernel k defined on \mathcal{D} , one may build a Reproducing Kernel Hilbert Space (RKHS) of functions defined on \mathcal{D} which we denote by \mathcal{H}_k , see **N.2**. The inner product of \mathcal{H}_k verifies the so called reproducing property :

$$(2.10) \quad \forall x, x' \in \mathcal{D}, \langle k(x, \cdot), k(x', \cdot) \rangle_{\mathcal{H}_k} = k(x, x')$$

In the *meshfree interpolation* framework [9] [28], one may formulate the following constrained (interpolation) optimization problem

$$(2.11) \quad \min_{v \in \mathcal{H}_k} \|v\|_{\mathcal{H}_k} \quad \text{s.t.} \quad v(x_i) = u(x_i) \quad \forall i \in \{1, \dots, n\}$$

Solving (2.11) leads to the Kriging equation for \tilde{m} in (2.3); the second equation (2.4) is what is called the power function in [28]. One may also show [9] that equation (2.3) can be summerized as

$$(2.12) \quad \tilde{m} = m + p_F(u - m)$$

with F is the finite dimensional space $F = \text{Span}(k(x_1, \cdot), \dots, k(x_n, \cdot)) \subset \mathcal{H}_k$ and p_F stands for the orthogonal projection operator on F w.r.t. the inner product of \mathcal{H}_k . In particular, when $m \equiv 0$, equation (2.12) amounts to $\tilde{m} = p_F(u)$. Likewise, equation (2.4) amounts to

$$(2.13) \quad \tilde{k}(x, \cdot) = P_{F^\perp}(k(x, \cdot))$$

$$(2.14) \quad \text{with} \quad \tilde{k}(x, x) = \|P_{F^\perp} k(x, \cdot)\|_{\mathcal{H}_k}^2 \leq \|k(x, \cdot)\|_{\mathcal{H}_k}^2 = k(x, x)$$

One perk of this approach is that the Kriging mean can now be understood as an orthogonal projection over a finite dimensional deterministic space, which is reminiscent of Fourier series or Galerkin reconstruction approaches.

2.4. Generalized functions. We refer to [62] and [76] for further details on generalized functions and Radon measures. In this whole subsection, \mathcal{D} is an open set of \mathbb{R}^d .

2.4.1. *Definitions and properties.* Endow $\mathcal{D}(\mathcal{D})$ with its usual LF-space topology, defined for example in [62]. We call generalized function any continuous linear form on $\mathcal{D}(\mathcal{D})$, i.e. any element of $\mathcal{D}(\mathcal{D})'$, the topological dual of $\mathcal{D}(\mathcal{D})$. We will rather denote it by $\mathcal{D}'(\mathcal{D})$ as in [62]. The topology of $\mathcal{D}(\mathcal{D})$ is such that $T \in \mathcal{D}'(\mathcal{D})$ if and only if for all compact set $K \subset \mathcal{D}$, there exists $C_K > 0$ and a non negative integer n_K such that

$$(2.15) \quad \forall \varphi \in \mathcal{D}(\mathcal{D}) \text{ s.t } \text{Supp}(\varphi) \subset K, |T(\varphi)| \leq C_K \sum_{|k| \leq n_K} \|\partial^k \varphi\|_\infty$$

Generalized functions are also called “distributions”, a terminology we will only use when there is no risk of confusion with probability distributions. The duality bracket will be denoted $\langle \cdot, \cdot \rangle$: for $\varphi \in \mathcal{D}(\mathcal{D})$ and $T \in \mathcal{D}'(\mathcal{D})$, we have $\langle T, \varphi \rangle = T(\varphi)$.

- Any function $f \in L^1_{loc}(\mathcal{D})$ can be injectively identified to a generalized function T_f [62] defined as follow

$$(2.16) \quad \forall \varphi \in \mathcal{D}(\mathcal{D}), \quad \langle T_f, \varphi \rangle := \int_{\mathcal{D}} f(x) \varphi(x) dx$$

The map $L^1_{loc}(\mathcal{D}) \ni f \mapsto T_f$ is linear and injective. Throughout this article, we will use the abusive notation $\langle T_f, \varphi \rangle = \langle f, \varphi \rangle$, as if $\langle \cdot, \cdot \rangle$ were the L^2 inner product.

- Any generalized function T can be indefinitely differentiated [62] with the following definition (see **N.6**)

$$(2.17) \quad \partial^k T : \varphi \mapsto \langle T, (-1)^{|k|} \partial^k \varphi \rangle$$

which coincides with the definition of weak derivatives when T is a function that admits the according weak derivatives [62].

In particular, (2.16) and (2.17) combined provide a flexible definition for the derivatives of any function $f \in L^1_{loc}(\mathcal{D})$ up to any order.

2.4.2. *Radon measures.* In this paper, we call positive Radon measure any positive measure over \mathcal{D} that is Borel regular ([26], Def 1.9) and that has finite mass over any compact subset of \mathcal{D} . Borel regularity is a standard regularity hypothesis from measure theory. We call real-valued Radon measure, or simply Radon measure, any linear combination of positive Radon measures. In [70], Chapter IX, it is proved that the space of Radon measures over \mathcal{D} is isomorphic to the space of continuous linear forms over $\mathcal{C}_c(\mathcal{D})$, the space of compactly supported continuous functions on \mathcal{D} endowed with its usual LF-space topology described e.g. in [76]. The corresponding isomorphism is given by

$$(2.18) \quad \mu \mapsto \begin{cases} \mathcal{C}_c(\mathcal{D}) & \longrightarrow \mathbb{R} \\ f & \longmapsto \int_{\mathcal{D}} f(x) \mu(dx) \end{cases}$$

We have the following facts :

- any signed measure that admits a density f w.r.t. the Lebesgue measure such that $f \in L^1_{loc}(\mathcal{D})$ is a Radon measure ([76], p.217).
- mimicking (2.16) and (2.18), any Radon measure can be injectively identified to a generalized function with the following identification [76]

$$(2.19) \quad \forall \varphi \in \mathcal{D}(\mathcal{D}), \quad \langle \mu, \varphi \rangle := \int_{\mathcal{D}} \varphi(x) \mu(dx)$$

In particular, Radon measures can be differentiated up to any order through equation (2.17).

- for any Radon measure μ , there is a unique couple (μ^+, μ^-) of positive Radon measures such that $\mu = \mu^+ - \mu^-$ ([70], Chapter IX). We then define $|\mu|$ as

$$(2.20) \quad |\mu| := \mu^+ + \mu^-$$

- If μ and ν are two finite Radon measures over \mathbb{R}^d (i.e. $\int_{\mathbb{R}^d} |\mu|(dx) < \infty$ and likewise for ν), their convolution $\mu * \nu$ is defined as follow : let $\mathcal{B}(\mathbb{R}^d)$ be the Borel σ -algebra of \mathbb{R}^d , then

$$(2.21) \quad \forall A \in \mathcal{B}(\mathbb{R}^d), \quad (\mu * \nu)(A) = \int_{\mathbb{R}^d} \int_{\mathbb{R}^d} \mathbb{1}_A(x+y) \mu(dx) \nu(dy)$$

and $\mu * \nu$ is also a Radon measure over \mathbb{R}^d . When μ and ν have densities f_μ and f_ν , $\mu * \nu$ has the density $f_\mu * f_\nu$ defined by

$$(f_\mu * f_\nu)(x) = \int_{\mathbb{R}^d} f_\mu(y) f_\nu(x-y) dy$$

Remark 2.1. What is meant behind the terminology of Radon measures varies between authors. [26] calls Radon measure what we call *positive* Radon measure in this article. [70] proves that continuous linear forms over $\mathcal{C}_c(\mathcal{D})$ are differences of Radon measures in the sense of the Radon measures defined in [26], but [70] never uses the term of Radon measures, positive or not. Likewise, [76] calls *positive* Radon measure any *positive* linear form over $\mathcal{C}_c(\mathcal{D})$ which, thanks to the proof from [70], reduces to Radon measures in the sense of [26].

2.4.3. Finite order generalized functions. Let k be a non negative integer, we consider $\mathcal{C}_c^k(\mathcal{D})$ the space of compactly supported functions of class \mathcal{C}^k endowed with its usual LF-space topology [62]. We denote $\mathcal{C}_c^k(\mathcal{D})'$ its topological dual. The topologies of $\mathcal{C}_c^k(\mathcal{D})$ and $\mathcal{D}(\mathcal{D})$ are such that the canonical injection $\mathcal{D}(\mathcal{D}) \rightarrow \mathcal{C}^k(\mathcal{D})$ is continuous [76], which yields that $\mathcal{C}^k(\mathcal{D})' \subset \mathcal{D}'(\mathcal{D})$: continuous linear forms over $\mathcal{C}^k(\mathcal{D})$, when restricted to $\mathcal{D}(\mathcal{D})$, become continuous linear forms over $\mathcal{D}(\mathcal{D})$, i.e. generalized functions. We then have the following definitions and facts.

- Generalized functions $T \in \mathcal{D}'(\mathcal{D})$ that are restrictions of continuous linear forms over $\mathcal{C}_c^k(\mathcal{D})$ are called generalized functions of order k . If T is of order k for some $k \in \mathbb{N}$, T is said to be of finite order.
- $T \in \mathcal{D}'(\mathcal{D})$ is at most of order k if in equation (2.15), the integer n_K can always be taken to be equal to n , whatever the compact set K .
- Let T be a generalized function of order k . Then ([76], p 259) there exists a family of Radon measures $\{\mu_p\}_{|p| \leq k}$ over \mathcal{D} such that

$$(2.22) \quad T = \sum_{|p| \leq k} \partial^p \mu_p$$

where the equality in (2.22) holds in $\mathcal{D}'(\mathcal{D})$ and $\mathcal{C}_c^k(\mathcal{D})'$. Note that we recover (2.19) when $k = 0$.

- Among the finite order generalized functions are those that are *compactly supported*, i.e. those for which the measures μ_p such that $T = \sum_{|p| \leq k} \partial^p \mu_p$ all have compact support. One property is that one can define the Fourier transform of any compactly supported generalized functions [62].

2.4.4. Convolution with generalized functions. Let k be a non negative integer. As above, we consider $\mathcal{C}_c^k(\mathbb{R}^d)$ endowed with its usual topology. Let $f \in \mathcal{C}_c^k(\mathbb{R}^d)$ and $T \in \mathcal{C}_c^k(\mathbb{R}^d)'$. Note $\tau_x f$ the function $y \mapsto f(y - x)$ and \check{f} the function $y \mapsto f(-y)$. Then [76] one may define the convolution between T and f by

$$(2.23) \quad T * f : x \mapsto \langle T, \tau_{-x} \check{f} \rangle$$

and $T * f$ is a function in the classical sense, i.e. defined pointwise. When T lies in $L_{loc}^1(\mathcal{D})$, equation (2.23) reduces to the usual convolution of functions through the identification defined in equation (2.16) :

$$(2.24) \quad (T * f)(x) = \int_{\mathbb{R}^d} T(y) f(x - y) dy$$

Similarly if T is in fact a Radon measure μ :

$$(2.25) \quad (T * f)(x) = \int_{\mathbb{R}^d} f(x - y) \mu(dy)$$

More general definitions of generalized function convolution are available [76] but this one is sufficient for our use.

2.4.5. Tensor product of generalized functions. For two generalized functions $T_1 \in \mathcal{D}'(\mathcal{D}_1)$ and $T_2 \in \mathcal{D}'(\mathcal{D}_2)$, $T_1 \otimes T_2 \in \mathcal{D}'(\mathcal{D}_1 \times \mathcal{D}_2)$ denotes their tensor product [76], which is uniquely determined by the following tensor property :

$$(2.26) \quad \forall \varphi_1 \in \mathcal{D}(\mathcal{D}_1), \forall \varphi_2 \in \mathcal{D}(\mathcal{D}_2), \langle T_1 \otimes T_2, \varphi_1 \otimes \varphi_2 \rangle = \langle T_1, \varphi_1 \rangle \times \langle T_2, \varphi_2 \rangle$$

$T_1 \otimes T_2$ reduces to the tensor product of functions when T_1 and T_2 are functions through the identification of equation (2.16), and the product measure when T_1 and T_2 are Radon measures through (2.19).

3. STOCHASTIC PROCESSES UNDER LINEAR DIFFERENTIAL CONSTRAINTS

One may wish to force the trajectories of a stochastic process $U = (U(x))_{x \in \mathcal{D}}$ to verify linear constraints, i.e. to lie in the kernel of some linear operator. This is a priori an ambitious task as the trajectories of U form a vast set of functions. However, if U is a second order stochastic process (i.e. $\forall x \in \mathcal{D}, \text{Var}(U(x)) < +\infty$), then in many cases linear constraints on the trajectories of U can be completely translated as linear constraints on the covariance kernel of U . In particular, these new linear constraints are imposed on a much smaller set of accessible “explicit” functions. Overall, the resulting constraints on the covariance kernel of U are much easier to handle than the constraints on the trajectories of U . This idea was thoroughly explored in [31], where different general frameworks were studied in order to formulate mathematical results on linearly constrained stochastic processes. In proposition 1, we recall a particular result from [31] that was then applied to the stationary heat equation in the same article.

Note $\mathcal{F}(\mathcal{D}, \mathbb{R})$ the space of real-valued functions defined on \mathcal{D} . Proposition 1 is based on the so called Loève isometry [9] between $\mathcal{L}(U)$ and $L^2(\mathbb{P})$ (see **N.3** for notations), which in turn leads to the following theorem.

Proposition 1 (Trajectories of GPs under linear constraints [31]). *Let $(U(x))_{x \in \mathcal{D}} \sim GP(0, k)$ be a centered GP. Note for all $x \in \mathcal{D}$ the function $k_x : y \mapsto k(x, y)$. Let E be a real vector space of functions defined on \mathcal{D} that contains the trajectories of U almost surely and $T : E \rightarrow \mathcal{F}(\mathcal{D}, \mathbb{R})$ be a linear operator. Suppose*

that for all $x \in \mathcal{D}$, $T(U)(x) \in \mathcal{L}(U)$. Then there exists a unique linear operator $\mathcal{T} : \mathcal{H}_k \longrightarrow \mathcal{F}(\mathcal{D}, \mathbb{R})$ such that for all $x, x' \in \mathcal{D}$,

$$\mathbb{E}[T(U)(x)U(x')] = \mathcal{T}(k_{x'})(x)$$

and $\forall x \in \mathcal{D}, \forall h_n \xrightarrow{\mathcal{H}_k} h$, $\mathcal{T}(h_n)(x) \longrightarrow \mathcal{T}(h)(x)$. Moreover, the following statements are equivalent :

- (i) $\mathbb{P}(\{\omega \in \Omega : T(U_\omega) = 0\}) = 1$
- (ii) $\forall x \in \mathcal{D}, \mathcal{T}(k_x) = 0$
- (iii) $\mathcal{T}(\mathcal{H}_k) = \{0\}$

This theorem can be applied when T is a differential operator as discussed in [31]. However, in Proposition 1, the differential operator T of order n has to be valued in the space of (classical, pointwise defined) functions $\mathcal{F}(\mathcal{D}, \mathbb{R})$; in particular for $u \in E$, the function $T(u)$ has to be defined pointwise in order to use the Loève isometry. To summarize, in all generality the derivatives in T have to be understood in a classical sense and E has to be contained in $\mathcal{D}^n(\mathcal{D})$, the space of n times differentiable functions on \mathcal{D} . Requiring that $E \subset \mathcal{D}^n(\mathcal{D})$ is a very strong assumption w.r.t. the trajectories of U ; furthermore, this is not compliant with the usual way of studying PDEs where derivatives are understood in a weaker sense. We present in Proposition 2 an adaptation of Proposition 1 where we make use of the distributional definition of derivatives and relax the assumptions made on U and its trajectories. In this proposition, $(U(x))_{x \in \mathcal{D}}$ is not supposed Gaussian and is only required to be second order. We refer to the notation paragraphs **N.5** and **N.6**.

Proposition 2 (Trajectories of stochastic processes under linear differential constraints). *Let $\mathcal{D} \subset \mathbb{R}^d$ be an open set and let $T = \sum_{|k| \leq n} a_k(x) \partial^k$ be a linear differential operator with coefficients $a_k(x) \in \mathcal{C}^{|k|}(\mathcal{D})$. Let $U = (U(x))_{x \in \mathcal{D}}$ be a second order stochastic process with mean function $m(x)$ and covariance kernel $k(x, x')$. For all $x \in \mathcal{D}$, note $k_x : y \longmapsto k(x, y)$. Suppose that its mean function m lies in $L^1_{loc}(\mathcal{D})$ as well as its standard deviation function $\sigma : x \longmapsto \sqrt{k(x, x)}$.*

- 1) *Then on a set of probability 1, the trajectories of U lie in $L^1_{loc}(\mathcal{D})$ as well as the functions k_x for all $x \in \mathcal{D}$.*
- 2) *Suppose that $T(m) = 0$ in the sense of distributions. Then the following statements are equivalent :*

- (i) $\mathbb{P}(T(U) = 0 \text{ in the sense of distributions}) = 1$
- (ii) $\forall x \in \mathcal{D}, T(k_x) = 0 \text{ in the sense of distributions.}$

Here we write down precisely what we mean by (i) and (ii). Note T^* the formal adjoint of T defined by $T^*u = \sum_{|k| \leq n} (-1)^{|k|} \partial^k (a_k(x)u)$. By (i), we mean that

$$(3.1) \quad \exists A \in \mathcal{F}, \quad \mathbb{P}(A) = 1, \quad \forall \omega \in A, \quad \forall \varphi \in \mathcal{D}(\mathcal{D}), \quad \langle U_\omega, T^* \varphi \rangle = \int_{\mathcal{D}} U_\omega(x) T^* \varphi(x) dx = 0$$

Similarly, (ii) means that

$$(3.2) \quad \forall x \in \mathcal{D}, \quad \forall \varphi \in \mathcal{D}(\mathcal{D}), \quad \langle k_x, T^* \varphi \rangle = \int_{\mathcal{D}} k_x(y) T^* \varphi(y) dy = 0$$

This definition can be found e.g. in [34]. The fact that the functions $x \longmapsto U_\omega(x)$ and $y \longmapsto k_x(y)$ lie in $L^1_{loc}(\mathcal{D})$ ensure the existence of the integrals in equations

(3.1) (see point 2 of the proof of Proposition 2) as well as the continuity of the associated linear forms over $\mathcal{D}(\mathcal{D})$, following the definition (2.16). In every case, the term “in the sense of distributions” can be replaced by “in $\mathcal{D}'(\mathcal{D})$ ” : stating that $T(f) = 0$ in the sense of distributions means that $T(f)$, seen as an element of $\mathcal{D}'(\mathcal{D})$, is equal to the null generalized function $0_{\mathcal{D}'(\mathcal{D})} : \varphi \mapsto 0$.

Proof. Suppose first that U is centered, i.e. $m \equiv 0$.

1) We begin by showing that the trajectories of U almost surely lie in $L^1_{loc}(\mathcal{D})$. Note first that thanks to the Cauchy-Schwarz inequality, $\mathbb{E}[|U(x)|] \leq \sigma(x)$. Now, let $(K_n)_{n \in \mathbb{N}}$ be an increasing sequence of compact subsets of \mathcal{D} such that $\bigcup_{n \in \mathbb{N}} K_n = \mathcal{D}$. Using Tonelli's theorem, we have that for any $n \in \mathbb{N}$,

$$(3.3) \quad \mathbb{E}\left[\int_{K_n} |U(x)| dx\right] = \int_{K_n} \mathbb{E}[|U(x)|] dx \leq \int_{K_n} \sigma(x) dx < +\infty$$

since $\sigma \in L^1_{loc}(\mathcal{D})$. Using the property that “ $\mathbb{E}[|X|] < +\infty \implies |X| < +\infty$ almost surely”, this yields a set $B_n \subset \Omega$ of probability 1 such that the random variable $\omega \mapsto \int_{K_n} |U_\omega(x)| dx$ takes finite values over B_n . Consider now the set $B = \bigcap_{n \in \mathbb{N}} B_n$ which remains of probability 1. For all compact subset $K \subset \mathcal{D}$, there exists an integer n_K such that $K \subset K_{n_K}$ and thus for all $\omega \in B$,

$$\int_K |U_\omega(x)| dx \leq \int_{K_{n_K}} |U_\omega(x)| dx < +\infty$$

which shows that the trajectories of U lie in $L^1_{loc}(\mathcal{D})$ almost surely.

Now, we check that for all $x \in \mathcal{D}$, $k_x \in L^1_{loc}(\mathcal{D})$: for any compact set K , since $\sigma \in L^1_{loc}(\mathcal{D})$ and because of (2.2),

$$\int_K |k_x(y)| dy = \int_K |k(x, y)| dy \leq \sigma(x) \int_K \sigma(y) dy < \infty$$

2) Let us check in advance that whatever $f \in L^1_{loc}(\mathcal{D})$, the map $T(f) : \varphi \mapsto \langle f, T^* \varphi \rangle$ is a continuous linear form over $\mathcal{D}(\mathcal{D})$. Since $a_k \in \mathcal{C}^k(\mathcal{D})$, we can apply Leibniz' rule on $T^* \varphi = \sum_{|k| \leq n} (-1)^{|k|} \partial^k (a_k \varphi)$. This yields a family $\{f_k\}_{|k| \leq n}$ of continuous functions over \mathcal{D} such that

$$(3.4) \quad \forall \varphi \in \mathcal{D}(\mathcal{D}), \quad \forall x \in \mathcal{D}, \quad T^* \varphi(x) = \sum_{|k| \leq n} f_k(x) \partial^k \varphi(x)$$

For all $f \in L^1_{loc}(\mathcal{D})$, for all compact set $K \subset \mathcal{D}$ and for all $\varphi \in \mathcal{D}(\mathcal{D})$ such that $\text{Supp}(\varphi) \subset K$, (3.4) yields

$$(3.5) \quad \begin{aligned} |\langle f, T^* \varphi \rangle| &\leq \int_{\mathcal{D}} |f(x)| |T^* \varphi(x)| dx \\ &\leq \left(\int_K |f(x)| dx \times \max_{|k| \leq n} \sup_{x \in K} |f_k(x)| \right) \sum_{|k| \leq n} \|\partial^k \varphi\|_\infty < +\infty \end{aligned}$$

This proves that $T(f) : \varphi \mapsto \langle f, T^* \varphi \rangle$ is a continuous linear form over $\mathcal{D}(\mathcal{D})$ (see equation (2.15)).

(i) \implies (ii) : Suppose (i). Let $\varphi \in \mathcal{D}(\mathcal{D})$. There exists a set $A \subset \Omega$ such that $\mathbb{P}(A) = 1$ and such that for all $\omega \in A$,

$$\int_{\mathcal{D}} U_\omega(x) T^* \phi(x) dx = 0$$

Multiplying equation above with $U_\omega(x')$, taking the expectancy and formally permuting (for now) the integral and the expectancy, we obtain

$$\begin{aligned} 0 &= \mathbb{E} \left[U(x') \int_{\mathcal{D}} U(x) T^* \varphi(x) dx \right] = \int_{\mathcal{D}} T^* \varphi(x) \mathbb{E}[U(x) U(x')] dx \\ &= \int_{\mathcal{D}} T^* \varphi(x) k(x, x') dx = \langle k_{x'}, T^* \varphi \rangle \end{aligned}$$

The integral-expectancy permutation is justified by writing down the expectancy as an integral and using Fubini's theorem, checking that the below quantity is finite. We use Tonelli's theorem and the Cauchy-Schwarz inequality :

$$\begin{aligned} \mathbb{E} \left[\int_{\mathcal{D}} |U(x') U(x) T^* \varphi(x)| dx \right] &= \int_{\mathcal{D}} |T^* \varphi(x)| \mathbb{E}[|U(x) U(x')|] dx \\ &\leq \int_{\mathcal{D}} |T^* \varphi(x)| \mathbb{E}[U(x)^2]^{1/2} \mathbb{E}[U(x')^2]^{1/2} dx \\ &\leq \sigma(x') \int_{\mathcal{D}} |T^* \varphi(x)| \sigma(x) dx < +\infty \end{aligned}$$

Indeed, since $\sigma \in L^1_{loc}(\mathcal{D})$, setting $f = \sigma$ in (3.5) shows that the last integral is finite. Thus, $\forall x \in \mathcal{D}, \forall \varphi \in \mathcal{D}(\mathcal{D}), \langle k_x, T^* \varphi \rangle = 0$ which proves that (i) \implies (ii).

(ii) \implies (i) : Suppose (ii). Let $\varphi \in \mathcal{D}(\mathcal{D})$, we have $\langle k_{x'}, T^* \varphi \rangle = 0$. Multiplying this with $T^* \varphi(x')$ and integrating w.r.t. x' yields

$$0 = \int_{\mathcal{D}} T^* \varphi(x') \int_{\mathcal{D}} T^* \varphi(x) k(x, x') dx dx' = \int_{\mathcal{D}} \int_{\mathcal{D}} T^* \varphi(x) T^* \varphi(x') \mathbb{E}[U(x) U(x')] dx dx'$$

Permuting formally the expectancy and the integrals (justified in equation (3.6)) yields

$$\begin{aligned} 0 &= \int_{\mathcal{D}} \int_{\mathcal{D}} T^* \varphi(x) T^* \varphi(x') \mathbb{E}[U(x) U(x')] dx dx' \\ &= \mathbb{E} \left[\left(\int_{\mathcal{D}} T^* \varphi(x) U(x) dx \right)^2 \right] = \mathbb{E}[\langle U, T^* \varphi \rangle^2] \end{aligned}$$

and thus $\langle U, T^* \varphi \rangle = 0$ a.s. : there exists $A_\varphi \in \mathcal{F}$ with $\mathbb{P}(A_\varphi) = 1$ such that $\forall \omega \in A_\varphi, \langle U_\omega, T^* \varphi \rangle = 0$. We justify the expectancy-integral permutation with the computation below

$$\begin{aligned} (3.6) \quad &\int_{\mathcal{D}} \int_{\mathcal{D}} |T^* \varphi(x) T^* \varphi(x')| \mathbb{E}[|U(x) U(x')|] dx dx' \\ &\leq \int_{\mathcal{D}} \int_{\mathcal{D}} |T^* \varphi(x) T^* \varphi(x')| \sigma(x) \sigma(x') dx dx' \\ &\leq \left(\int_{\mathcal{D}} |T^* \varphi(x)| \sigma(x) dx \right)^2 < +\infty \end{aligned}$$

As previously, setting $f = \sigma$ in (3.5) shows that the integral above is finite.

This does not finish the proof as we need to find a set A with $\mathbb{P}(A) = 1$, independently from φ , such that $\forall \omega \in A, \langle U_\omega, T^* \varphi \rangle = 0$. For this we use the fact that $\mathcal{D}(\mathcal{D})$ is a separable topological space, which we prove at the end of this proof. Let $F \subset \mathcal{D}(\mathcal{D})$ be a countable dense subset of $\mathcal{D}(\mathcal{D})$, let $A := B \cap \left(\bigcap_{\varphi \in F} A_\varphi \right)$ and let

$\omega \in A$. Since $U_\omega \in L^1_{loc}(\mathcal{D})$, (3.5) shows that the map $L_\omega : \varphi \mapsto \langle U_\omega, T^* \varphi \rangle$ is a continuous linear form on $\mathcal{D}(\mathcal{D})$. Even though $\mathcal{D}(\mathcal{D})$ is not a metric space, theorem 2.1.4 from [34] states that L_ω is in fact *sequentially* continuous. Let $\varphi \in \mathcal{D}(\mathcal{D})$ and a sequence $(\varphi_n) \subset F$ such that $\varphi_n \rightarrow \varphi$ (in the sense of the topology of $\mathcal{D}(\mathcal{D})$). Then $L_\omega(\varphi) = \lim_n L_\omega(\varphi_n) = 0$ since $\forall n, L_\omega(\varphi_n) = 0$. That is, we have proved that

$$\forall \omega \in A, \quad \forall \varphi \in \mathcal{D}(\mathcal{D}), \quad \langle U_\omega, T^* \varphi \rangle = L_\omega(\varphi) = 0$$

Since $\mathbb{P}(A) = 1$, this shows that (ii) \implies (i).

When U is not centered, consider the centered stochastic process V defined by $V(x) = U(x) - m(x)$ for which the above proof can be applied. Since T is linear and m is supposed to verify $T(m) = 0$ in the sense of distributions, the probabilistic events $\{T(U) = 0 \text{ in the sense of distributions}\}$ and $\{T(V) = 0 \text{ in the sense of distributions}\}$ coincide and thus have the same probability measure. Finally, U and V have the same covariance kernel $k(x, x')$. Thus,

$$\mathbb{P}(T(U) = 0 \text{ in the sense of distributions}) = 1$$

$$\iff \mathbb{P}(T(V) = 0 \text{ in the sense of distributions}) = 1 \iff \forall x \in \mathcal{D}, T(k_x) = 0$$

which finishes the proof in the general case.

Proof that $\mathcal{D}(\mathcal{D})$ is separable : $\mathcal{D}(\mathcal{D})$ is an LF-space as the inductive limit of the Fréchet spaces $\mathcal{D}_{K_i}(\mathcal{D}) := \{\varphi \in C^\infty(\mathcal{D}) : \text{Supp}(\varphi) \subset K_i\}, i \in \mathbb{N}$, where $K_1 \subset K_2 \subset \dots$ are compact subsets of \mathcal{D} such that $\bigcup_i K_i = \mathcal{D}$ ([76], p.131-133). As such, $\mathcal{D}(\mathcal{D})$ is separable iff $\mathcal{D}_{K_i}(\mathcal{D})$ is separable for all $i \in \mathbb{N}$ [78], which we now show. The Fréchet topology of $\mathcal{D}_{K_i}(\mathcal{D})$ is the one induced by the usual Fréchet topology of $C^\infty(\mathcal{D})$ when $\mathcal{D}_{K_i}(\mathcal{D})$ is seen as a subspace of $C^\infty(\mathcal{D})$ ([62], section 1.46). As a Fréchet space, $C^\infty(\mathcal{D})$ is metrizable. But $C^\infty(\mathcal{D})$ is also a Montel space ([76], Prop 34.4) : as a metrizable space, it is automatically separable ([66], p.195). Thus $\mathcal{D}_{K_i}(\mathcal{D})$ is also separable as a subspace of the separable metric space $C^\infty(\mathcal{D})$. \square

Remark 3.1. Distributional solutions are the weakest types of solutions for PDEs. In general, additional regularity conditions have to be imposed to obtain physically realistic solutions, such as Sobolev regularity or entropy conditions as for non linear hyperbolic PDEs [69]. However, every step in the above proof remains valid when replacing $\varphi \in \mathcal{D}(\mathcal{D})$ with $\varphi \in \mathcal{C}_c^n(\mathcal{D})$. Although we have not clarified the usual topology of $\mathcal{C}_c^n(\mathcal{D})$ in this article, we state that this is enough to show that the equalities stated in Proposition 2 also hold in $\mathcal{C}_c^n(\mathcal{D})'$, the space of finite order generalized functions of order n , rather than just in $\mathcal{D}'(\mathcal{D})$. $\mathcal{C}_c^n(\mathcal{D})'$ is a smaller space than $\mathcal{D}'(\mathcal{D})$, though less used in PDE theory than $\mathcal{D}'(\mathcal{D})$.

Remark 3.2. We gave here an elementary proof that

$$(3.7) \quad \sigma \in L^1_{loc}(\mathcal{D}) \implies \text{the trajectories of } U \text{ lie in } L^1_{loc}(\mathcal{D}) \text{ almost surely}$$

Similar results on Sobolev regularity of the trajectories of second order stochastic processes are scarce in the literature. Some are available in [68], though the result (3.7) is actually not covered in [68], where additional continuity hypotheses would be required in the left hand side of (3.7) to apply results from [68].

We partially recover Proposition 1 when the trajectories of U lie in $\mathcal{C}^n(\mathcal{D})$ and $k \in \mathcal{C}^{n,n}(\mathcal{D} \times \mathcal{D})$. Indeed, in that case one can show that if $T = \sum_{|k| \leq n} a_k(x) \partial^k$,

then we simply have $\mathcal{T} = T$ in Proposition 1. Additionally, $T(U_\omega)$ and $T(k_x)$ both lie in $\mathcal{F}(\mathcal{D}, \mathbb{R}) \cap L_{loc}^1(\mathcal{D})$, and for any function g that lies in $L_{loc}^1(\mathcal{D})$, we have (see **N.4**)

$$(3.8) \quad g = 0 \text{ in the sense of distributions} \iff g = 0 \text{ a.e.}$$

Equation (3.8) is just another way of saying that the linear map $f \mapsto T_f$ given in (2.16) is injective. In that framework, Proposition 1 states that

$$(3.9) \quad \forall x \in \mathcal{D}, T(k_x) = 0 \iff \mathbb{P}(T(U) = 0) = 1$$

where the function equalities of the form $T(f) = 0$ in (3.9) are valid everywhere on \mathcal{D} . Following equation (3.8), Proposition 2 states a slightly weaker result, namely that

$$(3.10) \quad \forall x \in \mathcal{D}, T(k_x) = 0 \text{ a.e.} \iff \mathbb{P}(T(U) = 0 \text{ a.e.}) = 1$$

We can now state the following corollary, which draws the consequences of Proposition 2 when applied to GPR.

Proposition 3 (Heredity of Proposition 2 to conditioned GPs). *Let \mathcal{D} and T be as defined in Proposition 2. Let $(U(x))_{x \in \mathcal{D}} \sim GP(m, k)$ be a Gaussian process that verifies the hypotheses of Proposition 2. Suppose also that*

$$(3.11) \quad T(m) = 0 \text{ and } \forall x \in \mathcal{D}, T(k_x) = 0 \text{ both in the sense of distributions}$$

(i) *Then whatever the integer p , the vector $u = (u_1, \dots, u_p)^T \in \mathbb{R}^p$ and the vector $X = (x_1, \dots, x_p)^T \in \mathcal{D}^p$ such that $k(X, X)$ is invertible, the Kriging mean $\tilde{m}(x)$ and the Kriging standard deviation function $\tilde{\sigma}(x) = \sqrt{\tilde{k}(x, x)}$ both lie in $L_{loc}^1(\mathcal{D})$, and we have*

$$T(\tilde{m}) = 0 \text{ and } \forall x \in \mathcal{D}, T(\tilde{k}_x) = 0 \text{ both in the sense of distributions}$$

where \tilde{m} and \tilde{k} are defined in equations (2.3) and (2.4).

(ii) *As such, the trajectories of the conditioned Gaussian process $(\tilde{U}(x))_{x \in \mathcal{D}}$ defined by $\tilde{U}(x) = (U(x)|U(x_i) = u_i \forall i = 1, \dots, p)$ are almost surely solutions of the equation $T(f) = 0$ in the sense of distributions :*

$$\mathbb{P}(T(\tilde{U}) = 0 \text{ in the sense of distributions}) = 1$$

Proof. Note first that for all $x \in \mathcal{D}$, $\tilde{k}(x, x) \leq k(x, x)$, which is immediate from (2.13). Thus the function $\tilde{\sigma} : x \mapsto \sqrt{\tilde{k}(x, x)}$ also lies in $L_{loc}^1(\mathcal{D})$. Point (i) is then a direct consequence of the definition of \tilde{m} and \tilde{k} in equations (2.3) and (2.4), and the linearity of T . Proposition 2 can then be applied conjointly with (i), which yields point (ii) since the mean and covariance functions of the GP \tilde{U} are \tilde{m} and \tilde{k} (see section 2.2, equations (2.3) and (2.4)). \square

Proposition 3 shows that when U is a GP, the results of Proposition 2 are inherited on the conditioned posterior process \tilde{U} . One weak consequence of Proposition 3 is that if GPR is performed with a kernel k that verifies point (ii) of Proposition 2, then the predictions provided by GPR are all solutions of the PDE $T(\tilde{m}) = 0$.

The goal of the next section is to apply this idea to a special case of the (3 dimensional) wave equation defined in eq.(4.1), by building an “explicit” positive definite kernel k such that $\forall x' \in \mathcal{D}, \square k_{x'} = 0$ in the sense of distributions, where the box symbol \square classically denotes the linear wave operator a.k.a. the d’Alembert

operator. With this new kernel, we will perform GPR on observations of a function that is solution to the wave equation and draw a number of related consequences.

4. GAUSSIAN PROCESSES AND THE 3 DIMENSIONAL WAVE EQUATION

4.1. General Solution to the 3 Dimensional Wave Equation. Denote the 3D Laplace operator $\Delta = \partial_{xx}^2 + \partial_{yy}^2 + \partial_{zz}^2$ and the d'Alembert operator $\square = 1/c^2 \partial_{tt}^2 - \Delta$ with constant wave speed $c > 0$. We focus on the general initial value problem in the free space \mathbb{R}^3

$$(4.1) \quad \begin{cases} \square w &= 0 & \forall (x, t) \in \mathbb{R}^3 \times \mathbb{R}_+^* \\ w(x, 0) &= u_0(x) & \forall x \in \mathbb{R}^3 \\ (\partial_t w)(x, 0) &= v_0(x) & \forall x \in \mathbb{R}^3 \end{cases}$$

Throughout this article, we will refer to u_0 as the initial position and v_0 as the initial speed. The problem (4.1) is a Cauchy problem with initial conditions (IC) u_0 and v_0 . It admits a unique solution which can be extended to all times $t \in \mathbb{R}$, and is represented as follow ([27], section 4.3.1.b, example 4)

$$(4.2) \quad w(x, t) = (F_t * v_0)(x) + (\dot{F}_t * u_0)(x) \quad \forall (x, t) \in \mathbb{R}^3 \times \mathbb{R}$$

where F_t and \dot{F}_t are known generalized functions. Actually, F_t and \dot{F}_t are better known through their Fourier transforms [27], as

$$(4.3) \quad \mathcal{F}(F_t)(\xi) = \frac{\sin(ct|\xi|)}{c|\xi|} \quad \text{and} \quad \mathcal{F}(\dot{F}_t)(\xi) = \cos(ct|\xi|)$$

where $|\xi|$ is the euclidean norm of $\xi \in \mathbb{R}^3$. Note that the relation $\dot{F}_t = \partial_t F_t$ can be directly deduced from (4.3). Additionally, the representation (4.2) is valid in any dimension as well as the Fourier formulas (4.3), see [27]. Finally, F_t also corresponds to the Green's function of the wave equation [23].

In dimension 3, F_t and \dot{F}_t are compactly supported generalized functions of order 0 and 1 respectively. More explicitly, in dimension 3 F_t and \dot{F}_t are given by

$$(4.4) \quad F_t = \frac{\sigma_{c|t|}}{4\pi c^2 t} \quad \text{and} \quad \dot{F}_t = \partial_t F_t$$

where σ_R is the surface measure of the sphere of center 0 and radius R . $\dot{F}_t = \partial_t F_t$ means that

$$\forall \mathcal{C}_0^1(\mathbb{R}^3), \langle \dot{F}_t, f \rangle = \partial_t \langle F_t, f \rangle = \partial_t \int_{\mathbb{R}^3} f(x) F_t(dx)$$

Suppose that $u_0 \in \mathcal{C}^1(\mathbb{R}^3)$ and $v_0 \in \mathcal{C}^0(\mathbb{R}^3)$, then w as defined in (4.2) is a function in the classical sense [76] and in that case an explicit formula for such convolutions is reminded in equation (2.23) (yet one may actually make sense out of (4.2) when u_0 and v_0 are only required to be any generalized functions [76]). Combining formulas (4.2) and (4.4) leads to the Kirschhoff formula [27] (see **N.7** for spherical coordinates notations) :

$$(4.5) \quad w(x, t) = \int_{S(0,1)} tv_0(x - c|t|\gamma) + u_0(x - c|t|\gamma) - c|t|\gamma \cdot \nabla u_0(x - c|t|\gamma) \frac{d\Omega}{4\pi}$$

4.2. Gaussian Process Modelling of the Solution. Suppose now that u_0 and v_0 are unknown, and only pointwise values of w are observed. In a Bayesian approach, we model u_0 and v_0 as random functions and put a Gaussian process prior over u_0 and v_0 . More precisely, we make the following assumptions.

- (A₁) Suppose that the initial conditions u_0 and v_0 of Problem (4.1) are trajectories drawn from two independent Gaussian processes $U^0 \sim GP(0, k_u)$ and $V^0 \sim GP(0, k_v) : \exists \omega \in \Omega, \forall x \in \mathbb{R}^3, u_0(x) = U_\omega^0(x)$ and $v_0(x) = V_\omega^0(x)$.
- (A₂) Suppose that all trajectories of U^0 lie in $\mathcal{C}^1(\mathbb{R}^3)$ and that those of V^0 lie in $\mathcal{C}^0(\mathbb{R}^3)$ almost surely. A sufficient condition for this is given in [1], Thm 1.4.2. This theorem states that under mild technical assumptions, the paths of $(U(x))_{x \in \mathcal{D}} \sim GP(0, k)$ lie in \mathcal{C}^l a.s. as soon as $k \in \mathcal{C}^{2l}(\mathcal{D} \times \mathcal{D})$, which we assume from now on.

We now analyse the consequence of these two assumptions. First, they imply that by solving (4.1), one obtains a time-space stochastic process $W(x, t)$ defined by

$$(4.6) \quad W(x, t) : \Omega \ni \omega \longmapsto (F_t * V_\omega^0)(x) + (\dot{F}_t * U_\omega^0)(x)$$

Here again, V_ω^0 denotes the trajectory of V^0 at $\omega \in \Omega$ and likewise for U_ω^0 . In particular, thanks to assumption (A₂), (4.6) defines a random variable for all (x, t) . Note the space-time variable $z = (x, t)$ and note the random variables

$$(4.7) \quad V(z) : \omega \longmapsto (F_t * V_\omega^0)(x) \quad \text{and} \quad U(z) : \omega \longmapsto (\dot{F}_t * U_\omega^0)(x)$$

that is, $W(z) = U(z) + V(z)$. We show in the next proposition that the stochastic processes U, V and W are GPs as well. In particular we describe their covariance kernels.

Proposition 4. *Define the two functions*

$$(4.8) \quad k_v^{\text{wave}}(z, z') = [(F_t \otimes F_{t'}) * k_v](x, x')$$

$$(4.9) \quad k_u^{\text{wave}}(z, z') = [(\dot{F}_t \otimes \dot{F}_{t'}) * k_u](x, x')$$

(i) Then $U = (U(z))_{z \in \mathbb{R}^3 \times \mathbb{R}}$ and $V = (V(z))_{z \in \mathbb{R}^3 \times \mathbb{R}}$ as defined in (4.7) are two independent centered GPs with covariance kernels k_u^{wave} and k_v^{wave} respectively. Consequently, $(W(z))_{z \in \mathbb{R}^3 \times \mathbb{R}}$ is a centered GP whose covariance kernel is given by

$$(4.10) \quad k_W(z, z') = k_v^{\text{wave}}(z, z') + k_u^{\text{wave}}(z, z')$$

(ii) Conversely, any centered second order stochastic process with covariance kernel k_W has its sample paths solution of the 3 dimensional wave equation (4.1) almost surely.

Proof. (i) : first we prove that U and V are GPs. Since U^0 and V^0 are GPs, $\mathcal{L}(U^0)$ and $\mathcal{L}(V^0)$ are only comprised of Gaussian random variables (see **N.3**).

To prove that U and V are Gaussian processes, we rely on the Kirschhoff formula (4.5), writing the integrals as limits of Riemann sums. We start with V , that is, we focus on the first term in Kirschhoff's formula (4.5). To show that V is a Gaussian process, we only need to show that for any z , $V(z) \in \mathcal{L}(V^0)$ as this will ensure the Gaussian process property. Since the trajectories of V^0 are continuous almost surely, there exists a sequence of numbers a_k^n and points y_k^n such that for almost

any $\omega \in \Omega$,

$$\begin{aligned} V(z)(\omega) &= (F_t * V_\omega^0)(x) = t \int_{S(0,1)} V^0(x - c|t|\gamma)(\omega) \frac{d\Omega}{4\pi} \\ &= \frac{t}{4\pi} \int_0^{2\pi} \int_0^\pi V^0(x - c|t|\gamma(\theta, \phi))(\omega) \sin(\theta) d\theta d\phi = \lim_{n \rightarrow \infty} \sum_{k=1}^n a_k^n V^0(x - y_k^n)(\omega) \end{aligned}$$

This shows that $V(z)$ is an a.s. limit of a sequence of centered Gaussian random variables $(Y_n) \subset \mathcal{L}(V^0)$; a.s. convergence implies convergence in law. From [44], Proposition 1.1, $V(z)$ is normally distributed and the convergence also takes place in $L^2(\mathbb{P})$. Therefore, $V(z) \in \mathcal{L}(V^0)$ and V is a Gaussian process. From the same proposition, $V(z)$ is centered because the variables Y_n are centered. Note that since F_t is supported on the compact set $S(0, 1)$, we only required the trajectories of V^0 to be continuous rather than continuous and compactly supported.

We apply the same reasoning to U , by applying the above steps to the second part of Kirschhoff's formula (4.5). One's ability to write out the integrals as a limit of Riemann sums is ensured when the trajectories of U^0 lie in $\mathcal{C}^1(\mathbb{R}^3)$.

Finally, since U^0 and V^0 are independent, $\mathcal{L}(U^0)$ and $\mathcal{L}(V^0)$ are orthogonal in $L^2(\mathbb{P})$. Since $\mathcal{L}(U) \subset \mathcal{L}(U^0)$ and likewise for V , U and V are independent Gaussian processes (for Gaussian random variables, independence is equivalent to null covariance). Finally, the sum of independent Gaussian random variables is a Gaussian random variable. Therefore $\mathcal{L}(W) \subset \mathcal{L}(U) + \mathcal{L}(V)$ is only comprised of Gaussian random variables and W is a Gaussian process. Now, we prove that

$$(4.11) \quad \mathbb{E}[U(z)U(z')] = [(\dot{F}_t \otimes \dot{F}_{t'}) * k_u](x, x')$$

The main argument is Fubini's theorem. For this we use the fact that \dot{F}_t is a distribution of order 1 and can be identified to the a sum of derivatives of measures (see equation (2.22)) : for all $t \in \mathbb{R}$, there exists $\{\mu_k^t\}_{k \in \mathbb{N}^3, |k| \leq 1}$ a family of Radon measures such that

$$(4.12) \quad \dot{F}_t = \sum_{|k| \leq 1} \partial^k \mu_k^t \quad \text{in the sense of distributions}$$

Moreover, \dot{F}_t is compactly supported, therefore all the measures μ_k^t are also compactly supported. First, we write $U_\omega(z)$ in integral form :

$$(4.13) \quad U_\omega(z) = (\dot{F}_t * U_\omega^0)(x) = \langle \dot{F}_t, \tau_{-x} \check{U}_\omega^0 \rangle = \left\langle \sum_{|k| \leq 1} \partial^k \mu_k^t, \tau_{-x} \check{U}_\omega^0 \right\rangle$$

$$(4.14) \quad = \sum_{|k| \leq 1} \langle \mu_k^t, (-1)^{|k|} \partial^k \tau_{-x} \check{U}_\omega^0 \rangle = \sum_{|k| \leq 1} \int_{\mathbb{R}^3} (-1)^{|k|} \partial^k U_\omega^0(x - y) \mu_k^t(dy)$$

Before applying Fubini's theorem, we need to check an integrability condition. Let $k \in \mathbb{N}^3$ such that $|k| \leq 1$. Recall that $|\mu_k^t|$ is defined in (2.20); denote also $\sigma_{\partial^k U^0}(x) = \sqrt{\text{Var}(\partial^k U_0(x))}$. Since the trajectories of U^0 lie in $\mathcal{C}^1(\mathcal{D})$ a.s, those of $\partial^k U^0$ lie in $\mathcal{C}^0(\mathcal{D})$ and thus the function $x \mapsto \text{Var}(\partial^k U_0(x))$ also lies in $\mathcal{C}^0(\mathcal{D})$ ([8], chapter 1, section 4.3). Therefore the function $x \mapsto \sigma_{\partial^k U^0}(x)$ also lies in $\mathcal{C}^0(\mathcal{D})$. We now check that the integral I below is finite. We use Tonelli's theorem and the

Cauchy-Schwarz inequality:

$$\begin{aligned}
I &:= \int_{\Omega} \sum_{|k| \leq 1} \int_{\mathbb{R}^3} \left| \partial^k U_{\omega}^0(x-y) \right| |\mu_k^t|(dy) \sum_{|k'| \leq 1} \int_{\mathbb{R}^3} \left| \partial^{k'} U_{\omega}^0(x'-y') \right| |\mu_{k'}^{t'}|(dy') \mathbb{P}(d\omega) \\
&= \sum_{|k|, |k'| \leq 1} \int_{\mathbb{R}^3} \int_{\mathbb{R}^3} \int_{\Omega} \left| \partial^k U_{\omega}^0(x-y) \partial^{k'} U_{\omega}^0(x'-y') \right| \mathbb{P}(d\omega) |\mu_k^t|(dy) |\mu_{k'}^{t'}|(dy') \\
&= \sum_{|k|, |k'| \leq 1} \int_{\mathbb{R}^3} \int_{\mathbb{R}^3} \mathbb{E} \left[\left| \partial^k U^0(x-y) \partial^{k'} U^0(x'-y') \right| \right] |\mu_k^t|(dy) |\mu_{k'}^{t'}|(dy') \\
&\leq \sum_{|k|, |k'| \leq 1} \int_{\mathbb{R}^3} \int_{\mathbb{R}^3} \left(\mathbb{E} [\partial^k U^0(x-y)^2] \mathbb{E} [\partial^{k'} U^0(x'-y')^2] \right)^{1/2} |\mu_k^t|(dy) |\mu_{k'}^{t'}|(dy') \\
&\leq \left(\sum_{|k| \leq 1} \int_{\mathbb{R}^3} \left(\mathbb{E} [\partial^k U^0(x-y)^2] \right)^{1/2} |\mu_k^t|(dy) \right) \times \left(\sum_{|k'| \leq 1} \int_{\mathbb{R}^3} \left(\mathbb{E} [\partial^{k'} U^0(x'-y')^2] \right)^{1/2} |\mu_{k'}^{t'}|(dy') \right) \\
&\leq \left(\sum_{|k| \leq 1} (|\mu_k^t| * \sigma_{\partial^k U^0})(x) \right) \times \left(\sum_{|k'| \leq 1} (|\mu_{k'}^{t'}| * \sigma_{\partial^{k'} U^0})(x') \right) < +\infty
\end{aligned}$$

For all multi-index k , the quantity $(|\mu_k^t| * \sigma_{\partial^k U^0})(x)$ is finite because $x \mapsto \sigma_{\partial^k U^0}(x)$ is continuous and $|\mu_k^t|$ is compactly supported. Note also that from hypothesis (A_2) , the GP U^0 is *mean square differentiable* up to order 1, which implies ([61], section III.1.4) that we have, for all multi-indexes k, k' such that $|k|, |k'| \leq 1$, x and x' :

$$(4.15) \quad \mathbb{E}[\partial^k U^0(x) \partial^{k'} U^0(x')] = \partial_1^k \partial_2^{k'} k_u(x, x')$$

where ∂_1 (resp. ∂_2) denotes derivatives w.r.t. the first (resp. second) argument of k_u . We may thus permute integrals and differential operators in $\mathbb{E}[U(z)U(z')]$:

$$\begin{aligned}
\mathbb{E}[U(z)U(z')] &= \mathbb{E} \left[\sum_{|k| \leq 1} \int_{\mathbb{R}^3} (-1)^{|k|} \partial^k U^0(x-y) \mu_k^t(dy) \sum_{|k'| \leq 1} \int_{\mathbb{R}^3} (-1)^{|k'|} \partial^{k'} U^0(x'-y') \mu_{k'}^{t'}(dy') \right] \\
&= \sum_{|k|, |k'| \leq 1} \int_{\mathbb{R}^3} \int_{\mathbb{R}^3} (-1)^{|k|} (-1)^{|k'|} \partial_1^k \partial_2^{k'} \mathbb{E}[U^0(x-y) U^0(x'-y')] \mu_k^t(dy) \mu_{k'}^{t'}(dy') \\
&= \sum_{|k|, |k'| \leq 1} \int_{\mathbb{R}^3} \int_{\mathbb{R}^3} (-1)^{|k|} (-1)^{|k'|} \partial_1^k \partial_2^{k'} k_u(x-y, x'-y') \mu_k^t(dy) \mu_{k'}^{t'}(dy') \\
&= \left[\left(\sum_{|k| \leq 1} \partial^k \mu_k^t \otimes \sum_{|k'| \leq 1} \partial^{k'} \mu_{k'}^{t'} \right) * k_u \right](x, x') = [(\dot{F}_t \otimes \dot{F}_{t'}) * k_u](x, x')
\end{aligned}$$

which proves (4.11).

One proves that $\mathbb{E}[V(z)V(z')] = [(F_t \otimes F_{t'}) * k_v](x, x')$ the exact same way, which is actually simpler as F_t is directly a measure. To conclude,

$$\begin{aligned}
k_W(z, z') &= \text{Cov}(W(z), W(z')) \\
&= \mathbb{E}[(W(z)W(z'))] = \mathbb{E}[(U(z) + V(z))(U(z') + V(z'))] \\
&= \mathbb{E}[U(z)U(z')] + \mathbb{E}[U(z)V(z')] + \mathbb{E}[V(z)U(z')] + \mathbb{E}[V(z)V(z')] \\
(4.16) \quad &= [(\dot{F}_t \otimes \dot{F}_{t'}) * k_u](x, x') + [(F_t \otimes F_{t'}) * k_v](x, x')
\end{aligned}$$

The cross terms are null because $U(z)$ and $V(z')$ are independent as well as $U(z')$ and $V(z)$.

(ii) : with expression (4.10), one checks that for any fixed z' , the function $z \mapsto k_W(z, z')$ is of the form (4.2) and thus verifies $\square k_{x'} = 0$ in the sense of distributions. (ii) is then a direct consequence of Proposition 2. \square

Remark 4.1. If U and V are not independent, then the two terms $[(\dot{F}_t \otimes F_{t'}) * k_{uv}](x, x')$ and $[(F_t \otimes \dot{F}_{t'}) * k_{vu}](x, x')$ must be added to equation (4.10), where $k_{uv}(x, x')$ denotes the cross covariance between U and V : $k_{uv}(x, x') = \text{Cov}(U(x), V(x'))$ and $k_{vu}(x, x') = \text{Cov}(V(x), U(x')) = k_{uv}(x', x)$.

More explicitly, we have the following Kirschhoff-like integral formulas for k_v^{wave} and k_u^{wave} :

$$(4.17) \quad [(F_t \otimes F_{t'}) * k_v](x, x') = tt' \int_{S(0,1) \times S(0,1)} k_v(x - c|t|\gamma, x' - c|t'|\gamma') \frac{d\Omega d\Omega'}{(4\pi)^2}$$

$$\begin{aligned}
[(\dot{F}_t \otimes \dot{F}_{t'}) * k_u](x, x') &= \int_{S(0,1) \times S(0,1)} \left(k_u(x - c|t|\gamma, x' - c|t'|\gamma') \right. \\
&\quad - ct \nabla_1 k_u(x - c|t|\gamma, x' - c|t'|\gamma') \cdot \gamma \\
&\quad - c|t'|\nabla_2 k_u(x - c|t|\gamma, x' - c|t'|\gamma') \cdot \gamma' \\
(4.18) \quad &\quad \left. + c^2 tt' \gamma^T \nabla_1 \nabla_2 k_u(x - c|t|\gamma, x' - c|t'|\gamma') \gamma' \right) \frac{d\Omega d\Omega'}{(4\pi)^2}
\end{aligned}$$

where $\nabla_1 k_u(x, x')$ is the gradient vector of k_u w.r.t. x , $\nabla_2 k_u(x, x')$ is the gradient vector of k_u w.r.t. x' and $\nabla_1 \nabla_2 k_u(x, x')$ is the matrix whose entry (i, j) is given by $\partial_{x_i^1} \partial_{x_j^2} k_u(x, x')$ ($\partial_{x_i^1}$ is the partial derivative w.r.t. the i^{th} coordinate of x , $\partial_{x_j^2}$ is the partial derivative w.r.t. the j^{th} coordinate of x'). From now on, we call WIGPR the act of performing GPR with a covariance kernel of the form (4.10).

4.2.1. *Stationary kernel for the initial conditions.* Many standard covariance kernels used for GPR are stationary [60]. For this reason, we study equation (4.8) when k_v is stationary. For conciseness, we restrict ourselves to the case where $u_0 = 0$, i.e. $k_u = 0$ (and we discard (4.9)).

Proposition 5. *Suppose that k_v is stationary : $k_v(x, x') = k_S(x - x')$.*

(i) *Then k_v^{wave} is stationary in space and*

$$(4.19) \quad [(F_t \otimes F_{t'}) * k_v](x, x') = (F_t * F_{t'} * k_S)(x - x')$$

(ii) Moreover, the measure $F_t * F_{t'}$ is absolutely continuous over \mathbb{R}^3 and identifying it to its density, we have

$$(4.20) \quad (F_t * F_{t'})(h) = \frac{\text{sgn}(t)\text{sgn}(t')}{8\pi c^2 |h|} \mathbb{1}_{[c||t|-|t'||, c(|t|+|t'|)]}(|h|)$$

where $|h|$ is the euclidean norm of $h \in \mathbb{R}^3$.

Proof. (i) : Suppose for simplicity that $c = 1$. Using (2.25),

$$\begin{aligned} [(F_t \otimes F_{t'}) * k_v](x, x') &= \int_{\mathbb{R}^3 \times \mathbb{R}^3} k(x - s_1, x' - s_2) dF_t(s_1) dF_{t'}(s_2) \\ &= \int_{\mathbb{R}^3 \times \mathbb{R}^3} k_S(x - x' - s_1 + s_2) dF_t(s_1) dF_{t'}(s_2) \end{aligned}$$

But $S(0, 1)$ is invariant under the change of variable $\gamma \mapsto -\gamma$ and thus for any function f , $\int_{\mathbb{R}^3} f(s_2) dF_{t'}(s_2) = \int_{\mathbb{R}^3} f(-s_2) dF_{t'}(s_2)$. This yields

$$[(F_t \otimes F_{t'}) * k_v](x, x') = \int_{\mathbb{R}^3 \times \mathbb{R}^3} k_S(x - x' - s_1 - s_2) dF_t(s_1) dF_{t'}(s_2)$$

Then, using the definition of $F_t * F_{t'}$ in (2.21),

$$(F_t * F_{t'} * k_S)(h) = \int_{\mathbb{R}^3} k_S(h - s) d(F_t * F_{t'})(s) = \int_{\mathbb{R}^3} \int_{\mathbb{R}^3} k_S(h - s_1 - s_2) dF_t(s_1) dF_{t'}(s_2)$$

Setting $h = x - x'$ finishes the proof.

(ii) : Without loss of generality we suppose that $c = 1$. The computation is derived in the Fourier domain. We use here the following convention for the Fourier transform of functions and measures over \mathbb{R}^d , along with its inverse transform

$$(4.21) \quad \mathcal{F}(f)(\xi) = \int_{\mathbb{R}^d} f(x) e^{-i\langle x, \xi \rangle} dx$$

$$(4.22) \quad f(x) = \frac{1}{(2\pi)^d} \int_{\mathbb{R}^d} \mathcal{F}(f)(\xi) e^{i\langle x, \xi \rangle} d\xi$$

$$(4.23) \quad \mathcal{F}(\mu)(\xi) = \int_{\mathbb{R}^d} f(x) e^{-i\langle x, \xi \rangle} \mu(dx)$$

Above, \langle, \rangle denotes the usual dot product of \mathbb{R}^d . Equation (4.23) for an absolutely continuous measure $\mu(dx) = f(x)dx$ reduces to (4.21), i.e. the Fourier transform of its density f . This convention is the one that yields the expressions (4.3) and it is such that $\mathcal{F}(f * g)(\xi) = \mathcal{F}(f)(\xi)\mathcal{F}(g)(\xi)$ [62] whatever f and g , functions or measures. Thus,

$$(4.24) \quad \mathcal{F}(F_t * F_{t'})(\xi) = \mathcal{F}(F_t)(\xi)\mathcal{F}(F_{t'})(\xi) = \frac{\sin(t|\xi|)\sin(t'|\xi|)}{|\xi|^2} = \frac{\cos(a|\xi|) - \cos(b|\xi|)}{2|\xi|^2}$$

with $a = t - t'$, $b = t + t'$. We then compute the inverse Fourier transform of the quantity above. Let $h \in \mathbb{R}^3$. In spherical coordinates (see **N.7**), noting the unit

vectors $\gamma_h = \frac{h}{|h|}$ and $\gamma = \frac{\xi}{|\xi|} = \frac{\xi}{r}$, we define f_a by

$$(4.25) \quad f_a(h) = \int_{\mathbb{R}^3} e^{i\langle h, \xi \rangle} \frac{\cos(a|\xi|)}{|\xi|^2} d\xi = \int_0^{+\infty} \int_0^{2\pi} \int_0^\pi e^{ir\langle h, \gamma \rangle} \frac{\cos(ar)}{r^2} r^2 \sin \theta d\theta d\phi dr$$

$$= \int_0^{+\infty} \cos(ar) \int_{S(0,1)} e^{ir|h|\langle \gamma, \gamma_h \rangle} d\Omega dr$$

In the lines above, we used the spherical coordinate change $\xi = r\gamma$, $d\xi = r^2 \sin \theta d\theta d\phi dr$. We then make use of radial symmetry in the interior integral. Note e_3 the third vector of the canonical basis of \mathbb{R}^3 and let M be an orthogonal matrix such that $M\gamma_h = e_3$. We perform the change of variable $\gamma' = M\gamma$, using that $MS(0,1) = S(0,1)$ and that the corresponding Jacobian is equal to 1:

(4.26)

$$\int_{S(0,1)} e^{ir|h|\langle \gamma, \gamma_h \rangle} d\Omega = \int_{MS(0,1)} e^{ir|h|\langle M^T \gamma', \gamma_h \rangle} d\Omega'$$

$$(4.27) \quad = \int_{S(0,1)} e^{ir|h|\langle \gamma', M\gamma_h \rangle} d\Omega'$$

$$= \int_{S(0,1)} e^{ir|h|\langle \gamma, e_3 \rangle} d\Omega = 2\pi \int_0^\pi e^{ir|h| \cos(\theta)} \sin(\theta) d\theta$$

$$(4.28) \quad = 2\pi \left[-\frac{e^{ir|h| \cos(\theta)}}{ir|h|} \right]_0^\pi = 2\pi \frac{e^{ir|h|} - e^{-ir|h|}}{ir|h|} = 4\pi \frac{\sin(r|h|)}{r|h|}$$

and thus

$$f_a(h) = 4\pi \int_0^\infty \frac{\cos(ar) \sin(r|h|)}{r|h|} dr = 4\pi \int_0^\infty \frac{\sin((|h|+a)r) + \sin((|h|-a)r)}{2r|h|} dr$$

$$(4.29) \quad = \frac{2\pi}{|h|} \int_0^\infty \frac{\sin(\alpha r)}{r} + \frac{\sin(\beta r)}{r} dr$$

with $\alpha = |h| + a$, $\beta = |h| - a$. Finally, we have the Dirichlet integral

$$(4.30) \quad \int_0^\infty \frac{\sin(\alpha r)}{r} dr = \operatorname{sgn}(\alpha) \frac{\pi}{2}$$

We define the function f_b exactly as f_a , and compute it by replacing a by b in every step above. Putting (4.24), (4.29) and (4.30) together, the inverse Fourier transform of $F_t * F_{t'}$ computed as in equation (4.22) is an absolutely continuous measure with density

$$f(h) = \frac{1}{(2\pi)^3} \frac{1}{2} (f_a(h) - f_b(h))$$

$$= \frac{1}{16\pi|h|} \left(\operatorname{sgn}(|h| + t - t') + \operatorname{sgn}(|h| - t + t') \right.$$

$$(4.31) \quad \left. - \operatorname{sgn}(|h| + t + t') - \operatorname{sgn}(|h| - t - t') \right)$$

$$=: \frac{1}{16\pi|h|} K(|h|, t, t')$$

$K(|h|, t, t')$ is defined in the line above. Note that $K(|h|, -t, t') = -K(|h|, t, t')$ and likewise with t' , thus $K(|h|, t, t') = \operatorname{sgn}(t)\operatorname{sgn}(t')K(|h|, T, T')$ with $T = |t|$, $T' = |t'|$.

Using the symmetries in t and t' in (4.31) and the fact that $\text{sgn}(s) = 1$ if $s > 0$, we obtain

$$\begin{aligned} K(|h|, T, T') &= \text{sgn}(|h| + |T - T'|) + \text{sgn}(|h| - |T - T'|) \\ &\quad - \text{sgn}(|h| + T + T') - \text{sgn}(|h| - T - T') \\ &= 1 + \text{sgn}(|h| - |T - T'|) - 1 - \text{sgn}(|h| - T - T') \\ &= \text{sgn}(|h| - |T - T'|) - \text{sgn}(|h| - T - T') \end{aligned}$$

Therefore,

$$K(|h|, T, T') = \begin{cases} 0 & \text{if } |h| < |T - T'| \\ 2 & \text{if } |T - T'| < |h| < T + T' \\ 0 & \text{if } |h| > T + T' \end{cases} = 2 \times \mathbb{1}_{[|T-T'|, T+T']}(|h|)$$

Identifying the measure $F_t * F_{t'}$ with its density, we have

$$(4.32) \quad (F_t * F_{t'})(h) = \frac{\text{sgn}(t)\text{sgn}(t')}{8\pi|h|} \mathbb{1}_{[||t|-|t'||, |t|+|t'|]}(|h|)$$

□

The proof above makes extensive use of the specificities of the dimension 3. First in equation (4.25), where the scalars r^2 cancel each other out; second in (4.28) where an exact antiderivative of the integrated function can be computed. None of these two simplifications hold in higher dimension or in dimension 2.

Remark 4.2. Note that expression (4.20) with $h = x - x'$ is the covariance kernel of the solution process U with initial condition the “formal” white noise process V^0 with the stationary Dirac delta covariance kernel $k_v(x, x') = \delta_0(x - x')$:

$$(4.33) \quad [(F_t \otimes F_{t'}) * k_v](x, x') = (F_t * F_{t'} * \delta_0)(x - x') = (F_t * F_{t'})(x - x')$$

Somewhat surprisingly, although formula (4.20) yields a summable function over \mathbb{R}^3 when t and t' are fixed, it is not directly usable for practical computations as the diagonal terms of the related covariance matrices are all singularities : $(F_t * F_t)(0) = +\infty \dots$. Yet, formula (4.20) may be used together with explicit kernels k_S to yield usable expressions. For instance, if $k_v(x, x') = k_S(x - x') = C \exp\left(-\frac{|x-x'|^2}{2L^2}\right)$, we state without proof that :

$$(4.34) \quad (F_t * F_{t'} * k_S)(h) = \text{sgn}(tt') \frac{C' L^3}{c^2} \left(\frac{\Phi\left(\frac{R_1+|h|}{L}\right) - \Phi\left(\frac{R_1-|h|}{L}\right)}{2|h|} - \frac{\Phi\left(\frac{R_2+|h|}{L}\right) - \Phi\left(\frac{R_2-|h|}{L}\right)}{2|h|} \right)$$

where $h = x - x'$, $\Phi(s) = \int_{-\infty}^s \frac{\exp(-t^2/2)}{\sqrt{2\pi}} dt$, $R_1 = c||t| - |t'||$, $R_2 = c(|t| + |t'|)$. Such a kernel always takes finite values : when h goes to 0, the above formula reduces to computable finite derivatives.

Although these formulas are interesting in themselves, the study of propagation phenomena is usually done thanks to compactly supported initial conditions, which can never be modelled with a stationary GP. Compactly supported initial conditions are dealt with in subsection 4.4 within the context of radial symmetry.

4.3. Initial Condition Reconstruction and Error control.

4.3.1. *Initial condition reconstruction.* Consider a set of locations $(x_i)_{1 \leq i \leq q}$ and moments $(t_j)_{1 \leq j \leq N}$ (imagine q sensors each collecting an observation at time t_j for all j). Consider now the following inverse problem

$$(4.35) \quad \begin{aligned} &\text{Recover } u_0 \text{ and } v_0 \text{ from the set of observations } \{w(x_i, t_j)\}_{i,j} \\ &\text{where } (w, u_0, v_0) \text{ are subject to (4.1)} \end{aligned}$$

We will see that WIGPR provides an answer to the problem (4.35). This is not surprising because the model described in the previous section was derived under the hypothesis that u_0 and v_0 were unknown.

We first detail some background from the inverse problem community for the problem (4.35). The general problem of reconstructing the initial conditions u_0 and v_0 from some observations of the solution w of (4.1) is known as Photoacoustic Tomography (PAT) ([40], [6]). In the usual inverse problem approach, the solution is accessible over a whole surface $S \subset \mathbb{R}^3$ or an open subset of \mathbb{R}^3 . The initial conditions are recovered from the observations over S thanks to an integral transform such as the Radon transform ([40], [6]). Under certain geometric conditions, the corresponding inverse problem is known to be well-posed ([40]). In real life applications though, only discrete finite dimensional data is available : one then has to discretize the integrals of the inversion step ([6], chapter 3). This means that a sufficiently large amount of sensors is needed for the numerical integration step to yield satisfying results; additionally, the sensors have to be located at specific locations dictated by the numerical integration method used. General Bayesian inversion approaches are also standard for this type of; see the state of the art section for a discussion and references.

We now return to WIGPR. From Proposition 3, we observe that performing GPR on any data with kernel (4.10) automatically produces a prediction \tilde{m} that verifies $\square \tilde{m} = 0$ in the sense of distributions. Therefore this function \tilde{m} is the solution of problem (4.1) for some initial conditions \tilde{u}_0 and \tilde{v}_0 :

$$(4.36) \quad \tilde{m}(x, t) = (F_t * \tilde{v}_0)(x) + (\dot{F}_t * \tilde{u}_0)(x)$$

These initial conditions are simply given by $\tilde{u}_0(x) = \tilde{m}(x, 0)$ and $\tilde{v}_0(x) = \partial_t \tilde{m}(x, 0)$. If the data $(w_1, \dots, w_n)^T$ on which GPR is performed is comprised of observations of a function w that is another solution of problem (4.1), the initial conditions $(\tilde{u}_0, \tilde{v}_0)$ can be understood as approximations of the initial conditions (u_0, v_0) corresponding to w . More precisely, following equation (2.12), we have

$$(4.37) \quad \tilde{m}(x, t) = p_F(w)(x, t) \quad \forall (x, t) \in \mathbb{R}^3 \times \mathbb{R}^+$$

$$(4.38) \quad \tilde{u}_0(x) = \tilde{m}(x, 0) = p_F(w)(x, 0) \quad \forall x \in \mathbb{R}^3$$

$$(4.39) \quad \tilde{v}_0(x) = \partial_t \tilde{m}(x, 0) = \partial_t p_F(w)(x, 0) = p_F(\partial_t w)(x, 0) \quad \forall x \in \mathbb{R}^3$$

where F denotes the finite dimensional space $\text{Span}(k_W(z_1, \cdot), \dots, k_W(z_n, \cdot))$ and p_F is the orthogonal projection on F defined right after equation (2.12). Here, z_m is of the form $z_m = (x_i, t_k) \in \mathbb{R}^4$. We see here that this use of WIGPR provides a flexible framework for tackling the problem (4.35) : the sensors are not constrained in number or location by any integration scheme. Taking a look at equations (4.38) and (4.39), we can quickly discuss the matter of optimal sensor locations for WIGPR. First, we expect that \tilde{m} will provide a better approximation of w when the functions $k_W(z_i, \cdot)_{i=1, \dots, n}$ are as orthogonal as possible in \mathcal{H}_{k_W} since \tilde{m} is an

orthogonal projection on F w.r.t. the \mathcal{H}_{k_W} metric. That is, the following inequality should be required

$$(4.40) \quad \langle k_W((x_i, t_k), \cdot), k_W((x_j, t_l), \cdot) \rangle_{\mathcal{H}_{k_W}} = k_W((x_i, t_k), (x_j, t_l)) \ll 1$$

A close inspection of expressions (4.17) and (4.18) shows that the property (4.40) can be obtained for most times t_k and t_l when the sensors are far apart from each other, as soon as the kernels k_u and k_v are such that $k(x, x') \rightarrow 0$ when $|x - x'| \rightarrow +\infty$ (which is common, see e.g. the kernel (5.1)).

4.3.2. Error Control. Now that we have showed that WIGPR can provide approximations of the initial conditions of (4.1), we underline the fact that these initial condition reconstructions are enough to control the spatial error between the target function u and the Kriging mean \tilde{m} , at all times. Indeed, we have the following L^p control in terms of the initial condition reconstruction error. For $p \in [1, +\infty]$, denote the Sobolev space $W^{1,p}(\mathbb{R}^3) = \{f \in L^p(\mathbb{R}^3) : \forall |k| \leq 1, \partial^k f \in L^p(\mathbb{R}^3)\}$.

Proposition 6. *For any $p \in [1, +\infty]$ and any pair $v_0 \in L^p(\mathbb{R}^3)$, $u_0 \in W^{1,p}(\mathbb{R}^3)$ we have the L^p estimates for all $t \in \mathbb{R}$*

$$(4.41) \quad \|F_t * v_0\|_p \leq |t| \|v_0\|_p$$

$$(4.42) \quad \|\dot{F}_t * u_0\|_p \leq \|u_0\|_p + C_p c |t| \|\nabla u_0\|_p$$

with $C_p = \left(\int_S |\gamma|^p \frac{d\Omega}{4\pi} \right)^{1/p} \leq 3^{1/q} \leq 3, 1/p + 1/q = 1$. Supposing that the correct speed c is known and plugged in k_W , equations (4.41) and (4.42) lead to the following L^p error estimate between the target w and its approximation \tilde{m}

$$(4.43) \quad \|w(\cdot, t) - \tilde{m}(\cdot, t)\|_p \leq |t| \|v_0 - \tilde{v}_0\|_p + \|u_0 - \tilde{u}_0\|_p + C_p c |t| \|\nabla(u_0 - \tilde{u}_0)\|_p$$

where \tilde{u}_0 and \tilde{v}_0 are defined in (4.38) and (4.39).

Equations (4.41) and (4.42) are simple stability estimates for the 3D wave equation, though they do not seem to have been documented in that form in the literature (notably the explicit control constants $|t|$ and $C_p c |t|$). They fall in the category of Strichartz estimates with L^p control for the space variable and L^∞ control for the time variable. We thus provide a proof of the Proposition 6.

Proof. We have

$$(4.44) \quad (F_t * v_0)(x) = t \int_{S(0,1)} v_0(x - c|t|\gamma) \frac{d\Omega}{4\pi}$$

$\frac{d\Omega}{4\pi}$ is the normalized Lebesgue measure on $S(0,1)$. For $p \in [1, +\infty[$, since $t \mapsto t^p$ is convex on \mathbb{R}^+ , Jensen's inequality yields

$$\begin{aligned} \|F_t * v_0\|_p^p &= t^p \int_{\mathbb{R}^3} |(F_t * v_0)(x)|^p dx = |t|^p \int_{\mathbb{R}^3} \left| \int_{S(0,1)} v_0(x - c|t|\gamma) \frac{d\Omega}{4\pi} \right|^p dx \\ &\leq |t|^p \int_{\mathbb{R}^3} \int_{S(0,1)} |v_0(x - c|t|\gamma)|^p \frac{d\Omega}{4\pi} dx = |t|^p \int_{S(0,1)} \int_{\mathbb{R}^3} |v_0(x - c|t|\gamma)|^p dx \frac{d\Omega}{4\pi} \\ &\leq \int_{S(0,1)} \|v_0\|_p^p \frac{d\Omega}{4\pi} = |t|^p \|v_0\|_p^p \end{aligned}$$

Which yields the first estimate. Next,

$$\begin{aligned} (\dot{F}_t * u_0)(x) &= \partial_t(F_t * u_0)(x) = \partial_t \left(t \int_{S(0,1)} u_0(x - c|t|\gamma) \frac{d\Omega}{4\pi} \right) \\ &= \int_{S(0,1)} u_0(x - c|t|\gamma) \frac{d\Omega}{4\pi} + t \int_{S(0,1)} -c\gamma \cdot \nabla u_0(x - c|t|\gamma) \frac{d\Omega}{4\pi} =: I_1(x) + I_2(x) \end{aligned}$$

Functions I_1 and I_2 are defined in the line above. We have $\|\dot{F}_t * u_0\|_p = \|I_1 + I_2\|_p \leq \|I_1\|_p + \|I_2\|_p$. As above, $\|I_1\|_p \leq \|u_0\|_p$. Using again Jensen's inequality,

$$\|I_2\|_p^p = c^p |t|^p \int_{\mathbb{R}^3} \left| \int_{S(0,1)} \gamma \cdot \nabla u_0(x - c|t|\gamma) \frac{d\Omega}{4\pi} \right|^p dx \leq c^p |t|^p \int_{\mathbb{R}^3} \int_{S(0,1)} |\gamma \cdot \nabla u_0(x - c|t|\gamma)|^p \frac{d\Omega}{4\pi} dx$$

Next, we use Hölder's inequality in \mathbb{R}^3 : $|\gamma \cdot \nabla u_0| \leq |\nabla u_0|_p \times |\gamma|_q$ with $\frac{1}{p} + \frac{1}{q} = 1$, where $|v|_p = (|v_1|^p + |v_2|^p + |v_3|^p)^{1/p}$ is the p -norm of $v \in \mathbb{R}^3$ and likewise for $|v|_q$. Thus,

$$\begin{aligned} \|I_2\|_p^p &\leq c^p |t|^p \int_{\mathbb{R}^3} \int_{S(0,1)} |\nabla u_0(x - c|t|\gamma)|_p^p \times |\gamma|_q^p \frac{d\Omega}{4\pi} dx \\ &\leq c^p |t|^p \int_{S(0,1)} |\gamma|_q^p \int_{\mathbb{R}^3} |\nabla u_0(x - c|t|\gamma)|_p^p dx \frac{d\Omega}{4\pi} = c^p |t|^p \left(\int_{S(0,1)} |\gamma|_q^p \frac{d\Omega}{4\pi} \right) \|\nabla u_0\|_p^p \end{aligned}$$

which yields the second estimate. Finally, the case $p = +\infty$ is trivial.

Equation (4.43) is then the result of equations (4.41) and (4.42) applied to the function

$$w(x, t) - \tilde{m}(x, t) = [F_t * (v_0 - \tilde{v}_0)](x) + [\dot{F}_t * (u_0 - \tilde{u}_0)](x)$$

□

Equation (4.43) shows that L^p approximations of the initial conditions provide L^p control between the solution w and the approximation \tilde{m} for any time t . This is why in our numerical applications (Section 5), we only focus on initial condition reconstruction.

When c is unknown and estimated by \hat{c} through maximizing the log marginal likelihood, we have (highlighting the c dependence $F_t^c = \frac{\sigma c |t|}{4\pi c^2 t}$)

$$\begin{aligned} \|w(\cdot, t) - \tilde{m}(\cdot, t)\|_p &= \|F_t^c * u_0 - F_t^{\hat{c}} * \tilde{u}_0 + \dot{F}_t^c * v_0 - \dot{F}_t^{\hat{c}} * \tilde{v}_0\|_p \\ &= \|F_t^c * (u_0 - \tilde{u}_0) + (F_t^c - F_t^{\hat{c}}) * \tilde{u}_0 + \dot{F}_t^c * (v_0 - \tilde{v}_0) + (\dot{F}_t^c - \dot{F}_t^{\hat{c}}) * \tilde{v}_0\|_p \end{aligned}$$

and thus

$$\begin{aligned} (4.45) \quad \|w(\cdot, t) - \tilde{m}(\cdot, t)\|_p &\leq |t| \|v_0 - \tilde{v}_0\|_p + \|u_0 - \tilde{u}_0\|_p + C_p c |t| \|\nabla(u_0 - \tilde{u}_0)\|_p \\ &\quad + \|(F_t^c - F_t^{\hat{c}}) * \tilde{u}_0\|_p + \|(\dot{F}_t^c - \dot{F}_t^{\hat{c}}) * \tilde{v}_0\|_p \end{aligned}$$

The terms with $F_t^c - F_t^{\hat{c}}$ and $\dot{F}_t^c - \dot{F}_t^{\hat{c}}$ may be further controlled in terms of $|c - \hat{c}|$ with additional hypotheses such as Lipschitz continuity of u_0 and v_0 . Likewise, the quantity $\|w(\cdot, t) - \tilde{m}(\cdot, t)\|_p$ may be further controlled if additional hypotheses are made on u_0 and/or v_0 , such as the ones presented in the next section.

4.4. The special case of radial symmetry. Suppose that the trajectories of V^0 have radial symmetry centered on some $x_0 \in \mathbb{R}^3$, which can be expressed in terms of linear operators with the spherical coordinates (r, θ, ϕ) around x_0 :

$$(4.46) \quad \mathbb{P}(\{\omega \in \Omega : \partial_\theta V_\omega^0 = 0\}) = 1 \quad \text{and} \quad \mathbb{P}(\{\omega \in \Omega : \partial_\phi V_\omega^0 = 0\}) = 1$$

Then by Proposition 2, it is equivalent to k_v verifying (in the sense of distributions)

$$\forall x \in \mathcal{D}, \quad \partial_\theta(k_v(x, \cdot)) = 0 \quad \text{and} \quad \partial_\phi(k_v(x, \cdot)) = 0$$

This means that there exists a kernel k_v^0 on \mathbb{R}_+ such that $k_v(x, x') = k_v^0(r^2, r'^2)$. Suppose also that the trajectories of U^0 exhibit radial symmetry : there exists k_u^0 such that $k_u(x, x') = k_u^0(r^2, r'^2)$. Then we have the following “explicit” formulas :

Proposition 7. *Set $K_v(r, r') = \int_0^R \int_0^{r'} k_v^0(s, s') ds ds'$. Then $\forall z = (x, t) \in \mathbb{R}^3 \times \mathbb{R}$, $\forall z' = (x', t') \in \mathbb{R}^3 \times \mathbb{R}$,*

$$(4.47) \quad k_v^{\text{wave}}(z, z') = \frac{\text{sgn}(tt')}{16c^2 rr'} \sum_{\varepsilon, \varepsilon' \in \{-1, 1\}} \varepsilon \varepsilon' K_v((r + \varepsilon c|t|)^2, (r' + \varepsilon' c|t'|)^2)$$

(4.48)

$$k_u^{\text{wave}}(z, z') = \frac{1}{4rr'} \sum_{\varepsilon, \varepsilon' \in \{-1, 1\}} (r + \varepsilon c|t|)(r' + \varepsilon' c|t'|) k_u^0((r + \varepsilon c|t|)^2, (r' + \varepsilon' c|t'|)^2)$$

Proof. Without loss of generality, we suppose that $c = 1$ and $x_0 = 0$. We first derive expression (4.47). Let f be a function defined on \mathbb{R}_+ and g the function defined on \mathbb{R}^3 by $g(x) = f(|x|^2)$. Let F be an antiderivative of f . Recall γ and $d\Omega$ defined in **N.7**. As in (4.26), let M be an orthogonal matrix such that $M(x/|x|) = e_3$ and use the change of variable $\gamma' = M\gamma$. Note that $MS(0, 1) = S(0, 1)$:

$$\begin{aligned} (F_t * g)(x) &= \frac{1}{4\pi t} \int_{S(0,1)} g(x - t\gamma) t^2 d\Omega = \frac{t}{4\pi} \int_{S(0,1)} f(|x - t\gamma|^2) d\Omega \\ &= \frac{t}{4\pi} \int_{S(0,1)} f(|x|^2 + t^2 - 2|t|\langle x, \gamma \rangle) d\Omega \\ &= \frac{t}{4\pi} \int_{MS(0,1)} f(|x|^2 + t^2 - 2|t||x|\langle \frac{x}{|x|}, M^T \gamma' \rangle) d\Omega' \\ &= \frac{t}{4\pi} \int_{S(0,1)} f(|x|^2 + t^2 - 2|t||x|\langle e_3, \gamma \rangle) d\Omega \\ &= \frac{t}{4\pi} \int_{\phi=0}^{2\pi} \int_{\theta=0}^{\pi} f(|x|^2 + t^2 - 2|t||x|\cos(\theta)) \sin(\theta) d\theta d\phi \\ &= \frac{t}{2} \int_{\theta=0}^{\pi} f(|x|^2 + t^2 - 2|t||x|\cos(\theta)) \sin(\theta) d\theta \\ &= \frac{t}{4|x||t|} \left[F(|x|^2 + t^2 - 2|t||x|\cos(\theta)) \right]_{\theta=0}^{\theta=\pi} \\ &= \frac{\text{sgn}(t)}{4|x|} \left(F((|x| + |t|)^2) - F((|x| - |t|)^2) \right) \\ (4.49) \quad &= \frac{\text{sgn}(t)}{4|x|} \sum_{\varepsilon \in \{-1, 1\}} \varepsilon F((|x| + \varepsilon|t|)^2) \end{aligned}$$

First, we note

$$(4.50) \quad k_0^1(r, r') := \int_0^{r'} k_0(r, s) ds \quad \text{and} \quad K_v(r, r') := \int_0^R \int_0^{r'} k(s, s') ds' ds$$

We apply twice result (4.49) on k_v : first by setting $g(x') = k_0(|x - t\gamma|^2, |x'|^2)$ where $x - t\gamma$ is fixed, which integrates to $F(s) = k_0^1(|x - t\gamma|^2, s)$. Second, by setting $g(x) = k_0^1(|x|^2, (|x'| + \varepsilon|t'|)^2)$ where $|x'| + \varepsilon|t'|$ is fixed, which integrates to $F(s) = K_v(s, (|x'| + \varepsilon|t'|)^2)$:

$$(4.51) \quad \begin{aligned} [(F_t \otimes F_{t'}) * k_v](x, x') &= \frac{1}{4\pi t} \frac{1}{4\pi t'} \int_{S(0,1)} \int_{S(0,1)} k_0(|x - t\gamma|^2, |x' - t'\gamma'|^2) t'^2 d\Omega' t^2 d\Omega \\ &= \frac{1}{4\pi t} \frac{\text{sgn}(t')}{4|x'|} \int_{S(0,1)} \sum_{\varepsilon' \in \{-1,1\}} \varepsilon' k_0^1(|x - t\gamma|^2, (|x'| + \varepsilon'|t'|)^2) t'^2 d\Omega \\ &= \frac{\text{sgn}(tt')}{16rr'} \sum_{\varepsilon, \varepsilon' \in \{-1,1\}} \varepsilon \varepsilon' K_v((r + \varepsilon|t|)^2, (r' + \varepsilon'|t'|)^2) \end{aligned}$$

We can then use this result to compute

$$(4.52) \quad [(\dot{F}_t \otimes \dot{F}_{t'}) * k_u](x, x') = \partial_t \partial_{t'} [(F_t \otimes F_{t'}) * k_u](x, x')$$

First, we compute it for $t \neq 0$ and $t' \neq 0$ by derivating (4.51) w.r.t. t and t' , using that for $t \neq 0$, $d|t|/dt = \text{sgn}(t)$ and $d\text{sgn}(t)/dt = 0$. It immediately yields

$$(4.53) \quad [(\dot{F}_t \otimes \dot{F}_{t'}) * k_u](x, x') = \frac{1}{4rr'} \sum_{\varepsilon, \varepsilon' \in \{-1,1\}} (r + \varepsilon|t|)(r' + \varepsilon'|t'|) k_u^0((r + \varepsilon|t|)^2, (r' + \varepsilon'|t'|)^2)$$

For the case where $t = 0$ or $t' = 0$, note from (4.3) that $\mathcal{F}(\dot{F}_0)(\xi) = 1$ and thus $\dot{F}_0 = \delta_0$, the Dirac mass at 0, which is the neutral element for the convolution. Therefore, when we have both $t = 0$ and $t' = 0$:

$$[(\dot{F}_0 \otimes \dot{F}_0) * k_u](x, x') = [(\delta_0 \otimes \delta_0) * k_u](x, x') = [\delta_{(0,0)} * k_u](x, x') = k_u(x, x')$$

which is also the result provided by (4.53) evaluated at $t = t' = 0$. When $t' = 0$ and $t \neq 0$, then we still have $d|t|/dt = \text{sgn}(t)$ and $d\text{sgn}(t)/dt = 0$:

$$\begin{aligned} [(\dot{F}_t \otimes \dot{F}_0) * k_u](x, x') &= [(\dot{F}_t \otimes \delta_0) * k_u](x, x') = \partial_t [(F_t \otimes \delta_0) * k_u](x, x') \\ &= \partial_t \int_{\mathbb{R}^3} \int_{\mathbb{R}^3} k_u^0(|x - y|^2, |x' - y'|^2) F_t(dy) \delta_0(dy') \\ &= \partial_t \frac{1}{4\pi t} \int_{S(0,1)} k_u^0(|x - t\gamma|^2, |x'|^2) t^2 d\Omega \\ &= \partial_t \frac{\text{sgn}(t)}{4r} \sum_{\varepsilon \in \{-1,1\}} \varepsilon k_0^1((r + \varepsilon|t|)^2, |x'|^2) \\ &= \frac{1}{2r} \sum_{\varepsilon \in \{-1,1\}} (r + \varepsilon|t|) k_u^0((r + \varepsilon|t|)^2, |x'|^2) \end{aligned}$$

which is also the result provided by (4.53) evaluated at $t' = 0$. The same arguments apply to show that expression (4.53) is valid when $t = 0$ and $t' \neq 0$. Therefore the expression (4.53) is valid whatever the value of $t, t' \in \mathbb{R}$. \square

Remark 4.3. Note that expressions (4.47) and (4.48) are much faster to compute numerically than (4.9) and (4.8), which require to compute convolutions.

4.4.1. *Compactly supported Initial Conditions and Finite Speed Propagation.* Suppose that v_0 is compactly supported on a ball $B(x_0, R)$. The Strong Huygens Principle for the 3 dimensional wave equation ([27], p.80) states that $F_t * v_0$ is supported on the ring $B(x_0, R + c|t|) \setminus B(x_0, (R - c|t|)_+)$, where $x_+ := \max(0, x)$. From a Gaussian process modelling point of view, supposing that $\text{Supp}(V^0) \subset B(x_0, R)$ amounts to imposing that if $x \notin B(x_0, R)$, then $V^0(x) = 0$ a.s.. This is equivalent to $\text{Var}(V^0(x)) = k_v(x, x) = 0$ since V^0 is supposed centered. The same reasoning in terms of compactly supported initial conditions can be applied to u_0 and $U(z)$. In the next proposition, we explore this possibility by forcing the covariance kernels of U^0 and V^0 to be zero outside of a ball centered on x_0 and identifying the consequences on the formulas (4.47) and (4.48). These formulas are the ones used in section 5.

Proposition 8. *Let $R_v > 0$ and $R_u > 0$. Let $\alpha \in (0, 1)$, $\varphi_\alpha : \mathbb{R}_+ \rightarrow [0, 1]$ be a C^∞ decreasing function such that*

$$\varphi_\alpha(s) = \begin{cases} 1 & \text{if } s < \alpha \\ 0 & \text{if } s \geq 1 \end{cases}$$

Set the truncated kernels

$$(4.54) \quad k_v^{R_v}(x, x') = k_v^{0, R_v}(r^2, r'^2) = k_v^0(r^2, r'^2) \mathbb{1}_{[0, R_v]}(r) \mathbb{1}_{[0, R_v]}(r')$$

$$(4.55) \quad k_u^{R_u}(x, x') = k_u^{0, R_u}(r^2, r'^2) = k_u^0(r^2, r'^2) \varphi(r/R_u) \varphi(r'/R_u)$$

Suppose now that $V^0 \sim GP(0, k_v^{R_v})$ and $U^0 \sim GP(0, k_u^{R_u})$. Then, with $K_v(r, r') = \int_0^R \int_0^{r'} k_v^0(s, s') ds ds'$,

$$(4.56) \quad k_v^{\text{wave}}(z, z') = \frac{\text{sgn}(tt')}{16c^2 r r'} \sum_{\varepsilon, \varepsilon' \in \{-1, 1\}} \varepsilon \varepsilon' K_v \left(\min((r + \varepsilon c|t|)^2, R_v^2), \min((r' + \varepsilon' c|t'|)^2, R_v^2) \right)$$

$$(4.57) \quad k_u^{\text{wave}}(z, z') = \frac{1}{4r r'} \sum_{\varepsilon, \varepsilon' \in \{-1, 1\}} (r + \varepsilon c|t|)(r' + \varepsilon' c|t'|) k_u^{0, R_u}((r + \varepsilon c|t|)^2, (r' + \varepsilon' c|t'|)^2)$$

Proof. When using kernel k_v^{0, R_v} , we can directly use equation (4.47) by substituting K_v with $K_v^{R_v}(r, r') := \int_0^r \int_0^{r'} k_v^{0, R_v}(s, s') ds ds'$ and realizing that for all $r, r' \geq 0$,

$$K_v^{R_v}(r^2, r'^2) := \int_0^{r^2} \int_0^{r'^2} k_v^{0, R_v}(s, s') ds ds' = K_v \left(\min(r^2, R_v^2), \min(r'^2, R_v^2) \right)$$

which directly proves (4.56). Additionally, (4.57) is only a substitution of k_u^0 with k_u^{0, R_u} in (4.48) : all the mathematical steps are justified as $\varphi \in C^\infty(\mathbb{R}_+)$. \square

Remark 4.4. $k_v^{R_v}$ and $k_u^{R_u}$ are the covariance kernels of the truncated processes $V_{\text{trunc}}^0(x) = \mathbb{1}_{[0, R_v]}(|x - x_0|) V^0(x)$ and $U_{\text{trunc}}^0(x) = \varphi(|x - x_0|/R_u) U^0(x)$ respectively. These kernels can never be stationary as their trajectories are compactly supported.

Using equation (4.56), one can then check that $k_v^{\text{wave}}(z, z) = \text{Var}(V(z)) = 0$ as soon as $(r - c|t|)^2 > R_v^2$, ie $V(z) = 0$ a.s. and likewise for k_u^{wave} : this is the expression of the strong Huygens principle on the kernels k_v^{wave} and k_u^{wave} .

Such compactly supported kernels may lead to sparse covariance matrices which may then be used for computational speedups, see section 3.6.

4.4.2. Estimation of physical parameters. The wave kernel (4.10), using for k_u and k_v radially symmetric kernels supported in $B(x_0^u, R_u)$ and $B(x_0^v, R_v)$ respectively, has for hyperparameters

$$\theta = (c, x_0^u, R_u, \theta_{k_u^0}, x_0^v, R_v, \theta_{k_v^0})$$

Among those, $(c, x_0^u, R_u, x_0^v, R_v)$ all correspond to physical parameters that can be estimated via likelihood maximisation. This is numerically investigated in Section 5.

Remark 4.5. Note that finding the correct R_u and R_v is not a well posed problem : if $\text{Supp}(U^0) \subset B(x_0^u, R_u)$ then $\text{Supp}(U^0) \subset B(x_0^u, \alpha R_u)$ for any $\alpha \geq 1$ and αR_u is also a correct solution. This is discussed in Section 5.

4.4.3. Gaussian process regression, radial symmetry and the 1D wave equation. Note that supposing that the initial conditions exhibit radial symmetry reduces Problem (4.1) to the 1D wave equation since for a radially symmetric function f defined on \mathbb{R}^3 , we have $(\Delta_{3D}f)(r) = \frac{1}{r^2}[\partial_{rr}^2(r^2f)](r)$ and thus if w in (4.1) exhibits radial symmetry,

$$\begin{aligned} \square_{3D}w = 0 &\iff \frac{1}{c^2}\partial_{tt}^2w - \Delta_{3D}w = 0 \iff \frac{1}{c^2}\partial_{tt}^2w - \frac{1}{r^2}\partial_{rr}^2(r^2w) = 0 \\ &\iff \frac{1}{c^2}\partial_{tt}^2\tilde{w} - \partial_{rr}^2\tilde{w} = 0 \end{aligned}$$

with $\tilde{w}(r, t) = r^2w(r, t)$. However, the joint problem of approximating the solution w of Problem (4.1) with GPR in presence of radial symmetry *and* searching for the real source location parameters (x_0^u, R_u, x_0^v, R_v) cannot be reduced to the one dimensional case, as the centers x_0^u and x_0^v both belong to \mathbb{R}^3 .

4.5. The Point Source Limit. When studying linear PDEs, the case of the point source is very important. From an application point of view, modelling the source term as a point source (i.e. a Dirac mass) is relevant in a number of real life cases : a localized detonation in acoustics, an electric point source in electromagnetics, a mass point in mechanics, and so forth. From a theoretical point of view, the solution of a linear PDE when the source is a Dirac mass also plays a special role. This solution is called the PDE's Green's function and encodes all of the mathematical properties of the corresponding PDE [23]. In this section, we will not make use of the Kriging equations (2.3) and (2.4) as reconstructing an initial condition that is a point source is actually of little interest. Also, reconstructing the wave equation's Green function thanks to GPR is expected to yield very poor results because this Green's function in particular is extremely irregular; it is not even a function, it is a family of singular measures, see equation (4.4). However, estimating the physical parameters attached to it, essentially the position parameter x_0 , is a relevant question and an attainable goal. This is what we do in this section, by studying the behaviour of the log marginal likelihood that comes with WIGPR when the initial condition reduces to point source. Here, we restrict ourselves to the case $u_0 = 0$ in (4.1) and thus focus on the kernel $k_v^{\text{wave}}(z, z')$. We begin by clarifying the setting in which we will work.

4.5.1. *Setting.*

- Note x_1, \dots, x_q the q sensor locations and suppose we have N time measurements in $[0, T]$ corresponding to times $0 = t_1 < \dots < t_N = T$ for each sensor ; we have overall $n = Nq$ pointwise observations of a function w that is a solution of the problem (4.1). These observations are stored in a vector $w_{\text{obs}} \in \mathbb{R}^{Nq}$.
- We suppose that the initial condition v_0 that corresponds to w is almost a point source : in particular it is supported on a small ball $B(x_0^*, R^*)$ where $R^* \ll 1$.
- We are interested in finding x_0^* , the correct source location. To do so, we study the log marginal likelihood that corresponds to the observations w_{obs} using the following truncated kernel

$$(4.58) \quad k_{\text{nor}, x_0}^{\text{R}}((x, t), (x', t')) = \left(\frac{1}{\frac{4}{3}\pi R^3} \right)^2 [(F_t \otimes F_{t'}) * k_{x_0}^{\text{R}}](x, x')$$

where $k_{x_0}^{\text{R}}(x, x') = k_{\text{v}}(x, x') \mathbb{1}_{B(x_0, R)}(x) \mathbb{1}_{B(x_0, R)}(x')$

The renormalization by the constant $(\frac{4}{3}\pi R^3)^2$ is an anticipation of the upcoming Proposition 9. Note that the kernel $k_{x_0}^{\text{R}}$ corresponds to the kernel (4.54) in Proposition 8, though we do not make any radial symmetry assumption here (in the point source limit, radial symmetry appears by itself anyway). Here, (x_0^*, R^*) denotes the real source position and source size corresponding to the observations w_{obs} while (x_0, R) denotes the position and source size hyperparameter of $k_{\text{nor}, x_0}^{\text{R}}$. We suppose that except for x_0 , all the other hyperparameters θ of $k_{\text{nor}, x_0}^{\text{R}}$ are fixed. In particular, we suppose that the kernel speed c is fixed to the correct speed value c^* ; we also suppose that $R = R^*$ for simplicity.

In that framework, the log-marginal likelihood $p(w_{\text{obs}}|\theta)$ only depends on x_0 . We thus write $K_{x_0} = k_{x_0}^{\text{R}}(X, X)$ and $\mathcal{L}(\theta, \lambda) = \mathcal{L}(x_0, \lambda)$. The log-marginal likelihood then writes

$$(4.59) \quad \mathcal{L}(\theta, \lambda) = \mathcal{L}(x_0, \lambda) = w_{\text{obs}}^T (K_{x_0} + \lambda I_n)^{-1} w_{\text{obs}} + \log \det(K_{x_0} + \lambda I_n)$$

In Figure 1, we provide a 3 dimensional image that shows some numerical values of (4.59) as a function of x_0 on a test case. This figure constitutes visual evidence that in the limit $R \rightarrow 0$, trying to recover a point source location from minimizing the log marginal likelihood provided by the kernel (4.58) reduces to the classic triangulation method used for example in GPS systems. More precisely, we observe three facts. (i) As a function of x_0 , $\mathcal{L}(x_0, \lambda)$ reaches local minima over the whole surface of spheres centered on each sensor. (ii) At the intersection of two of those spheres, the local minima are smaller. (iii) The spheres all intersect at a single point x_0^* , which is the global minima of $\mathcal{L}(x_0, \lambda)$ and the real source location.

Our task now is to explain why we observe such patterns on the Figure 1. In that sense, we begin with a convergence statement to understand what happens in the point source limit from a Gaussian process point of view.

Proposition 9. *Let k be a continuous PD kernel defined on $\mathbb{R}^3 \times \mathbb{R}^3$ and $x_0 \in \mathbb{R}^3$. For $R > 0$, define $k_{x_0}^{\text{R}}$ its truncation around x_0 by*

$$k_{x_0}^{\text{R}}(x, x') = k(x, x') \mathbb{1}_{B(x_0, R)}(x) \mathbb{1}_{B(x_0, R)}(x')$$

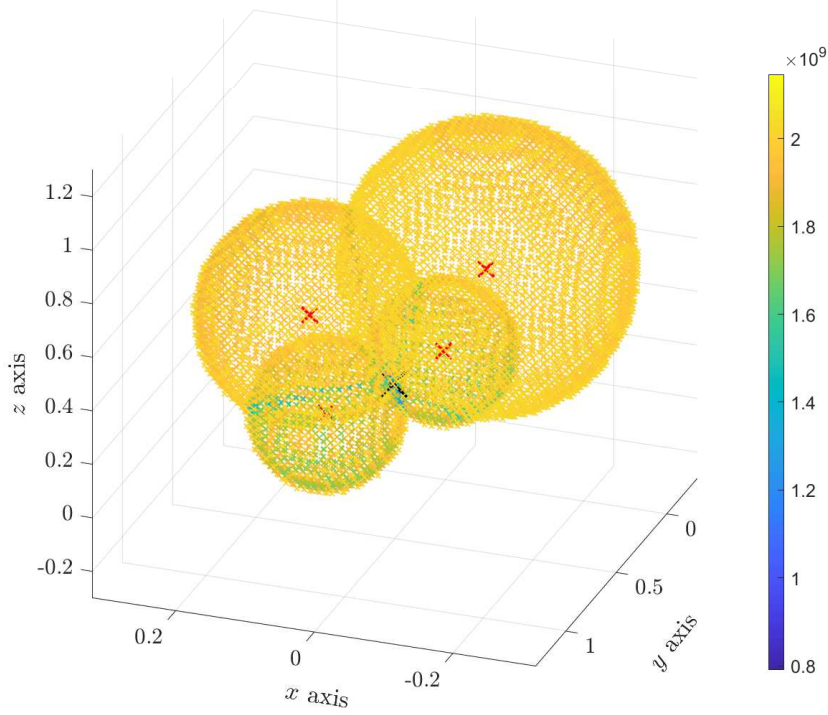


FIGURE 1. Negative log marginal likelihood as a function of $x_0 \in \mathbb{R}^3$. Are only represented values of the negative log marginal likelihood that are below 2.035×10^9 . There only remains thin spherical shells. Red crosses : sensor locations. Black cross : source position. The source is located at the intersection of thin spherical shells centered at the sensor locations.

Let $t, t' \in \mathbb{R}$. Then $(F_t \otimes F_{t'}) * k_{x_0}^R$ defines an absolutely continuous Radon measure over $\mathbb{R}^3 \times \mathbb{R}^3$. Furthermore we have the following weak- \star convergence in the space of Radon measures :

$$(4.60) \quad \frac{1}{\left(\frac{4}{3}\pi R^3\right)^2} [(F_t \otimes F_{t'}) * k_{x_0}^R] \xrightarrow[R \rightarrow 0]{\mathcal{C}_c(\mathbb{R}^3 \times \mathbb{R}^3)'} k(x_0, x_0) \times (\tau_{x_0} F_t) \otimes (\tau_{x_0} F_{t'})$$

where $\tau_x \mu$, the translation of a measure μ by x , is defined by

$$\int f(y) \tau_x \mu(dy) := \int f(x + y) \mu(dy)$$

Proof. First, using equation (4.17), we have

$$(4.61) \quad [(F_t \otimes F_{t'}) * k_{x_0}^R](x, x') = tt' \int_{S(0,1) \times S(0,1)} k_{x_0}^R(x - c|t|\gamma, x' - c|t'|\gamma') \frac{d\Omega d\Omega'}{(4\pi)^2}$$

The integrated function in equation (4.61) is piecewise continuous over $\mathbb{R}^3 \times \mathbb{R}^3$ and the integral in (4.61) is well defined, whatever the values of x and x' . Let f be a continuous compactly supported function on $\mathbb{R}^3 \times \mathbb{R}^3$. We define

$$I_R := \frac{1}{(\frac{4}{3}\pi R^3)^2} \langle (F_t \otimes F_{t'}) * k_{x_0}^R, f \rangle$$

and wish to show that $I_R \rightarrow k(x_0, x_0) \langle \tau_{x_0} F_t \otimes \tau_{x_0} F_{t'}, f \rangle$ when $R \rightarrow 0$. Using equation (4.17), we have

$$\begin{aligned} I_R &= \frac{1}{(\frac{4}{3}\pi R^3)^2} \int_{\mathbb{R}^3 \times \mathbb{R}^3} f(x, x') [(F_t \otimes F_{t'}) * k_{x_0}^R](x, x') dx dx' \\ &= \frac{1}{(\frac{4}{3}\pi R^3)^2} \int_{\mathbb{R}^3 \times \mathbb{R}^3} f(x, x') tt' \int_{S(0,1) \times S(0,1)} k_{x_0}^R(x - c|t|\gamma, x' - c|t'|\gamma') \frac{d\Omega d\Omega'}{(4\pi)^2} dx dx' \\ &= \frac{1}{(\frac{4}{3}\pi R^3)^2} tt' \int_{S(0,1) \times S(0,1)} \int_{\mathbb{R}^3 \times \mathbb{R}^3} \left(f(x, x') k_{x_0}(x - c|t|\gamma, x' - c|t'|\gamma') \right. \\ &\quad \left. \times \mathbb{1}_{[0,R]}(|x - c|t|\gamma - x_0|) \mathbb{1}_{[0,R]}(|x' - c|t'|\gamma' - x_0|) \right) dx dx' \frac{d\Omega d\Omega'}{(4\pi)^2} \end{aligned}$$

The first indicator function restricts the integration domain of x to $B(x_0 + ct\gamma, R)$, and likewise for the second indicator function and x' . In spherical coordinates, write $x = x_0 + ct\gamma + R\rho\gamma_x$ with $\rho \in [0, 1]$ and $\gamma_x \in S(0, 1)$ and likewise for x' .

$$\begin{aligned} I_R &= tt' \int_{S(0,1) \times S(0,1)} \int_{S(0,1) \times S(0,1)} \int_0^1 \int_0^1 \left(f(x_0 + ct\gamma + R\rho\gamma_x, x_0 + c|t'|\gamma' + R\rho'\gamma_{x'}) \right. \\ &\quad \left. \times k(x_0 + R\rho\gamma_x, x_0 + R\rho'\gamma_{x'}) \right) \times 9\rho^2 d\rho\rho'^2 d\rho' \frac{d\Omega_x d\Omega_{x'}}{(4\pi)^2} \frac{d\Omega d\Omega'}{(4\pi)^2} \end{aligned}$$

The integration domain above is a compact subset of \mathbb{R}^{10} . Since f is continuous and k is supposed continuous in the vicinity of (x_0, x_0) , Lebesgue's dominated convergence theorem can be applied when $R \rightarrow 0$, which yields

$$\begin{aligned} I_R &\xrightarrow{R \rightarrow 0} tt' k(x_0, x_0) \int_{S(0,1) \times S(0,1)} f(x_0 + ct\gamma, x_0 + c|t'|\gamma') \frac{d\Omega d\Omega'}{(4\pi)^2} \\ &= k(x_0, x_0) \langle \tau_{x_0} F_t \otimes \tau_{x_0} F_{t'}, f \rangle \end{aligned}$$

□

In the Proposition 9 and as in the propositions 8, the kernel $k_{x_0}^R$ is the covariance kernel of the truncated process $V_{\text{trunc}}^0(x) = \mathbb{1}_{B(x_0, R)}(x) V^0(x)$.

Remark 4.6. We provided above an ad hoc proof of Proposition 9, tailored to the measures F_t and $F_{t'}$. Proposition 9 is actually a consequence of a more general fact, where F_t and $F_{t'}$ are replaced by any Radon measure μ and ν . However, the corresponding proof is much more tedious (though not much more difficult) and the truncation function $\mathbb{1}_{B(x_0, R)}$ should be replaced by a continuous counterpart, to ensure minimal regularity for integrability conditions. Finally, Proposition 9 can also be seen as a weak-* convergence statement of mollifications of $F_t \otimes F_{t'}$ when convolved with k_{nor, x_0}^R , although the authors could not find references in the literature that state such weak-* convergence theorems in the space of Radon measures.

The limit object we obtain by inspecting equation (4.60) is not a function, it is only a measure; and thus it is not a covariance kernel. This means that we do not obtain a Gaussian process in the point source limit. Rather, we obtain a generalized stochastic process in the sense of [9], paragraph 2.2.1.1. This is actually not surprising as the Green function F_t of the wave equation is only a measure. This is another manifestation of the fact that the wave equation exhibits no regularization effect, because of its hyperbolicity. Yet, Proposition 9 provides an entry point for studying the log marginal likelihood (4.59) associated with the kernel (4.58) when R is small. Indeed, Proposition 9 states that for small values of R , the kernel (4.58) behaves like a rank one kernel, i.e. a kernel of the form $k(z, z') = f(z)f(z')$ for some particular function f . We will see that this observation is actually enough to provide mathematical understanding of the patterns observed in Figure 1.

Rather than proving that we can use the tensor shape of the limit object in Proposition 9 even though it is not a function, we prefer to introduce regularized versions of both this limit object and of $\mathcal{L}(x_0, \lambda)$, and study these regularized terms instead. This will be enough to exhibit a limit object that explains the patterns visible on Figure 1. This is done in propositions 10 and 11, which are statements on the regularized log marginal likelihood $\mathcal{L}_{\text{reg}}(x_0, \lambda)$ defined in equation (4.62) rather than on $\mathcal{L}(x_0, \lambda)$. Note however that proving a complete mathematical statement linking the behaviours of $\mathcal{L}(x_0, \lambda)$ and $\mathcal{L}_{\text{reg}}(x_0, \lambda)$ is lacking for the moment.

4.5.2. Regularizing the point source and corresponding approximations. First, we regularize F_t thanks to a mollifier $\varphi(x)$ on \mathbb{R}^3 which we choose to be radially symmetric as in [26], section 4.2.1. Define $\varphi_R(y) = \varphi(y/R)/R^3$, then a \mathcal{C}_c^∞ regularization of F_t is obtained by

$$f_t^R(x) := (F_t * \varphi_R)(x) \quad \forall x \in \mathbb{R}^3$$

As F_t, f_t^R exhibits radial symmetry. We will next use the following approximated objects :

- Note $k_{x_0}^{\text{reg}}((x, t), (x', t')) := f_t^R(x - x_0)f_{t'}^R(x' - x_0)$ a regularized version of the limit object in Proposition 9. Proposition 9 states that in some sense, when R approaches 0, k_{nor, x_0}^R is close to $k_{x_0}^{\text{reg}}$.
- We also assume that $w(x_i, t_j)$ may be approximated by $\tilde{w}(x_i, t_j) = f_{t_j}^R(x_i - x_0^*)$ as in the point source limit, $v_0 = \delta_{x_0^*}$ and in that case we would have $w(x_i, t_j) = (F_{t_j} * v_0)(x_i) = F_{t_j}(x_i - x_0^*)$ (forgetting for a second that F_t is not defined pointwise). We thus introduce the column vector of “approximated observations” $W = (\tilde{w}(x_i, t_j))_{i,j}$ and we suppose that W is ordered in the following way :

$$W = \begin{pmatrix} \overline{W_1} \\ \vdots \\ \overline{W_q} \end{pmatrix}$$

where W_i corresponds to the sensor i : $W_i = (\tilde{w}(x_i, t_1), \dots, \tilde{w}(x_i, t_N))^T$.

These approximated objects enable us to introduce the “regularized” log marginal likelihood built by replacing k with $k_{x_0}^{\text{reg}}$ and w_{obs} by W :

$$(4.62) \quad \mathcal{L}_{\text{reg}}(x_0, \lambda) := W^T (K_{x_0}^{\text{reg}} + \lambda I_n)^{-1} W + \log \det(K_{x_0}^{\text{reg}} + \lambda I_n)$$

with $K_{x_0}^{\text{reg}} = k_{x_0}^{\text{reg}}(X, X)$. Instead of studying $\mathcal{L}(x_0, \lambda)$, we now rather analyse $\mathcal{L}_{\text{reg}}(x_0, \lambda)$; we expect $\mathcal{L}_{\text{reg}}(x_0, \lambda)$ to be close to $\mathcal{L}(x_0, \lambda)$ in some sense, although here we do not state any approximation theorem w.r.t. the approximation of $\mathcal{L}(x_0, \lambda)$ with $\mathcal{L}_{\text{reg}}(x_0, \lambda)$.

Because of the tensor product shape of $k_{x_0}^{\text{reg}}$, $K_{x_0}^{\text{reg}}$ has rank one : $K_{x_0}^{\text{reg}} = F_{x_0} F_{x_0}^T$ with

$$F_{x_0} = \begin{pmatrix} \frac{F_{x_0}^1}{F_{x_0}^q} \\ \vdots \\ \frac{F_{x_0}^q}{F_{x_0}^q} \end{pmatrix}$$

and $F_{x_0}^i = (f_{t_1}^R(x_i - x_0), \dots, f_{t_N}^R(x_i - x_0))^T$. Below, we write a proposition which describes the asymptotic behaviour of $\mathcal{L}_{\text{reg}}(x_0, \lambda)$ in the limit of $\lambda \rightarrow 0$. This limit corresponds to noiseless observations; we will see that the limit object in Proposition 10 provides an explanation of the patterns of Figure 1. We note $\|\cdot\|$ and $\langle \cdot, \cdot \rangle$ the usual Euclidean norm and dot product in \mathbb{R}^n .

Proposition 10 (Asymptotic behaviour of $\mathcal{L}_{\text{reg}}(x_0, \lambda)$ when $\lambda \rightarrow 0$). *Let $\varepsilon > 0$ and $E_\varepsilon := \{x_0 \in \mathbb{R}^3 : \rho(K_{x_0}^{\text{reg}}) > \varepsilon\}$ where $\rho(A)$ denotes the spectral radius of A . Define the correlation coefficient between F_{x_0} and W by $r(x_0) = \text{Corr}(F_{x_0}, W) = \langle F_{x_0}, W \rangle / (\|W\| \times \|F_{x_0}\|) \in [-1, 1]$. We set $r(x_0) = 0$ if $F_{x_0} = 0$.*

Then we have the pointwise convergence

$$\forall x_0 \in \mathbb{R}^3, \quad |\lambda \mathcal{L}_{\text{reg}}(x_0, \lambda) - \|W\|^2 (1 - r(x_0)^2)| = O_{\lambda \rightarrow 0}(\lambda \log \lambda)$$

and the uniform convergence on E_ε

$$\sup_{x_0 \in E_\varepsilon} |\lambda \mathcal{L}_{\text{reg}}(x_0, \lambda) - \|W\|^2 (1 - r(x_0)^2)| = O_{\lambda \rightarrow 0}(\lambda \log \lambda)$$

Proof. Suppose first that $\|F_{x_0}\|^2 = 0$. Then obviously, $r(x_0) = 0$ and $\mathcal{L}_{\text{reg}}(x_0, \lambda) = \|W\|^2 / \lambda + n \log \lambda$ which shows that

$$(4.63) \quad |\lambda \mathcal{L}_{\text{reg}}(x_0, \lambda) - \|W\|^2| = O_{\lambda \rightarrow 0}(\lambda \log \lambda)$$

Now, suppose that $\|F_{x_0}\|^2 > 0$. Let $\varepsilon > 0$ such that $\|F_{x_0}\|^2 \geq \varepsilon$.

We first deal with the first term in (4.62). Using the Sherman–Morrison formula ([55], section 2.7.1), we may invert $(K_{x_0}^{\text{reg}} + \lambda I_n)$ explicitly :

$$(K_{x_0}^{\text{reg}} + \lambda I_n)^{-1} = \frac{1}{\lambda} I_n - \frac{1}{\lambda^2} \frac{F_{x_0} F_{x_0}^T}{1 + \frac{1}{\lambda} F_{x_0}^T F_{x_0}} = \frac{1}{\lambda} \left(I_n - \frac{F_{x_0} F_{x_0}^T}{\lambda + \|F_{x_0}\|^2} \right)$$

One also easily derives the determinant term as $F_{x_0} F_{x_0}^T$ only has one non zero eigenvalue equal to $\|F_{x_0}\|^2$, since $(F_{x_0} F_{x_0}^T) F_{x_0} = F_{x_0} (F_{x_0}^T F_{x_0}) = \|F_{x_0}\|^2 F_{x_0}$:

$$(4.64) \quad \log \det(K_{x_0}^{\text{reg}} + \lambda I_n) = (n-1) \log \lambda + \log \lambda + \|F_{x_0}\|^2$$

(The same argument shows that $\rho(K_{x_0}^{\text{reg}}) = \|F_{x_0}\|^2$.) Thus,

$$\begin{aligned} \mathcal{L}_{\text{reg}}(x_0, \lambda) &= W^T (K_{x_0}^{\text{reg}} + \lambda I_n)^{-1} W + \log \det(K_{x_0}^{\text{reg}} + \lambda I_n) \\ &= \frac{1}{\lambda} \left(\|W\|^2 - \frac{\langle F_{x_0}, W \rangle^2}{\lambda + \|F_{x_0}\|^2} \right) + (n-1) \log \lambda + \log(\lambda + \|F_{x_0}\|^2) \\ (4.65) \quad &= \frac{\|W\|^2}{\lambda} \left(1 - \frac{\langle F_{x_0}, W \rangle^2}{\|W\|^2 (\lambda + \|F_{x_0}\|^2)} \right) + (n-1) \log \lambda + \log(\lambda + \|F_{x_0}\|^2) \end{aligned}$$

and

$$\begin{aligned}
 \lambda \mathcal{L}_{\text{reg}}(x_0, \lambda) - \|W\|^2(1 - r(x_0)^2) \\
 (4.66) \quad &= \|W\|^2 \left(\frac{\langle F_{x_0}, W \rangle^2}{\|W\|^2 \|F_{x_0}\|^2} - \frac{\langle F_{x_0}, W \rangle^2}{\|W\|^2 (\lambda + \|F_{x_0}\|^2)} \right) \\
 &\quad + (n-1)\lambda \log \lambda + \lambda \log(\lambda + \|F_{x_0}\|^2)
 \end{aligned}$$

But for the term in (4.66) that is multiplied by $\|W\|^2$,

$$\begin{aligned}
 \frac{\langle F_{x_0}, W \rangle^2}{\|W\|^2 \|F_{x_0}\|^2} - \frac{\langle F_{x_0}, W \rangle^2}{\|W\|^2 (\lambda + \|F_{x_0}\|^2)} &= \frac{\langle F_{x_0}, W \rangle^2}{\|W\|^2} \left(\frac{1}{\|F_{x_0}\|^2} - \frac{1}{\lambda + \|F_{x_0}\|^2} \right) \\
 &= \frac{\langle F_{x_0}, W \rangle^2}{\|W\|^2} \frac{\lambda}{\|F_{x_0}\|^2 (\lambda + \|F_{x_0}\|^2)} \\
 (4.67) \quad &\leq r(x_0)^2 \frac{\lambda}{\lambda + \|F_{x_0}\|^2} \leq \frac{\lambda}{\|F_{x_0}\|^2} \leq \frac{\lambda}{\varepsilon}
 \end{aligned}$$

and obviously, since $\lambda > 0$,

$$(4.68) \quad \frac{\langle F_{x_0}, W \rangle^2}{\|W\|^2 \|F_{x_0}\|^2} - \frac{\langle F_{x_0}, W \rangle^2}{\|W\|^2 (\lambda + \|F_{x_0}\|^2)} \geq 0$$

Also, one sees that $F_{x_0} = 0$ as soon as $\sup_i |x_0 - x_i| > cT + R$, ie x_0 is too far from the receivers for them to capture non zero signal during the time interval $[0, T]$. Thus the function $x_0 \mapsto \|F_{x_0}\|^2$ is zero outside of a compact set. It is obviously continuous on \mathbb{R}^3 and is thus bounded on \mathbb{R}^3 by some constant $M > 0$. Using this together with (4.67) and (4.68) inside (4.66) and assuming that $\lambda \leq 1$ yields

$$(4.69) \quad |\lambda \mathcal{L}_{\text{reg}}(x_0, \lambda) - \|W\|^2(1 - r(x_0)^2)| \leq \frac{\lambda}{\varepsilon} \|W\|^2 + (n-1)|\lambda \log \lambda| + \lambda \log(M+1)$$

which shows the uniform convergence statement as well as the pointwise one (together with (4.63)). \square

The set E_ε is a set on which all the matrices $K_{x_0}^{\text{reg}}$ are all uniformly large enough in the spectral radius sense.

Remark 4.7. In the proof of Proposition 10, the second term in (4.62) has no influence in the limit object and only pollutes the rate of convergence. Discarding it leads to a $O_{\lambda \rightarrow 0}(\lambda)$ rate of convergence.

It also makes sense to inspect the limiting case $N \rightarrow \infty$, which corresponds to having the sampling frequency of the captors go to infinity. In this case, the discrete objects in Proposition 10 behave as Riemann sums if the time steps t_k are equally spaced; as a result, we obtain integrals in the limit $N \rightarrow \infty$. We state a weak asymptotic behaviour result of $\mathcal{L}_{\text{reg}}(x_0, \lambda)$ in that limit, with a very similar limit object. Highlight the dependence in N in $\mathcal{L}_{\text{reg}}(x_0, \lambda)$ by noting it instead $\mathcal{L}_{\text{reg}}^N(x_0, \lambda)$.

Proposition 11 (Asymptotic behaviour of $\mathcal{L}_{\text{reg}}^N(x_0, \lambda)$ when $N \rightarrow \infty$). *Define the following vector valued functions $L^2([0, T], \mathbb{R}^q)$:*

$$\begin{aligned}
 \forall t \in [0, T], \quad I_u(t) &:= (\tilde{u}(x_1, t), \dots, \tilde{u}(x_q, t))^T \\
 \forall t \in [0, T], \quad I_{x_0}(t) &:= (f_t^R(x_1 - x_0), \dots, f_t^R(x_q - x_0))^T
 \end{aligned}$$

and the scalar valued function

$$(4.70) \quad r_\infty(x_0) := \frac{\langle I_u, I_{x_0} \rangle}{\|I_u\| \|I_{x_0}\|}$$

whenever $\|I_{x_0}\| \neq 0$; in (4.70), the norms and the dot product are those of the usual euclidean structure of $L^2([0, T], \mathbb{R}^q)$. Suppose that for all $k \in \{1, \dots, N\}$, $t_k = T(k-1)/(N-1)$, i.e. the t_k are equally spaced in $[0, T]$.

Then whenever x_0 is such that $\|I_{x_0}\| \neq 0$, we have the following pointwise convergence at x_0

$$(4.71) \quad \frac{\lambda}{N} \mathcal{L}_{\text{reg}}^N(x_0, \lambda) \xrightarrow{N \rightarrow \infty} \|I_u\|_2^2 (1 - r_\infty(x_0)^2) + q \lambda \log \lambda$$

Proof. In all concerned mathematical objects, we highlight the N dependency with an exponent, i.e. W^N , $F_{x_0}^N$, etc. We use the exact same tool as in the previous proof, namely that we have

$$\mathcal{L}_{\text{reg}}^N(x_0, \lambda) = \frac{\|W^N\|^2}{\lambda} \left(1 - \frac{\langle F_{x_0}^N, W^N \rangle^2}{\|W^N\|^2 (\lambda + \|F_{x_0}^N\|^2)} \right) + (n-1) \log \lambda + \log(\lambda + \|F_{x_0}^N\|^2)$$

But

- $\|W^N\|^2 = \sum_{i=1}^q \sum_{k=1}^N \tilde{u}(x_i, t_k)^2$
- $\|F_{x_0}^N\|^2 = \sum_{i=1}^q \sum_{k=1}^N f_{t_k}^R(x_i - x_0)^2$
- $\langle F_{x_0}^N, W^N \rangle = \sum_{i=1}^q \sum_{k=1}^N f_{t_k}^R(x_i - x_0) \tilde{u}(x_i, t_k)$

Since the time steps are equally spaced, we can study the limit $N \rightarrow \infty$ of the above objects thanks to Riemann sums. When $N \rightarrow \infty$,

$$(4.72) \quad \frac{1}{N} \|W^N\|^2 \longrightarrow \sum_{i=1}^q \int_0^T \tilde{u}(x_i, t)^2 dt = \|I_u\|^2$$

$$(4.73) \quad \frac{1}{N} \|F_{x_0}^N\|^2 \longrightarrow \sum_{i=1}^q \int_0^T f_t(x_i - x_0)^2 dt = \|I_{x_0}\|^2$$

$$(4.74) \quad \frac{1}{N} \langle W^N, F_{x_0}^N \rangle \longrightarrow \sum_{i=1}^q \int_0^T \tilde{u}(x_i, t) f_t(x_i - x_0) dt = \langle I_u, I_{x_0} \rangle$$

Suppose that x_0 is such that $\|I_{x_0}\| \neq 0$, then because of (4.73), the quantity $\|F_{x_0}^N\|$ is bounded from below by $\|I_{x_0}\|/2$ for sufficiently large N . We then have the following convergence

$$(4.75) \quad \frac{\langle F_{x_0}^N, W^N \rangle^2}{\|W^N\|^2 (\lambda + \|F_{x_0}^N\|^2)} = \frac{(\frac{1}{N} \langle F_{x_0}^N, W^N \rangle)^2}{\frac{1}{N} \|W^N\|^2 (\frac{\lambda}{N} + \frac{1}{N} \|F_{x_0}^N\|^2)} \xrightarrow{N \rightarrow \infty} r_\infty(x_0)$$

Likewise, since $n = qN$, when $N \rightarrow \infty$:

$$(4.76) \quad \begin{aligned} & \frac{(n-1) \log \lambda}{N} + \frac{1}{N} \log(\lambda + \|F_{x_0}^N\|^2) \\ &= \frac{(Nq-1) \log \lambda}{N} + \frac{\log N}{N} + \frac{1}{N} \log \left(\frac{\lambda}{N} + \frac{1}{N} \|F_{x_0}^N\|^2 \right) \xrightarrow{N \rightarrow \infty} q \log \lambda \end{aligned}$$

which shows the announced result. \square

Remark 4.8. One could surely obtain better rates of convergence in Proposition 11 using basic convergence results for Riemann sums and regularity assumptions, but we restrict ourselves to a $o_{N \rightarrow \infty}(1)$ convergence to avoid further technicalities.

4.5.3. *Discussion : why do we observe that the actual source position is located at the intersection of spheres centered on receivers in Figure 1 ?*

The answer can be found by analysing the limit term in proposition 10 (or the one in Proposition 11). Note $L(x_0)$ the said limit object from Proposition 10 :

$$(4.77) \quad L(x_0) = \|W\|^2(1 - r(x_0)^2) = \|W\|^2 \left(1 - \frac{\text{Big}(\sum_{i=1}^q \langle F_{x_0}^i, W_i \rangle)^2}{\|W\|^2 \|F_{x_0}\|^2} \right)$$

Note T_i the time of arrival of the point source wave at sensor i : $|x_i - x_0^*| = c^* T_i$. Define also the sphere S_i centered on x_i and the thin spherical shell A_i of thickness $2R$ that surrounds it

$$(4.78) \quad S_i := S(x_i, cT_i)$$

$$(4.79) \quad A_i := A(x_i, cT_i - R, cT_i + R) = \overline{B(x_0, cT_i + R)} \setminus B(x_0, cT_i - R)$$

(i) $L(x_0)$ reaches a local minima over the whole sphere S_i . When x_0 is located inside A_i , the subvectors W_i and $F_{x_0}^i$ of W and F_{x_0} respectively become almost colinear because f_t^R is radially symmetric. They become exactly colinear when $x_0 \in S_i$. This maximizes the term $\langle F_i, W_i \rangle$ in virtue of the Cauchy-Schwarz inequality. When x_0 lies on one and only one of those spherical shells A_i , the other terms $\langle F_j, W_j \rangle$ are all zero.

(ii) The local minima of $L(x_0)$ located at the intersection of 2 or more spheres S_i are smaller. More generally, when I is a subset of $\{1, \dots, n\}$ and when $x_0 \in \bigcap_{i \in I} A_i \setminus \bigcap_{j \notin I} A_j$, the term $\sum_{i \in I} \langle F_i, W_i \rangle$ is (almost) maximized while $\sum_{j \notin I} \langle F_j, W_j \rangle = 0$, which explains why the intersection of spheres are darker coloured than the other parts of the spheres in Figure 1.

(iii) The spheres S_i intersect at a single point, which is exactly x_0^* as well as the global minima of $L(x_0)$. The quantity $r(x_0)$ reaches a global maximum when all subvectors W_i and $F_{x_0}^i$ are colinear, which is the case only when $x_0 \in \bigcap_i S_i$. When there are at least 4 sensors, the intersection of all the spheres $\bigcap_i S_i$ is reduced to at most one point. Recall that we have supposed that $c = c^*$: this implies that $x_0^* \in \bigcap_i S_i$, and thus the minimum of $L(x_0)$ is located at $x_0 = x_0^*$.

Note that if the speed c in $k_{x_0}^R$ does not correspond to the real speed c^* , the intersection $\bigcap_i S_i$ will be empty. Additionally, from an optimization point of view, numerically solving $\inf_{x_0} \mathcal{L}(x_0, \lambda)$ is obviously highly non convex and none of our numerical experiments lead to the correct solution.

4.6. Computational Speedups. In the Kriging formulas (2.3) and (2.4) as well as in the log marginal likelihood equation (2.9), we are interested in inverting matrices of the form $K + \lambda I$ where K is positive semidefinite. Using basic algebra, we show an exact computational shortcut to computing $(K + \lambda I)^{-1}$ when K has null lines, which is typically the case when using kernels (4.56) because of finite speed propagation. It may provide huge computational speedups in the limit of small source size as is the case in the previous subsection.

4.6.1. Inversion shortcut for Tichonov-regularized PSD matrices with null columns.

Let K be a symmetric semi-positive definite matrix of size n . Suppose it has p non zero columns i_1, \dots, i_p and $q = n - p$ zero columns i_{p+1}, \dots, i_n . Since K is symmetric, its lines i_1, \dots, i_p are also zero. Finally, a simple necessary and sufficient condition for its column j to be zero is $K_{jj} = 0$ because of the Cauchy-Schwarz inequality for PSD matrices : $|a_{ij}| \leq \sqrt{a_{ii}}\sqrt{a_{jj}}$. Define the matrix \tilde{K} of the extracted non-zero columns of K , of size $p \times p$ by $\tilde{K}_{k,l} = K_{i_k,i_l} \forall k, l \in \{1, \dots, p\}$. Note $\mathcal{E} = (e_1, \dots, e_n)$ the canonical basis of \mathbb{R}^n and $\mathcal{F} = (e_{i_1}, \dots, e_{i_n})$ a permutation according to the indexes i_1, \dots, i_p and i_{p+1}, \dots, i_n defined above (that permutation is unique up to additional permutations of the null columns of K). Then for the orthogonal permutation matrix P such that

$$(4.80) \quad \forall k \in \{1, \dots, n\}, \quad Pe_k = e_{i_k}$$

we have

$$(4.81) \quad K = P^T \times \left(\begin{array}{c|c} \tilde{K} & 0_{p,q} \\ \hline 0_{q,p} & 0_{q,q} \end{array} \right) \times P$$

Then we have blockwise,

$$(4.82) \quad (K + \lambda I_n)^{-1} = P^T \times \left(\begin{array}{c|c} (\tilde{K} + \lambda I_p)^{-1} & 0_{p,q} \\ \hline 0_{q,p} & \frac{1}{\lambda} I_q \end{array} \right) \times P$$

Note that matrix P is easy to find as one only has to compute the diagonal elements of K in order to find the null lines/columns of K , since K is PSD. That is, we only need to invert a $p \times p$ matrix. For a in \mathbb{R}^n , define $a_{in} \in \mathbb{R}^p$ the first p components of Pa and $a_{out} \in \mathbb{R}^{n-p}$ the last $n - p$ components of Pa , ie

$$(4.83) \quad Pa = \begin{pmatrix} (Pa)_1 \\ \vdots \\ (Pa)_p \\ (Pa)_{p+1} \\ \vdots \\ (Pa)_n \end{pmatrix} = \begin{pmatrix} a_{in} \\ a_{out} \end{pmatrix}$$

Using (4.82) and (4.83), we have immediately that

$$(4.84) \quad a^T (K + \lambda I_n)^{-1} a = a_{in}^T (\tilde{K} + \lambda I_p)^{-1} a_{in} + \frac{1}{\lambda} \|a_{out}\|^2$$

In the term $a^T (K + \lambda I_n)^{-1} a$, a_{in} corresponds to the coordinates of a that are "kept" by the non zero elements of K and a_{out} corresponds to those that are left out by the non zero elements of K .

4.6.2. Computational shortcuts for Kriging. We may now use the previous section to speed up GPR computations when using a covariance kernel k_θ . This is summarized in Proposition 12 in which we use the following notations.

- Note $X = (x_1, \dots, x_n)^T \in \mathbb{R}^n$ the observation locations, $Y \in \mathbb{R}^n$ the vector of observations ($Y_i = u(x_i)$ for noiseless observations).
- Note $K_\theta := k_\theta(X, X)$ the associated covariance matrix, P_θ and \tilde{K}_θ the matrices P and \tilde{K} defined by (4.80) for $K = K_\theta$, p_θ the number of non zero columns of K_θ and $q_\theta = n - p_\theta$.

- As in (4.83), note X_{in}^θ the first p_θ coordinates of $P_\theta X$ and X_{out}^θ the q_θ last, and likewise for Y_{in}^θ and Y_{out}^θ .

Plugging equation (4.82) in the log-marginal likelihood and Kriging formulas, we obtain Proposition 12.

Proposition 12. *If using a covariance kernel k_θ with hyperparameter θ for GPR, we have the following exact computational shortcuts.*

(i) *For the log-marginal likelihood,*

$$(4.85) \quad \begin{aligned} \mathcal{L}(\theta, \lambda) &= (Y_{in}^\theta)^T (\tilde{K}_\theta + \lambda I_{p_\theta})^{-1} Y_{in}^\theta \\ &\quad + \frac{1}{\lambda} \|Y_{out}^\theta\|^2 + \log \det(\tilde{K}_\theta + \lambda I_{p_\theta}) + q_\theta \log \lambda \end{aligned}$$

(ii) *For the Kriging formulas,*

$$(4.86) \quad \begin{cases} \tilde{m}(x) &= m(x) + k_\theta(X_{in}^\theta, x)^T (\tilde{K}_\theta + \lambda I_{p_\theta})^{-1} (Y_{in}^\theta - m(X_{in}^\theta)) \\ (4.87) \quad \tilde{k}(x, x') &= k_\theta(x, x') - k_\theta(X_{in}^\theta, x)^T (\tilde{K}_\theta + \lambda I_{p_\theta})^{-1} k_\theta(X_{in}^\theta, x') \end{cases}$$

(iii) *if $k_\theta(x, x) = 0$ then $\tilde{m}(x) = m(x)$ and $\tilde{k}(x, x') = 0$.*

Proof. As in equation (4.84), we have immediately that

$$(4.88) \quad Y^T (K_\theta + \lambda I_n)^{-1} Y = (Y_{in}^\theta)^T (\tilde{K}_\theta + \lambda I_{p_\theta})^{-1} Y_{in}^\theta + \frac{1}{\lambda} \|Y_{out}^\theta\|^2$$

It is also obvious from (4.81) that $\log \det(K_\theta + \lambda I_n) = \log \det(\tilde{K}_\theta + \lambda I_{p_\theta}) + q_\theta \log \lambda$, which proves (4.85).

For the Kriging equations, suppose without loss of generality that $m \equiv 0$. The Kriging mean is, as in (4.84),

$$(4.89) \quad \begin{aligned} \tilde{m}(x) &= k(X, x)^T (K + \lambda I_n)^{-1} Y \\ &= k(X_{in}^\theta, x)^T (\tilde{K}_\theta + \lambda I_{p_\theta})^{-1} Y_{in}^\theta + \frac{1}{\lambda} k(X_{out}^\theta, x)^T Y_{out}^\theta \end{aligned}$$

Now, suppose that the observation location x_i is such that $k_\theta(x_i, x_i) = (K_\theta)_{ii} = 0$, which is exactly the case of all the coordinates of X_{out}^θ (by definition). Then from the Cauchy-Schwarz inequality (2.2), the function $x \mapsto k(x, x_i)$ is identically zero. Thus for all x , we have $k(X_{out}^\theta, x)^T Y_{out}^\theta = 0$ which, when plugged in (4.89), proves (4.86). The exact same reasoning leads to (4.87). Finally, for the same reason, if $k_\theta(x, x) = 0$ then the vector $k_\theta(X_{in}^\theta, x)$ is null, which implies that $\tilde{m}(x) = 0$. \square

We remind that formulas (4.85), (4.86) and (4.87) are exact. There are actually three shortcuts for the Kriging equations (4.86) and (4.87). First, the fast matrix inversion, which is especially useful during the log marginal likelihood optimization step (hyperparameter calibration). Second, the selection of the pertinent data points in $k_\theta(X_{in}^\theta, x)$ by using X_{in} instead of X . Third, the selection of the pertinent evaluation points thanks to the point (iii) of Proposition 12. These last two are useful when \tilde{m} and/or \tilde{k} have to be evaluated many times. Note also that all the mathematical objects on the right-hand side of equations (4.85), (4.86) and (4.87) depend on θ and have to be recomputed for each new value of θ . However this is fast since checking which columns of K_θ are zero only requires to compute the diagonal of K_θ : this requires n calls to k_θ .

Remark 4.9. In equation (4.85), the term $\frac{1}{\lambda} \|Y_{out}^\theta\|^2$ can be understood as a very heavy penalization term that sanctions non zero observations that do not lie in the support of k_θ . When applying this to kernel (4.10), the term $\frac{1}{\lambda} \|Y_{out}^\theta\|^2$ penalizes the non zero observations that do not lie in the space time domain (aka light cone) allowed by Huygens' principle.

4.6.3. *Expected numerical gain when using the truncated wave kernel (4.10).*

In this case, to examine if a point (x, t) is such that $k_\theta((x, t), (x, t)) = 0$, one only needs to check that (x, t) lies in the light cone that corresponds to θ (among others, θ contains (x_0, R, c)). Explicitly, the condition to check is whether or not $x \in B(x_0, c|t| + R) \setminus B(x_0, (c|t| - R)_+)$ or equivalently, $c|t| - R \leq |x - x_0| \leq c|t| + R$. This is actually much cheaper than evaluating $k_\theta((x, t), (x, t))$.

For the log-marginal likelihood : using Cholesky decomposition to invert $\tilde{K}_\theta + \lambda I_{p_\theta}$, only $p_\theta^3/3$ flops are required versus $n^3/3$ previously (in both cases, the computation of the determinant term in (4.85) is immediate from the Cholesky decomposition).

For the Kriging formulas : here we suppose that we are performing GPR using the truncated wave kernel (4.10). Suppose that the hyperparameter vector θ has been previously estimated : in particular, it provides estimated wave speed c , radius R and source position x_0 . Now, equation (4.86) states that

$$(4.90) \quad \tilde{m}(x, t) = \sum_{i=1}^{p_\theta} a_i k_\theta((x, t), (X_{in}^\theta)_i)$$

for some fixed real numbers a_1, \dots, a_{p_θ} . Suppose that we want to compute $\tilde{m}(x, t)$ over a cubic spatial grid $[0, L]^3$ of side length L at a fixed time t . Suppose that the space step Δx of this grid verifies $\Delta x \ll L$: then the number of grid points inside a volume V is approximately $V/\Delta x^3$ (each grid point occupies a cubic volume of Δx^3). In compliance with the strong Huygens principle, computing $\tilde{m}(x, t)$ over the whole grid using Proposition 12 results in N_θ calls to k , with

$$(4.91) \quad N_\theta \simeq p_\theta \times \frac{\text{Vol}\left([B(x_0, ct + R) \setminus B(x_0, (ct - R)_+)] \cap [0, L]^3\right)}{\Delta x^3}$$

The set $B(x_0, ct + R) \setminus B(x_0, (ct - R)_+)$ corresponds to the admissible domain allowed by the strong Huygens principle at time t . This is to be compared to $N_{\text{full}} = n \times L^3/\Delta x^3$, the number of calls to k needed without using Proposition 12; obviously, $N_\theta < N_{\text{full}}$ and actually, $N_\theta \ll N_{\text{full}}$ when R is small. More precise estimations of the number of grid points inside the volume in equation (4.91) can be derived, though this is a difficult research topic in itself : see for instance [7] or the Gauss circle problem for its 2D counterpart. Also, the volume appearing in (4.91) can be explicitly derived but we consider the additional insights this provides to be negligible.

5. NUMERICAL EXPERIMENTS

In this section, we showcase WIGPR on functions w that are solutions of problem (4.1), using kernels (4.47) and (4.48) separately as well as together as in (4.10).

The goal is twofold : reconstructing the target function w , which amounts to reconstructing its initial conditions, and estimating the physical parameters attached. Note that with badly estimated physical parameters, the reconstruction step is more or less bound to fail, especially with inaccurate wave speed c and/or source centers x_0^u and x_0^v . Throughout this section, we only consider compactly supported and radially symmetric initial conditions, for which we can use the formulas (4.56) and (4.57).

At the end of this section, we also briefly show that perfect transparent boundary conditions are automatically enforced on the numerical reconstructions of w provided by WIGPR. This is true simply because the Kriging means provided by WIGPR are built to be exact solutions of the free space problem (4.1). Transparent boundary conditions are a well known research topic in the numerical analysis community ([11], [24], [35], [39]), which arises from the need to numerically simulate free space (unbounded) PDE problems on numerical simulation domains that are inherently finite.

5.1. General test protocol for WIGPR.

5.1.1. *Test cases.* Three general test cases for WIGPR are considered here. They correspond to different initial conditions (u_0, v_0) :

- (1) A test case for k_u^{wave} described in Subsection 5.2, for which $v_0 = 0$.
- (2) A test case for k_v^{wave} described in Subsection 5.3, for which $u_0 = 0$.
- (3) A test case for $k_u^{\text{wave}} + k_v^{\text{wave}}$ described in Subsection 5.4 using both of the non zero initial conditions of the two previous test cases.

For each test case, the complete procedure described below is performed.

5.1.2. *Numerical simulation.* Given initial conditions u_0 and v_0 , we numerically simulate the solution w over a given time period. We use a basic two step explicit finite difference time domain (FDTD) numerical scheme for the wave equation as described in [10], equation A.24, over the cube $[0, 1]^3$. The space unit is the meter (each side is $L = 1$ meter), the time unit is the second. We also use second order Engquist-Majda transparent boundary conditions [24]. The simulation parameters are as follows. We use a sample rate $SR = 200$ Hz (time step $\Delta t = 1/200$ s), a space step $\Delta x = 43$ mm, a wave speed $c = 0.5$ m/s. The simulation duration is $T = 1.5$ s $= 0.75$ L/c .

5.1.3. *Database generation.* 30 sensors are scattered in the cube $[0.2, 0.8]^3$ using a Latin hypercube repartition and a minimax space filling algorithm. Signal outputs correspond to time series for each sensor, with a sample rate of 50 Hz, so 75 data points altogether equally spanned over the interval $[0, 1.5]$ s for each sensor, which leads to $30 \times 75 = 2250$ observations. Each signal is then artificially polluted by a centered Gaussian white noise with standard deviation $\sigma_{\text{noise}} = 0.09$. This value corresponds to around 10% of the maximal amplitude of the signals, see Figures 2, 4 and 6.

5.1.4. *WIGPR.* We perform WIGPR on (portions of) the dataset obtained above, using the kergp package [21] from R [57]. For that we use kernels (4.56) and/or (4.57) which are “fast” to evaluate, with K_v and k_u^0 both 1D 5/2–Matérn kernels.

This Matérn kernel is stationary and writes, in term of the increment $h = x - x'$,

$$(5.1) \quad k_{5/2}(h) = \sigma^2 \left(1 + \frac{|h|}{\rho} + \frac{h^2}{3\rho^2} \right) \exp \left(-\frac{|h|}{\rho} \right)$$

It has two additional hyperparameters : ρ and σ^2 . ρ is the length scale of the kernel (5.1) and should correspond to the typical variation length scale of the function approximated with GPR. σ^2 is the variance of the kernel. We tackle two different questions related to WIGPR.

- (Q₁) We study how well the physical parameters (propagation speed c , source position x_0 and size R) can be estimated with WIGPR. For this, we first select N_s time series corresponding to the first N_s sensors with $N_s \in \{1, 2, 3, 4, 5, 6, 8, 10, 15, 20, 25, 30\}$. The corresponding database encompasses $75 \times N_s$ data points. For this database, we perform negative log marginal likelihood minimization to estimate the corresponding hyperparameters, which are either

$$\theta = \begin{cases} (x_0^a, R_a, \theta_{k_a^0}, c, \lambda) \in \mathbb{R}^8, a \in \{u, v\}, & \text{if } v_0 = 0 \text{ or } u_0 = 0 \\ (x_0^u, R_u, \theta_{k_u^0}, x_0^v, R_v, \theta_{k_v^0}, c, \lambda) \in \mathbb{R}^{14} & \text{if } v_0 \neq 0 \text{ and } u_0 \neq 0 \end{cases}$$

λ corresponds to σ^2 in (2.9), and is viewed as an additional hyperparameter in the log marginal likelihood. We use a COBYLA optimization algorithm to solve (2.5) and a multistart procedure with $n_{mult} = 100$ different starting points. That is, 100 different values of θ_0 are scattered over an hypercube $H \subset \mathbb{R}^8$ or $H \subset \mathbb{R}^{14}$, and the COBYLA log marginal likelihood optimization procedure is run using each value of θ_0 as a starting point. Among all the obtained results, the hyperparameter value that provides the maximal log marginal likelihood is selected. The multistart procedure mitigates the risk of getting stuck in local maxima. COBYLA is a gradient-free optimization method used in kergp and available in the `nloptr` package from R. We then reconstruct the initial conditions using WIGPR.

- (Q₂) We study the sensibility of the reconstruction step w.r.t. the sensor locations. Consider 40 different Latin hypercube layouts of the 30 sensors, each obtained with a minimax space filling algorithm. For each layout, we provide the correct hyperparameter values to the model; these values are described in each test case. We then reconstruct the initial conditions using GPR and N_s sensors, with $N_s \in \{1, 5, 10, 15, 20, 25, 30\}$. L^p relative errors (see equation (5.2)) are computed between the reconstructed initial condition and the real initial condition, and for each number of sensors N_s , statistics over the 40 different datasets for these L^p errors are summarized in boxplots.

In both cases, the approximated initial position \tilde{u}_0 is recovered by evaluating the WIGPR Kriging mean at $t = 0$ over a 3D grid and the initial speed \tilde{v}_0 is recovered by evaluating the Kriging mean at $t = 0$ and $t = dt = 10^{-7}$ over the same 3D grid: $\tilde{v}_0 \simeq (\tilde{m}(\cdot, dt) - \tilde{m}(\cdot, 0))/dt$ with $dt = 10^{-7}$.

5.1.5. *Result visualization.* For each test case are provided an example of captured data (observation points), for one particular design of experiment (out of 40) for 6 sensors (out of 30). This displayed data takes the form of a sequence of 6 time series (Figures 2, 4 and 6). For each test case, an example of initial condition reconstruction achieved thanks to WIGPR is also showcased. These examples take

the form of a slice of the corresponding 3D functions evaluated on some plane $z = Cst$. Figures are obtained with MATLAB [47].

5.1.6. Numerical indicators. Precise numerical results are displayed in appendix A; they are as follows.

For (Q_1) are plotted the distances between the correct physical parameters and the estimated ones, depending on the number of sensors used. Additionally, for every $p \in \{1, 2, \infty\}$ are plotted relative L^p errors $e_{p,rel}$ defined below depending on the number of sensors used.

$$(5.2) \quad e_{p,rel}^u = \frac{\|u_0 - \tilde{u}_0\|_p}{\|u_0\|_p} \quad \text{and} \quad e_{p,rel}^v = \frac{\|v_0 - \tilde{v}_0\|_p}{\|v_0\|_p}$$

A relative error of 50% means that $\|u_0 - \tilde{u}_0\|_p = 0.5\|u_0\|_p$. A relative error of over 100% means that $\|u_0 - \tilde{u}_0\|_p \geq \|u_0\|_p$, in which case the null estimator $\hat{u}_0 = 0$ performs better than the estimator \tilde{u}_0 provided by WIGPR. Note that obtaining a small L^p relative error is harder when the target function has a small L^p norm.

For (Q_2) are plotted boxplots of the relative L^p errors over the 40 different sensor layouts, depending on the number of sensors used.

Integrals for the L^p error plots are approximated using Riemann sums over a 3D grid with space step $dx = 0.01$.

5.2. Test case for k_u^{wave} . In this test case, v_0 is assumed null and thus we set $k_v = 0$, which yields $k_v^{\text{wave}} = 0$. We thus use k_u^{wave} defined in (4.57) for GPR. We use the 1D Matérn kernel (5.1) for k_u^0 in equation (4.57). The initial condition u_0 is a radial raised cosine described as follows. Set $x_0 = (0.65, 0.3, 0.5)^T$, $R = 0.25$ and $A = 5$, the corresponding initial conditions (IC) are given by :

$$\begin{cases} u_0(x) &= A \mathbb{1}_{[0,R]}(|x - x_0|) \left(1 + \cos \left(\frac{\pi|x - x_0|}{R} \right) \right) \\ v_0(x) &= 0 \end{cases}$$

See Figure 3, left column, for a graphical representation. For problem (Q_1) , the optimization domain is chosen to be the following hypercube

$$(5.3) \quad \theta = (x_0, R, \rho, \sigma^2, c, \lambda) \in [0, 1]^3 \times [0.03, 0.5] \times [0.02, 2] \times [0.1, 5] \times [0.2, 0.8] \times [10^{-8}, 10^{-2}]$$

For problem (Q_2) , the hyperparameter θ_0 provided to the model is

$$(5.4) \quad \theta_0 = (x_0, R, (\rho, \sigma^2), c, \lambda) = ((0.65, 0.3, 0.5), 0.3, (0.2, 3), 0.5, \sigma_{noise}^2)$$

with $\sigma_{noise}^2 = 0.0081$. The value of 0.2 provided for ρ is a visual estimation of the length scale of u_0 based on Figure 3. Additionally, the couple $(0.2, 3)$ provided for (ρ, σ^2) is more or less confirmed by the estimations of (ρ, σ^2) performed for problem (Q_1) , test case#1, visible in Table 1.

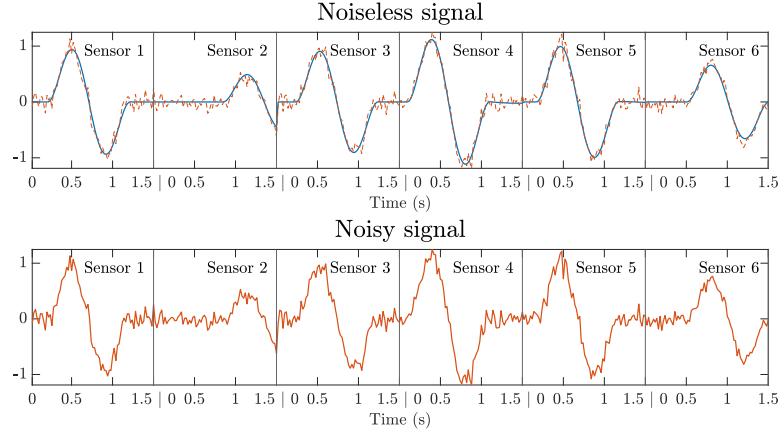


FIGURE 2. Example of captured signals for the test case #1

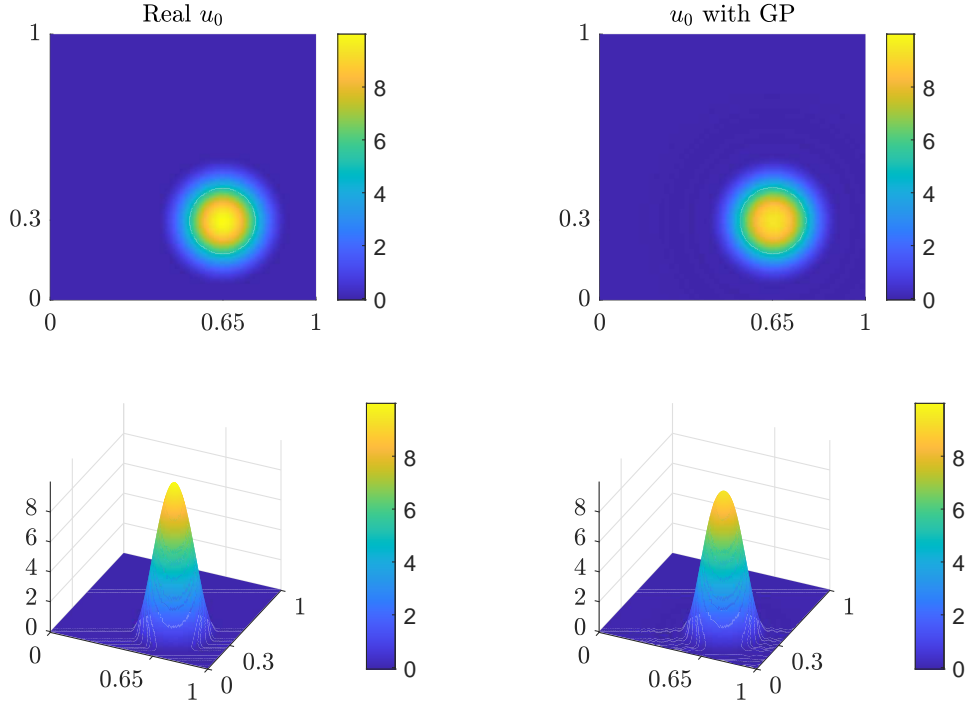


FIGURE 3. Test case #1 : top and lateral view of the reconstruction of u_0 provided by WIGPR in comparison with u_0 . Left : u_0 . Right : reconstruction of u_0 using WIGPR. 20 sensors were used. The images correspond to the 3D solutions evaluated at $z = 0.5$.

5.2.1. *Discussion on the numerical results.* For problem (Q_1) , Figures 10a and 10b show that the physical parameters x_0 and c are well estimated. Figure 10c shows that the source size parameter R is overestimated, as could be expected from Remark 4.5. The relative errors in Figures 10d, 10e and 10f show that the overall

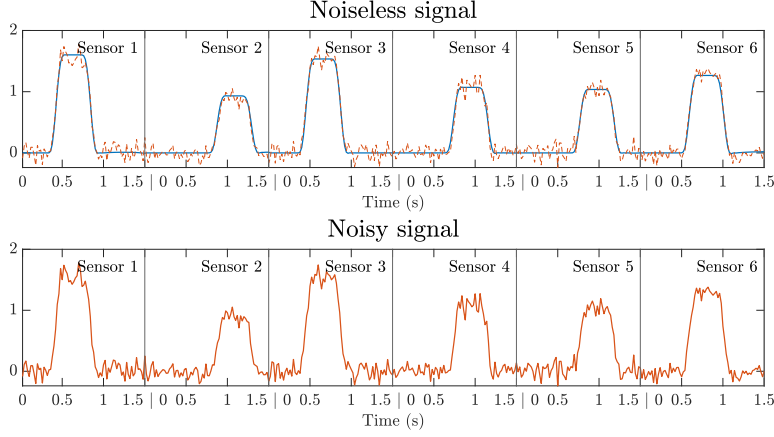


FIGURE 4. Example of captured signals for the test case #2

function reconstruction is satisfying, with around 10% relative error. For problem (Q_2) (figures 14a, 14c and 14e), the relative errors stagnate at around 2%. The data summarized by the boxplots are not very scattered, as is visible from the interquartile range (IQR) of the boxplots. The interquartile range is the difference between the 3rd and the 1st quartiles, and remains between 0.5% and 2% in the three figures aforementioned. This means that for this test case, the reconstruction step is not very sensitive to the sensors layout when they are scattered as a Latin hypercube. For problems (Q_1) and (Q_2) , the results are very good overall. Note though that this is a simple test case : the function to be reconstructed is differentiable and exhibits rather small variations compared to the next test case.

5.3. Test case for k_v^{wave} . We use the kernel (4.56) and the 1D Matérn kernel (5.1) for K_v in equation (4.56). The initial condition v_0 is a radial ring cosine described as follows. Set $x_0 = (0.3, 0.6, 0.7)^T$, $R_1 = 0.05$, $R_2 = 0.15$, $A = 50$, the corresponding IC are given by :

$$\begin{cases} u_0(x) &= 0 \\ v_0(x) &= A \mathbb{1}_{[R_1, R_2]}(|x - x_0|) \left(1 + \cos \left(\frac{2\pi(|x - x_0| - \frac{R_1 + R_2}{2})}{R_2 - R_1} \right) \right) \end{cases}$$

See Figure 5, left column, for a graphical representation. For problem (Q_1) , the optimization domain is chosen to be the one from the previous test case defined in (5.3). For problem (Q_2) , the hyperparameter θ_0 provided to the model is

$$(5.5) \quad \theta_0 = (x_0, R, (\rho, \sigma^2), c, \lambda) = ((0.3, 0.6, 0.7), 0.15, (0.03, 3), 0.5, \sigma_{\text{noise}}^2)$$

with $\sigma_{\text{noise}}^2 = 0.0081$. As in the test case #1, the value of 0.03 provided for ρ is a visual estimation of the length scale of v_0 based on Figure 5. Additionally, the couple $(0.03, 3)$ provided for (ρ, σ^2) is more or less confirmed by the estimations of (ρ, σ^2) performed for problem (Q_1) , test case #2, visible in Table 1.

5.3.1. Discussion of the numerical results. For problem (Q_1) , Figures 11a and 11b show that the physical parameters x_0 and c are well estimated. As in the first test case, Figure 11c shows that the source size parameter R is overestimated, see

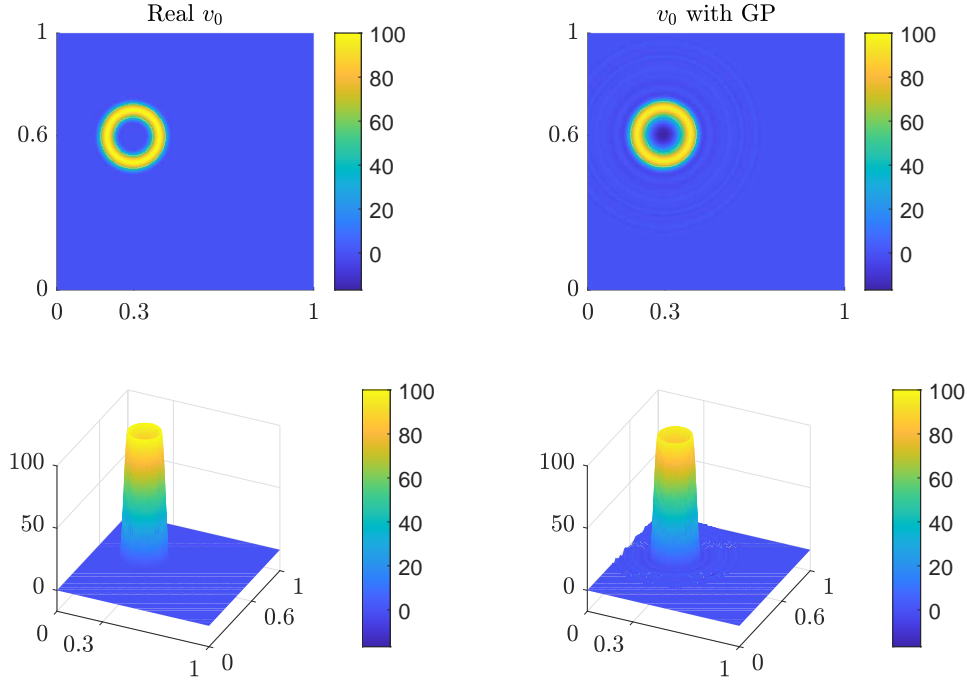


FIGURE 5. Test case #2 : top and lateral view of the reconstruction of v_0 provided by WIGPR in comparison with v_0 . Left : v_0 . Right : reconstruction of v_0 using WIGPR. 25 sensors were used. The images correspond to the 3D solutions evaluated at $z = 0.7$.

Remark 4.5. However, the relative error plots are not as good as in the previous example. The poor L^1 relative error between 60% and 100% in Figure 11f is an indicator that the reconstructed function (WIGPR Kriging mean) is supported on a set significantly larger than the original function, as the L^1 norm is minimized for sparse functions. This is indeed visible on Figure 5, and is partly due to the fact that R was overestimated. The L^2 and L^∞ plots in Figures 11d and 11e are not too bad, with 20% to 30% relative error. Although these errors are large when compared to the test case #1, WIGPR still managed to capture the structure of the initial condition, as is visible on Figure 5. For problem (Q_2) , the relative error plots are better than for (Q_1) . The L^2 and L^1 relative errors stagnate at around 6% with an IQR of around 2% (figures 14b and 14f). The L^∞ relative error stagnates at around 10% with an IQR of around 5% (figure 14d). Note finally that this test case is more difficult than the previous one : the initial condition to reconstruct has a smaller support and exhibits much larger variations.

5.4. **Test case for $k_u^{\text{wave}} + k_v^{\text{wave}}$.** Here, we combine the initial conditions from the two previous test cases. Set $x_0^u = (0.65, 0.3, 0.5)^T$, $R_u = 0.25$, $A_u = 2.5$, $x_0^v = (0.3, 0.6, 0.7)^T$, $R_1^v = 0.05$, $R_2^v = 0.15$ and $A_v = 30$. The corresponding IC are

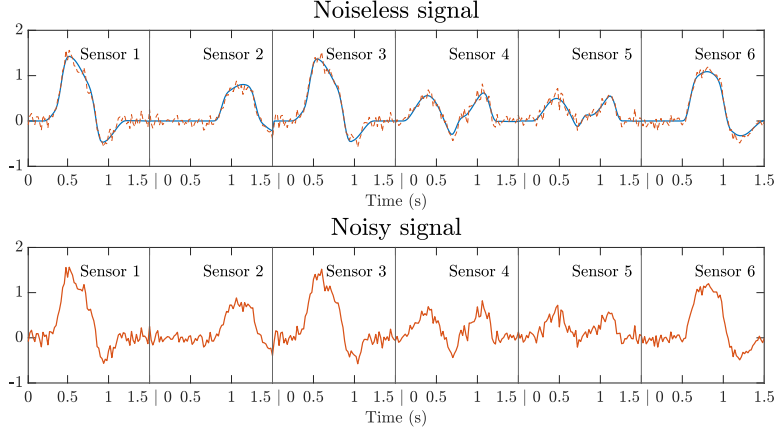


FIGURE 6. Example of captured signals for the test case #3

given by :

$$\begin{cases} u_0(x) &= A_u \mathbb{1}_{[0, R_u]}(|x - x_0^u|) \left(1 + \cos \left(\frac{\pi |x - x_0^u|}{R_u} \right) \right) \\ v_0(x) &= A_v \mathbb{1}_{[R_1^v, R_2^v]}(|x - x_0^v|) \left(1 + \cos \left(\frac{2\pi (|x - x_0^v| - \frac{R_1^v + R_2^v}{2})}{R_2^v - R_1^v} \right) \right) \end{cases}$$

See Figures 3 and 3, left columns, for graphical representations. For problem (Q_1) , the optimization domain is chosen to be the following hypercube

$$\begin{aligned} \theta &= (x_0^u, R_u, (\rho_u, \sigma_u^2), x_0^v, R_v, (\rho_v, \sigma_v^2), c, \lambda) \\ &\in [0, 1]^3 \times [0.05, 0.4] \times [0.02, 2] \times [0.1, 5] \\ (5.6) \quad &\times [0, 1]^3 \times [0.05, 0.4] \times [0.02, 2] \times [0.1, 5] \times [0.2, 0.8] \times [10^{-8}, 10^{-2}] \end{aligned}$$

For problem (Q_2) , the hyperparameter value θ_0 provided to the model is

$$(5.7) \quad \theta_0 = ((0.65, 0.3, 0.5), 0.3, (0.2, 0.3), (0.3, 0.6, 0.7), 0.15, (0.03, 3), 0.5, \sigma_{noise}^2)$$

with $\sigma_{noise}^2 = 0.0081$. The provided values for (ρ_u, σ_u^2) and (ρ_v, σ_v^2) are those of the two previous test cases; see Subsections 5.2 and 5.3.

5.4.1. Discussion of the numerical results. Figures 12a, 12b and 12e show that the physical parameters x_0^u , x_0^v and c are well estimated. Figures 12c and 12d show that the source sizes R_u and R_v are overestimated, see Remark 4.5. For the initial position u_0 , Figures 13a and 13c show that with $N_s = 30$ sensors, WIGPR yielded good results with around 10% L^2 and L^∞ of relative errors. However, for the other values of N_s , WIGPR did not perform as well with around 50% of L^2 and L^∞ relative error. As in the previous test case, the L^1 relative error plot in Figure 13e shows that the reconstructed function \tilde{u}_0 is usually supported on larger sets than the true function u_0 . With 30 sensors, WIGPR yielded 30% relative error and between 60% and 90% of relative L^1 error for the other values of N_s . The reconstruction of u_0 in the case $N_s = 30$ is displayed in Figure 7, showing a satisfactory result. For the reconstruction of the initial speed v_0 , all the numerical attempts failed. The best result is attained for $N_s = 30$ sensors with 65% of L^2 and L^∞ relative errors

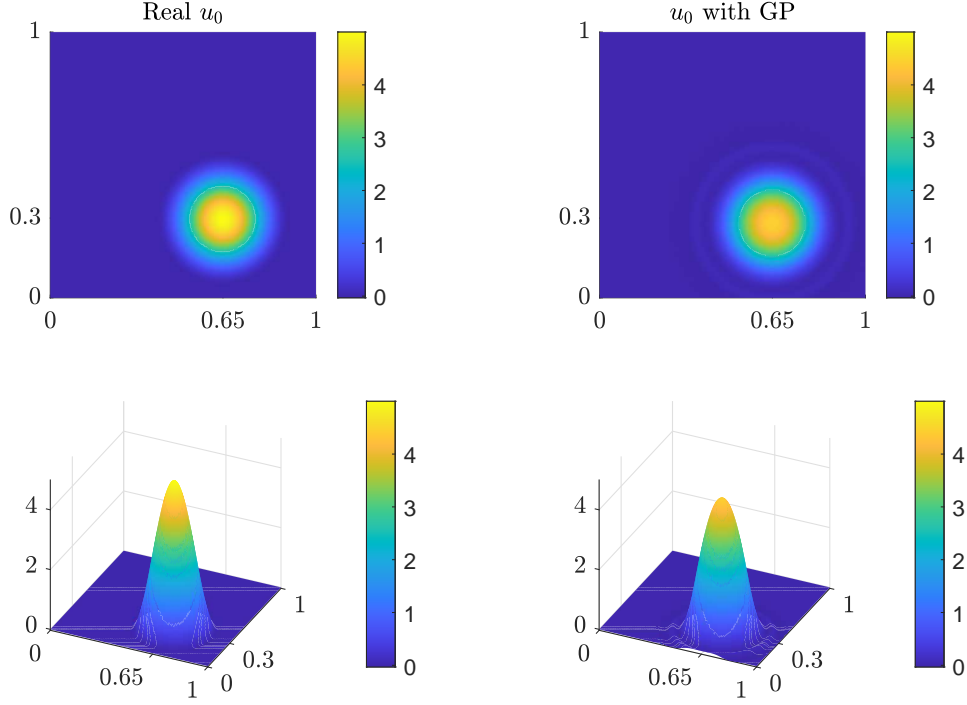


FIGURE 7. Test case #3 : top and lateral view of the reconstruction of u_0 provided by WIGPR in comparison with u_0 . Left : u_0 . Right : reconstruction of u_0 using WIGPR. 30 sensors were used. The images correspond to the 3D solutions evaluated at $z = 0.5$.

(13b and 13d). But for this case, Figure 8 shows that WIGPR failed to capture the structure of v_0 . One explanation of this is that for the test case #3, the value of the length scale hyperparameter ρ_v was overestimated by a factor of at least 10 (see the 4th row of Table 1 versus the 3rd row). Therefore the WIGPR model was never able to capture the fast variations of v_0 . For problem (Q_2) , the results are better. For the initial position u_0 , the results are very similar to those of the test case #1. Figures 15a, 15c and 15e show that relative errors stagnate at around 2% to 4% for the three relative errors. The corresponding IQR are of the same order of magnitude : 1% to 2%. For the initial speed v_0 (figures 15b, 15d and 15f), the results are very similar to those of the test case #2 but multiplied by a factor between 3 and 6. The L^2 and L^1 relative errors now stagnate below 30% and the L^∞ relative stagnates below 45%. The corresponding IQR are of around 10% for the L^2 and L^1 errors and 15% for the L^∞ error. Note finally that this test case combines the difficulties of the first and second test cases.

5.4.2. Noise level estimation. The estimated noise variance is displayed in the last three rows of Table 1. In all the test cases, the noise variance λ was rather well estimated for $N_s = 25$ or $N_s = 30$, relatively to the target value of $\sigma_{noise}^2 = 0.0081$.

5.5. Transparent boundary conditions. The search for perfect or approximated transparent boundary conditions for numerical schemes is an active research topic.

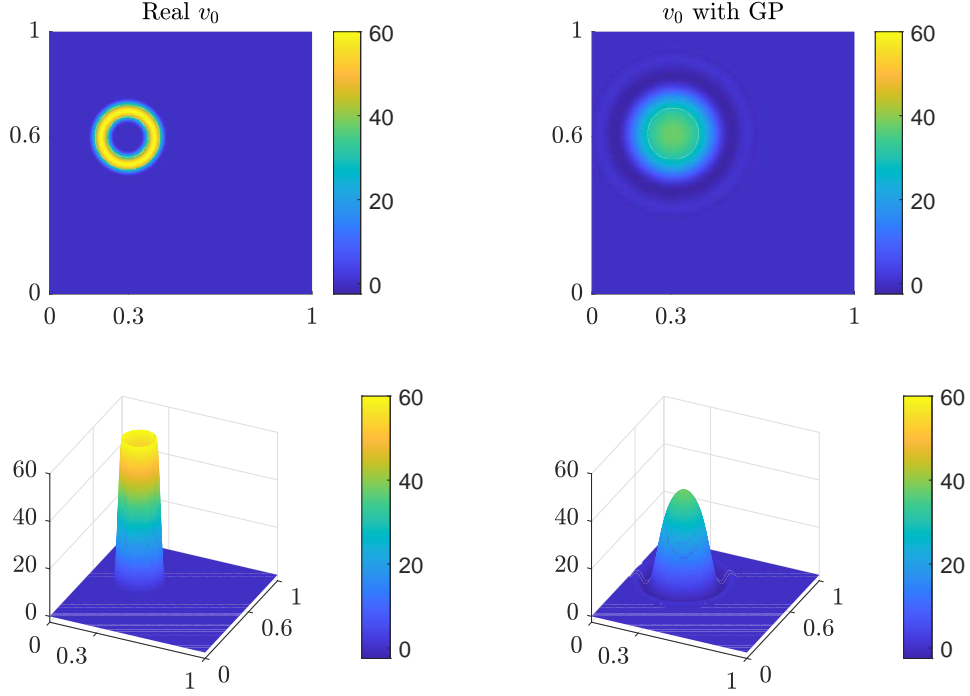


FIGURE 8. Test case #3 : top and lateral view of the reconstruction of v_0 provided by WIGPR in comparison with v_0 . Left : v_0 . Right : reconstruction of v_0 using WIGPR. 30 sensors were used. The images correspond to the 3D solutions evaluated at $z = 0.7$.

TABLE 1. Estimated Matérn hyperparams. and noise var. for (Q_1)

	Test case	$N_s = 10$	$N_s = 15$	$N_s = 20$	$N_s = 25$	$N_s = 30$
ρ_u	1	0.117	0.11	0.043	0.184	0.144
	3	1.145	0.357	0.891	0.529	0.088
ρ_v	2	0.105	0.149	0.023	0.068	0.046
	3	1.453	1.703	0.595	0.482	0.353
σ_u^2	1	4.97	3.88	4.23	3.09	4.89
	3	3.9	4.97	3.84	4.64	4.89
σ_v^2	2	4.25	5	1.61	4.17	4.89
	3	3.54	3.05	3.5	3.27	3.26
λ	1	0.01	0.0099	0.0088	0.0086	0.0096
	2	0.0097	0.0096	0.0036	0.0094	0.0095
	3	0.0098	0.01	0.0099	0.0083	0.0094

They became a popular research topic in 1970' [24] and several different strategies have since been set up to deal with them : see e.g. [11], [24], [35], or [39] for an overview of these different methods. The need for them rises from the fact that numerical simulation domains are necessarily finite and thus bounded; or at the

very least, discretized thanks to a finite grid. To numerically solve a free space PDE such as (4.1), one first uses an adapted numerical scheme (finite differences, finite elements, etc) for the desired PDE applied in the interior domain, i.e. at the interior points of the discretization grid. At the boundaries of the numerical domain, one is then forced to encode boundary conditions : common examples are the Dirichlet and Von Neumann boundary conditions, which cause reflections on the boundaries of the domain. For the free space problem, the question is then the following : can we numerically implement boundary conditions that produce no reflections?

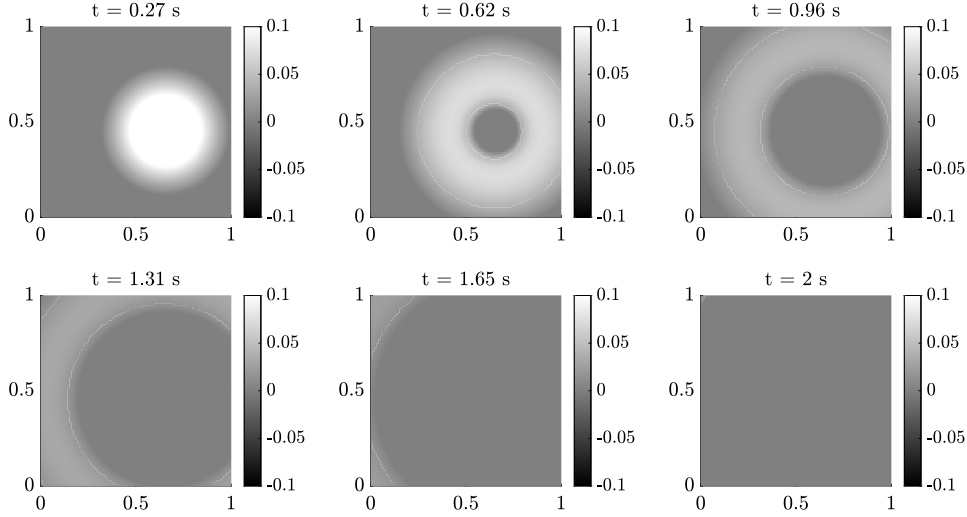


FIGURE 9. Numerical example showing that the outgoing waves produced by WIGPR do not suffer from numerical reflection issues.

Figure 9 shows that WIGPR provides numerical solutions for problem (4.1) that do not suffer from numerical reflection issues. The reason is simple : these numerical reconstructions are evaluations on a grid of functions that are exact solutions of the free space problem (4.1). While being a promising start for new types of transparent boundary conditions, the discussion above is not enough to provide viable transparent boundary conditions in the sense of numerical schemes. Given the covariance kernels from (4.9) and (4.8), two questions should now be investigated. 1) How can WIGPR be associated to classical numerical schemes such as finite difference schemes for the wave equation? 2) Is the corresponding numerical transparent boundary condition numerically stable?

6. CONCLUSION AND PERSPECTIVES

In Section 3, we have presented a new result that provides a simple characterization of the second order stochastic processes whose trajectories verify linear differential constraints within the framework of generalized functions. This result is one of the starting points of Section 4, in which a Gaussian process model of the wave equation was described and thoroughly studied. This model was derived by putting a GP prior on the wave equation's initial conditions, following a Bayesian

approach when considering these initial conditions to be unknown. We then showed that WIGPR naturally provides an approximation of the initial conditions of the wave equation, as expected with a Bayesian approach w.r.t. the initial conditions. The radial symmetry WIGPR formulas from Section 4 were then showcased in Section 5, where two practical questions were tackled. First, WIGPR can correctly estimate certain physical parameters attached to the corresponding wave equation, such as wave speed or source position. When these parameters are well estimated, the initial condition reconstruction step is rather satisfactory in terms of L^1 , L^2 and L^∞ relative errors. Second, we observed that the WIGPR reconstruction step is not very sensitive to the layout of sensors when they are spread according to a Latin hypercube, assuming that the correct set of hyperparameters is provided to the model.

Future possible investigations may concern the practical use of the more general formula (4.10) without any symmetry assumptions. To compute the convolution efficiently, one may then resort to Fast Fourier transforms (FFT). The case of the two dimensional wave equation is also of practical interest, notably in oceanography [43], and presents many different properties than its 3D counterpart ([27], p.80). It would thus deserve a theoretical and practical study in its own right when coupled with GPR. Moreover, proposition 2 constitutes a first step towards understanding PDE constrained stochastic processes in an integrated sense; different functional analysis frameworks can now be considered, for example by assuming Sobolev regularity of the coefficients of T instead of C^k regularity or by trying to work in smaller function spaces than $\mathcal{D}'(\mathcal{D})$ by transferring only a part of the derivatives of the PDE to the test function. A well known particular case is when the differential operator can be “split in two” by this procedure : it is then alternatively viewed as a bilinear form over some Hilbert space. This leads to the variational formulation of the PDE and is the canonical approach to studying elliptic PDEs.

Acknowledgements. We would like to thank the Service Hydrographique et Océanographique de la Marine (SHOM) for funding this work, and Rémy Baraille in particular for his personal involvement in the project. We thank the GMM laboratory of INSA Toulouse for providing us access to their servers on which we ran our numerical computations.

APPENDIX A : NUMERICAL RESULTS

7. HYPERPARAMETER ESTIMATION AND RELATED ERROR PLOTS

7.1. Test case #1 : k_u^{wave} . Here, $\theta = (x_0^u, R_u, (\rho_u, \sigma_u^2), c, \lambda) \in \mathbb{R}^8$. The target value is $\theta^* = ((0.65, 0.3, 0.5), 0.25, (\sim 0.15, ?), 0.5, 0.0081)$. The values (ρ_u, σ_u^2) are the hyperparameters of the underlying Matérn kernel k_u^0 . The a priori target value of 0.15 for ρ_u is a visual estimation of the characteristic length scale of u_0 from the figure 3. The corresponding variance σ_u^2 is difficult to estimate a priori and its target value is left at “?”.

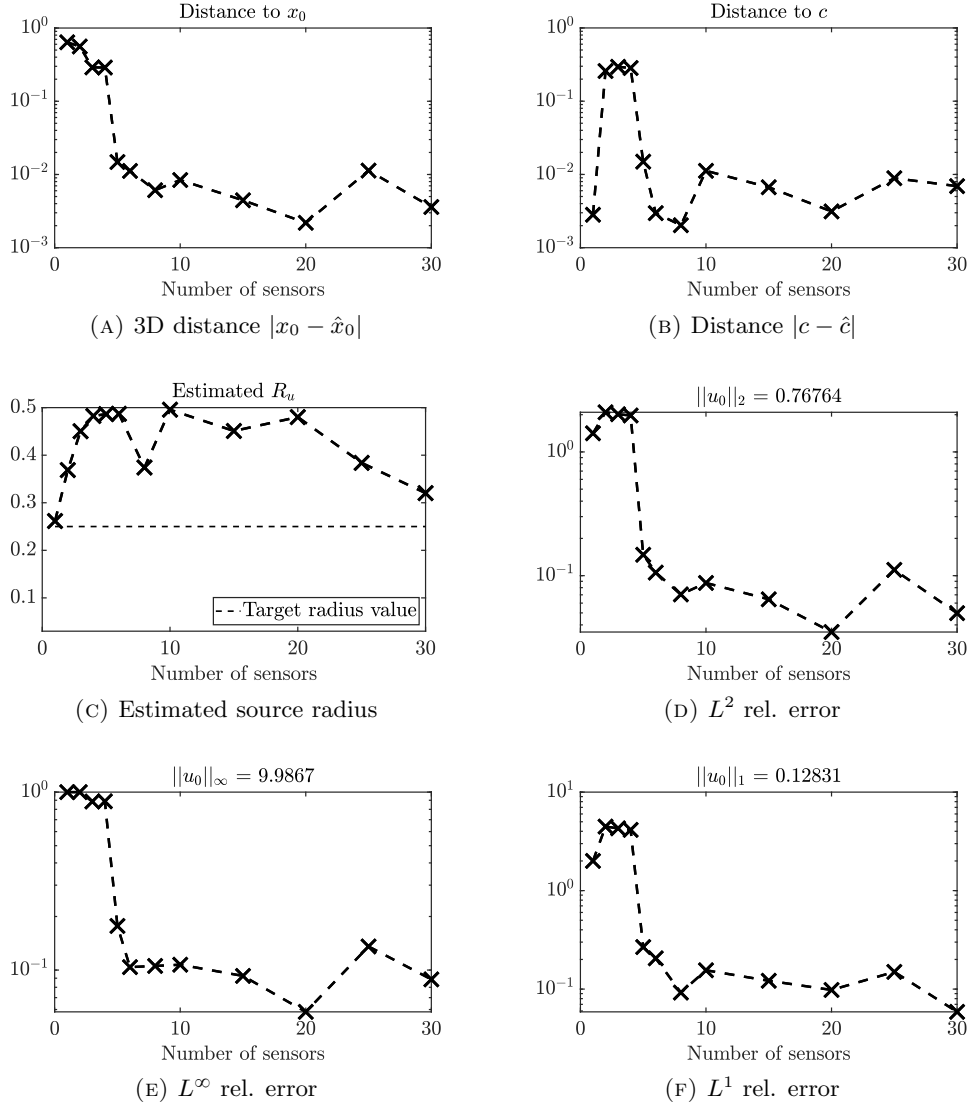


FIGURE 10. Hyperparameter estimation and error plots for the test case #1

7.2. Test case #2 : k_v^{wave} . Here, $\theta = (x_0^v, R_v, (\rho_v, \sigma_v^2), c, \lambda) \in \mathbb{R}^8$. The target value is $\theta^* = ((0.3, 0.6, 0.7), 0.15, (\sim 0.05, ?), 0.5, 0.0081)$. The values (ρ_v, σ_v^2) are the hyperparameters of the underlying Matérn kernel k_v^0 . The a priori target value of 0.05 for ρ_v is a visual estimation of the characteristic length scale of v_0 from the figure 5. The corresponding variance σ_v^2 is difficult to estimate a priori and its target value is left at “?”.

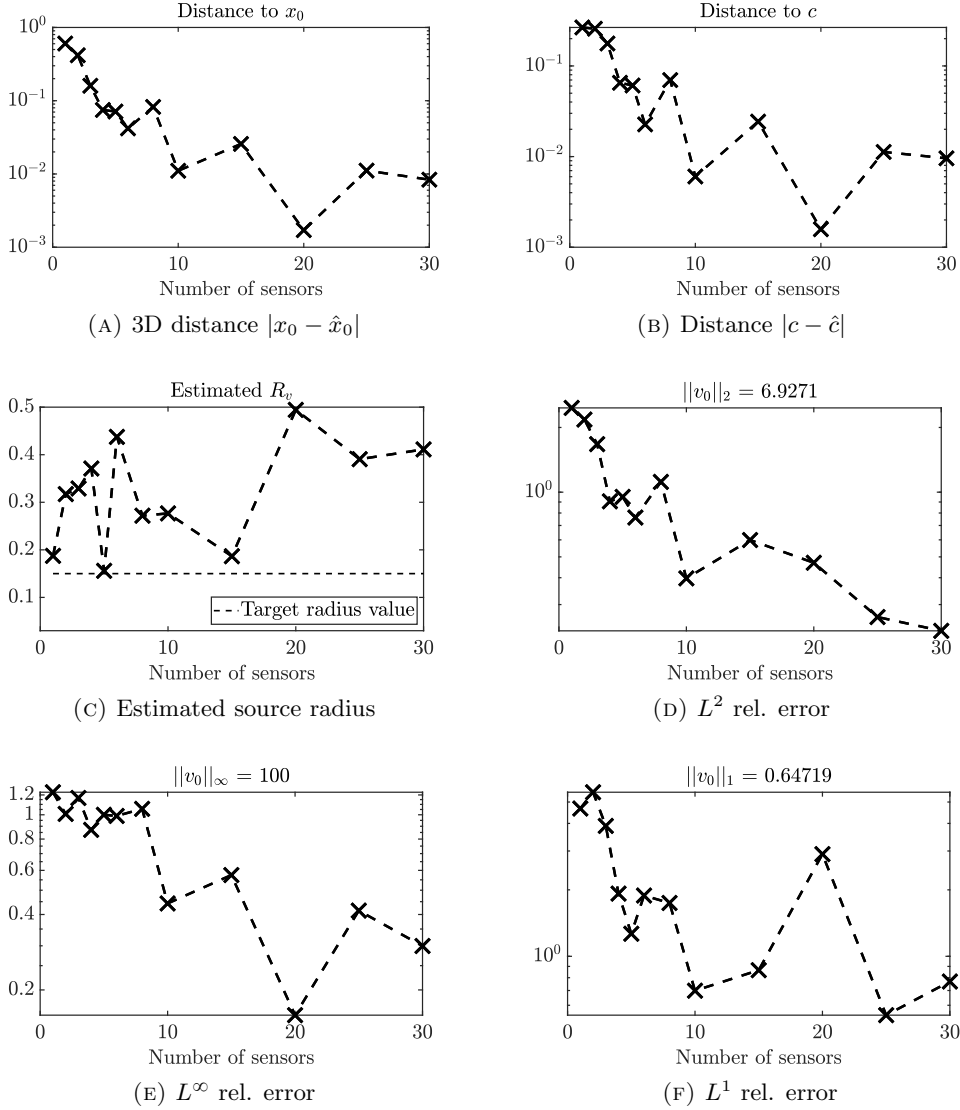


FIGURE 11. Hyperparameter estimation and error plots for the test case #2

7.3. Test case #3 : $k_u^{\text{wave}} + k_v^{\text{wave}}$. Here, $\theta = (x_0^u, R_u, (\rho_u, \sigma_u^2), x_0^v, R_v, (\rho_v, \sigma_v^2), c, \lambda) \in \mathbb{R}^{14}$. The target value is $\theta^* = ((0.65, 0.3, 0.5), 0.3, (\sim 0.15, ?), (0.3, 0.6, 0.7), 0.15, (\sim 0.05, ?), 0.5, \lambda)$. The values (ρ_u, σ_u^2) and (ρ_v, σ_v^2) are the hyperparameters of the underlying Matérn kernels k_u^0 and k_v^0 . The a priori target values of 0.15 for ρ_u and 0.05 for ρ_v are visual estimations of the characteristic length scale of u_0 and v_0 from the figures 3 and 5. The corresponding variances σ_u^2 and σ_v^2 are difficult to estimate a priori and the corresponding target values are left at “?”.

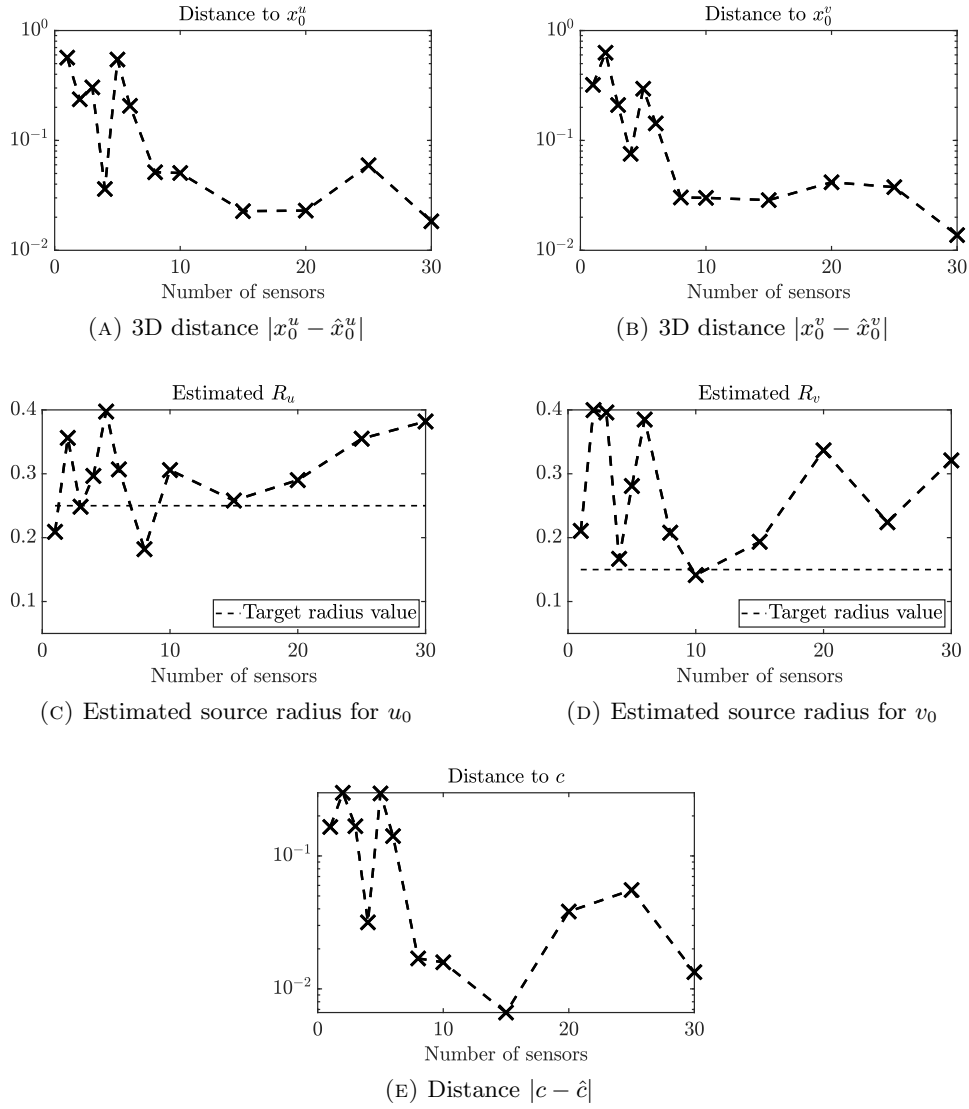


FIGURE 12. Hyperparameter estimation for the test case #3

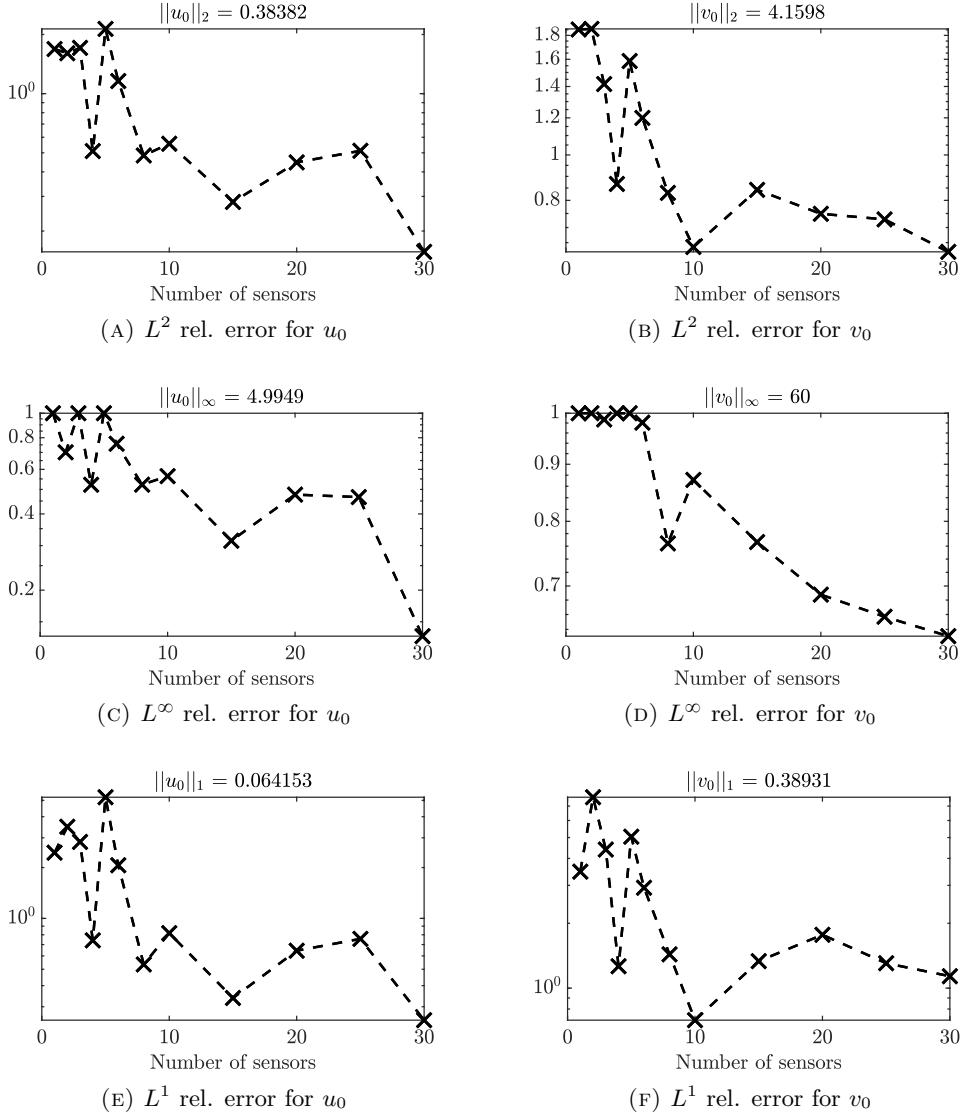


FIGURE 13. Error plots for the test case #3

8. EXPERIENCE PLAN SENSIBILITY RESULTS

In all the presented figures are represented the following objects. Each box plot shows the median, the first and the third quartiles of a dataset corresponding to results obtained on the 40 different receiver dispositions. The “targets” (dot inside a circle) correspond to the median of each boxplot. The dashed line links the mean of each box plot. The black crosses are the mean of each box plot, through which each dashed curve pass.

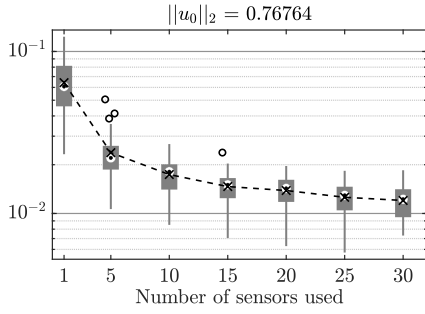
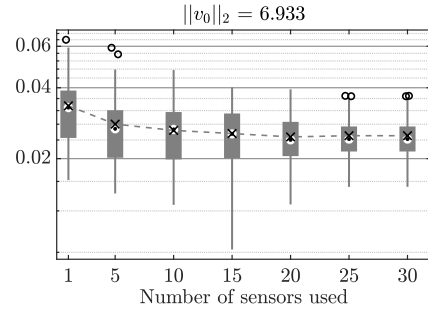
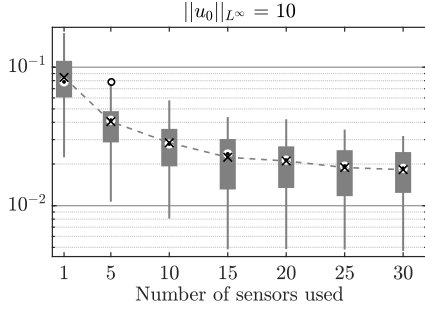
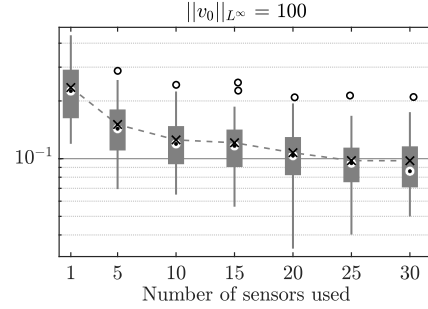
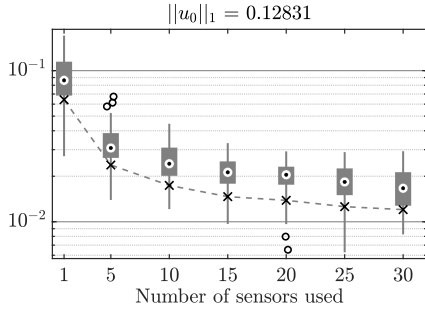
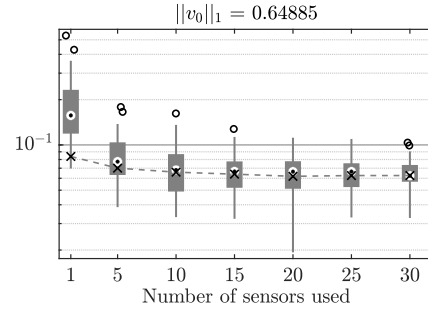
(A) L^2 rel. error for u_0 (test case #1)(B) L^2 rel. error for v_0 (test case #2)(C) L^∞ rel. error for u_0 (test case #1)(D) L^∞ rel. error for v_0 (test case #2)(E) L^1 rel. error for u_0 (test case #1)(F) L^1 rel. error for v_0 (test case #2)

FIGURE 14. Error plots for the test cases #1 and #2

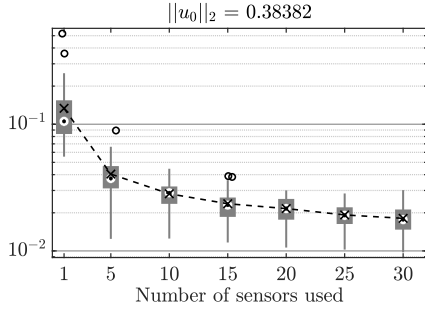
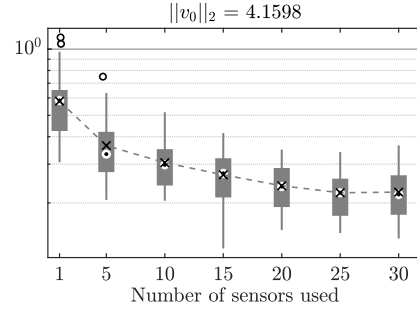
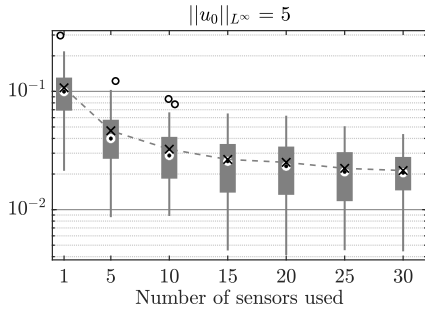
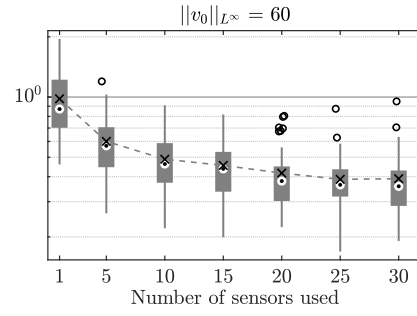
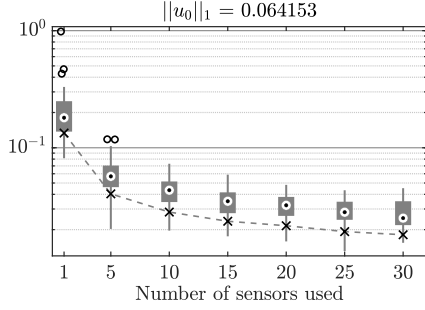
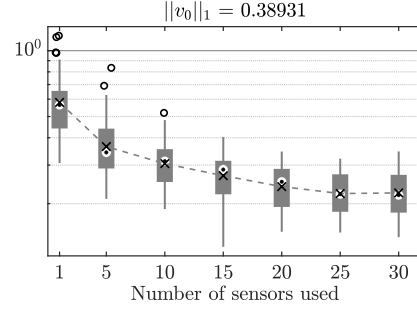
(A) L^2 rel. error for u_0 (test case #3)(B) L^2 rel. error for v_0 (test case #3)(C) L^∞ rel. error for u_0 (test case #3)(D) L^∞ rel. error for v_0 (test case #3)(E) L^1 rel. error for u_0 (test case #3)(F) L^1 rel. error for v_0 (test case #3)

FIGURE 15. Error plots for the test case #3

REFERENCES

1. R. J. Adler and J. E. Taylor, *Random fields and geometry*, Springer-Verlag New York, NY, 2007.
2. C. G. Albert and K. Rath, *Gaussian process regression for data fulfilling linear differential equations with localized sources*, *Entropy* **22** (2020), no. 2.
3. P. A. Alvarado, M. A. Alvarez, G. Daza-Santacoloma, A. Orozco, and G. Castellanos-Dominguez, *A latent force model for describing electric propagation in deep brain stimulation: A simulation study*, 2014 36th Annual International Conference of the IEEE Engineering in Medicine and Biology Society, 2014, pp. 2617–2620.
4. M. Álvarez, D. Luengo, and N. Lawrence, *Linear latent force models using Gaussian processes*, *IEEE Transactions on Pattern Analysis and Machine Intelligence* **35** (2013), 2693–2705.
5. W. F. Ames, *Numerical methods for partial differential equations (second edition)*, Academic Press, second edition ed., 1977.
6. Habib Ammari (ed.), *Mathematical modeling in biomedical imaging II. optical, ultrasound, and opto-acoustic tomographies*, *Lecture Notes in Mathematics*, vol. 2035, Springer, Berlin, Heidelberg, 2012.
7. L. Arkhipova, *Number of lattice points in a sphere*, *Moscow University Mathematics Bulletin* **63** (2008), 214–215.
8. Jean-Marc Azaïs and Mario Wschebor, *Level sets and extrema of random processes and fields*, Wiley & Sons, 2009.
9. A. Berline and C. Thomas-Agnan, *Reproducing kernel Hilbert spaces in probability and statistics*, Springer US, 2004.
10. S. Bilbao, *Wave and scattering methods for numerical simulations*, John Wiley & Sons, Ltd, 2004.
11. Jean-Pierre Bérenger, *Perfectly matched layer (PML) for computational electromagnetics*, *Synthesis Lectures on Computational Electromagnetics* **2** (2007), no. 1, 1–117.
12. Martin D. Buhmann, *Radial basis functions: Theory and implementations*, *Cambridge Monographs on Applied and Computational Mathematics*, Cambridge University Press, 2003.
13. Yifan Chen, Bamdad Hosseini, Houman Owadi, and Andrew M. Stuart, *Solving and learning nonlinear PDEs with Gaussian processes*, *Journal of Computational Physics* **447** (2021), 110668.
14. Igor Cialenco, Gregory E Fasshauer, and Qi Ye, *Approximation of stochastic partial differential equations by a kernel-based collocation method*, *International Journal of Computer Mathematics* **89** (2012), no. 18, 2543–2561.
15. J. Cockayne, C. Oates, T. Sullivan, and M. Girolami, *Probabilistic numerical methods for partial differential equations and bayesian inverse problems*, *ArXiv* (2017).
16. Jon Cockayne, Chris Oates, Tim Sullivan, and Mark Girolami, *Probabilistic numerical methods for pde-constrained bayesian inverse problems*, *AIP Conference Proceedings* **1853** (2017), no. 1, 060001.
17. Patrick R Conrad, Mark Girolami, Simo Särkkä, Andrew Stuart, and Konstantinos Zygalakis, *Statistical analysis of differential equations: introducing probability measures on numerical solutions*, *Statistics and Computing* **27** (2017), no. 4, 1065–1082.
18. S. L. Cotter, M. Dashti, and A. M. Stuart, *Approximation of Bayesian inverse problems for PDEs*, *SIAM Journal on Numerical Analysis* **48** (2010), no. 1, 322–345.
19. Robert C Dalang and Marta Sanz-Solé Sol, *Hölder-Sobolev regularity of the solution to the stochastic wave equation in dimension three*, vol. 199, *Memoirs of the American Mathematical Society*, no. 931, American Mathematical Society, 2009.
20. Masoumeh Dashti and Andrew M. Stuart, *The Bayesian approach to inverse problems*, *Handbook of Uncertainty Quantification (Cham)* (Roger Ghanem, David Higdon, and Houman Owadi, eds.), Springer International Publishing, 2017, pp. 311–428.
21. Y. Deville, D. Ginsbourger, and O. Roustant. Contributors: Nicolas Durrande., *kerpp: Gaussian process laboratory*, 2021, R package version 0.5.5.
22. R. M. Dudley, *Real analysis and probability*, 2 ed., *Cambridge Studies in Advanced Mathematics*, Cambridge University Press, 2002.
23. Dean G Duffy, *Green's functions with applications*, second edition ed., Chapman and Hall/CRC, 2015.

24. Bjorn Engquist and Andrew Majda, *Absorbing boundary conditions for the numerical simulation of waves*, Mathematics of Computation **31** (1977), no. 139, 629–651.
25. S. Esmailzadeh, Z. Medina-Cetina, J.W. Kang, and L.F. Kallivokas, *Varying dimensional Bayesian acoustic waveform inversion for 1d semi-infinite heterogeneous media*, Probabilistic Engineering Mechanics **39** (2015), 56–68.
26. Lawrence C Evans and Ronald F Garzepy, *Measure theory and fine properties of functions, revised edition (1st ed.)*, Chapman and Hall/CRC, 2015.
27. L.C. Evans, *Partial differential equations*, Graduate studies in mathematics, American Mathematical Society, 1998.
28. G. Fasshauer, *Meshfree approximation methods with MATLAB*, Interdisciplinary Mathematical Sciences, 2007.
29. Gregory E Fasshauer and Qi Ye, *Reproducing kernels of generalized Sobolev spaces via a Green function approach with distributional operators*, Numerische Mathematik **119** (2011), no. 3, 585–611.
30. ———, *Reproducing kernels of Sobolev spaces via a Green kernel approach with differential operators and boundary operators*, Advances in Computational Mathematics **38** (2013), no. 4, 891–921.
31. D. Ginsbourger, O. Roustant, and N. Durrande, *On degeneracy and invariances of random fields paths with applications in Gaussian process modelling*, Journal of Statistical Planning and Inference (2016), 170 :117 – 128.
32. T. Graepel, *Solving Noisy Linear Operator Equations by Gaussian Processes: Application to Ordinary and Partial Differential Equations*, Proceedings of the 20th International Conference on Machine Learning, AAAI Press, 2003, pp. 234–241.
33. M. Gulian, A. Frankel, and L. Swiler, *Gaussian process regression constrained by boundary value problems*, Computer Methods in Applied Mechanics and Engineering **388** (2022), 114117.
34. Lars Hörmander, *The analysis of linear partial differential operators I: Distribution theory and Fourier analysis*, Springer, 2015.
35. Fang Q. Hu, *Absorbing boundary conditions*, International Journal of Computational Fluid Dynamics **18** (2004), no. 6, 513–522.
36. Svante Janson, *Gaussian Hilbert spaces*, Cambridge Tracts in Mathematics, Cambridge University Press, 1997.
37. C. Jidling, J. Hendriks, N. Wahlstrom, A. Gregg, T. Schon, C. Wensrich, and A. Wills, *Probabilistic modelling and reconstruction of strain*, Nuclear Instruments & Methods in Physics Research Section B-beam Interactions With Materials and Atoms **436** (2018), 141–155.
38. C. Jidling, N. Wahlström, A. Wills, and T. B. Schön, *Linearly constrained Gaussian processes*, Advances in Neural Information Processing Systems (I. Guyon, U. V. Luxburg, S. Bengio, H. Wallach, R. Fergus, S. Vishwanathan, and R. Garnett, eds.), vol. 30, Curran Associates, Inc., 2017.
39. Maria Kazakova and Pascal Noble, *Discrete transparent boundary conditions for the linearized Green–Naghdi system of equations*, SIAM Journal on Numerical Analysis **58** (2020), no. 1, 657–683.
40. P. Kuchment and L. Kunyansky, *Mathematics of photoacoustic and thermoacoustic tomography*, Handbook of Mathematical Methods in Imaging **v. 2, Ch. 19** (2010), 817–866.
41. M. Lange-Hegemann, *Algorithmic linearly constrained Gaussian processes*, Advances in Neural Information Processing Systems (S. Bengio, H. Wallach, H. Larochelle, K. Grauman, N. Cesa-Bianchi, and R. Garnett, eds.), vol. 31, Curran Associates, Inc., 2018.
42. ———, *Linearly constrained Gaussian processes with boundary conditions*, Proceedings of The 24th International Conference on Artificial Intelligence and Statistics (A. Banerjee and K. Fukumizu, eds.), Proceedings of Machine Learning Research, vol. 130, PMLR, 13–15 Apr 2021, pp. 1090–1098.
43. David Lannes and Philippe Bonneton, *Derivation of asymptotic two-dimensional time-dependent equations for surface water wave propagation*, Physics of Fluids **21** (2009), no. 1, 016601.
44. Jean-François Le Gall, *Mouvement brownien, martingales et calcul stochastique*, Springer, 2013.

45. A. F. López-Lopera, N. Durrande, and M. Álvarez, *Physically-inspired Gaussian process models for post-transcriptional regulation in drosophila*, IEEE/ACM Transactions on Computational Biology and Bioinformatics **18** (2021), 656–666.
46. M. Álvarez, D. Luengo, and N. D. Lawrence, *Latent force models*, Proceedings of the Twelfth International Conference on Artificial Intelligence and Statistics (Hilton Clearwater Beach Resort, Clearwater Beach, Florida USA) (D. van Dyk and M. Welling, eds.), Proceedings of Machine Learning Research, vol. 5, PMLR, 16–18 Apr 2009, pp. 9–16.
47. The Mathworks, Inc., Natick, Massachusetts, *MATLAB version 9.8.0.1721703 (R2020a) Update 7*, 2020.
48. Fábio Macêdo Mendes and Edson Alves da Costa Júnior, *Bayesian inference in the numerical solution of Laplace's equation*, AIP Conference Proceedings **1443** (2012), no. 1, 72–79.
49. F. J. Narcowich and J. Ward, *Generalized Hermite interpolation via matrix-valued conditionally positive definite functions*, Mathematics of Computation **63** (1994), 661–687.
50. N.C. Nguyen and J. Peraire, *Gaussian functional regression for linear partial differential equations*, Computer Methods in Applied Mechanics and Engineering **287** (2015), 69–89.
51. A. P. Nikitin, ST John, A. Solin, and S. Kaski, *Non-separable spatio-temporal graph kernels via SPDEs*, ArXiv (2021).
52. Houman Owhadi, *Bayesian numerical homogenization*, Multiscale Modeling & Simulation **13** (2015), no. 3, 812–828.
53. M. Álvarez P. A. Alvarado and A. Orozco, *A three spatial dimension wave latent force model for describing excitation sources and electric potentials produced by deep brain stimulation*, arXiv (2016).
54. A. Pazy, *Semigroups of linear operators and applications to partial differential equations*, Applied Mathematical Sciences, 1983.
55. William H Press, Saul A Teukolsky, William T Vetterling, and Brian P Flannery, *Numerical recipes 3rd edition: The art of scientific computing*, Cambridge university press, 2007.
56. Zenith Purisha, Carl Jidling, Niklas Wahlström, Thomas B Schön, and Simo Särkkä, *Probabilistic approach to limited-data computed tomography reconstruction*, Inverse Problems **35** (2019), no. 10, 105004.
57. R Core Team, *R: A language and environment for statistical computing*, R Foundation for Statistical Computing, Vienna, Austria, 2020.
58. M. Raissi, P. Perdikaris, and G. E. Karniadakis, *Machine learning of linear differential equations using Gaussian processes*, Journal of Computational Physics **348** (2017), 683–693.
59. ———, *Numerical Gaussian processes for time-dependent and nonlinear partial differential equations*, SIAM Journal on Scientific Computing **40** (2018), no. 1, A172–A198.
60. C. E. Rasmussen and C.K.I. Williams, *Gaussian processes for machine learning*, the MIT Press, 2006.
61. K. Ritter, *Average-case analysis of numerical problems*, Lecture Notes in Mathematics, Springer Berlin Heidelberg, 2007.
62. W. Rudin, *Functional analysis*, McGraw-Hill, New York, 1991.
63. S. Särkkä, M. Álvarez, and N. Lawrence, *Gaussian process latent force models for learning and stochastic control of physical systems*, IEEE Transactions on Automatic Control **64** (2019), 2953–2960.
64. Simo Särkkä, *Linear operators and stochastic partial differential equations in Gaussian process regression*, Artificial Neural Networks and Machine Learning – ICANN 2011 (Berlin, Heidelberg) (Timo Honkela, Włodzisław Duch, Mark Girolami, and Samuel Kaski, eds.), Springer Berlin Heidelberg, 2011, pp. 151–158.
65. R. Schaback, *Solving the Laplace equation by meshless collocation using harmonic kernels*, Advances in Computational Mathematics **31** (2009), 457–470.
66. H.H. Schaefer, *Topological vector spaces*, Graduate Texts in Mathematics, Springer-Verlag New York, 1999.
67. M. Scheuerer and M. Schlather, *Covariance models for divergence-free and curl-free random vector fields*, Stochastic Models **28** (2012), 433 – 451.
68. Michael Scheuerer, *Regularity of the sample paths of a general second order random field*, Stochastic Processes and their Applications **120** (2010), no. 10, 1879–1897.
69. D. Serre, *Systems of conservation laws*, Cambridge University Press, 1999.
70. S.Lang, *Real and functional analysis*, Graduate Texts in Mathematics, Springer-Verlag New York, 1993.

71. A. Solin and Simo Särkkä, *Hilbert space methods for reduced-rank Gaussian process regression*, Statistics and Computing **30** (2020), 419–446.
72. Arno Solin, *Stochastic Differential Equation Methods for Spatio-Temporal Gaussian Process Regression*, Doctoral thesis, School of Science, 2016, pp. 68 + app. 72.
73. A. M. Stuart, *Inverse problems: A Bayesian perspective*, Acta Numerica **19** (2010), 451–559.
74. Laura P. Swiler, Mamikon Gulian, Ari L. Frankel, Cosmin Safta, and John D. Jakeman, *A survey of constrained Gaussian process regression: Approaches and implementation challenges*, Journal of Machine Learning for Modeling and Computing **1** (2020), no. 2, 119–156.
75. A. Tarantola, *Inverse problem theory and methods for model parameter estimation*, SIAM, 2005.
76. F. Trèves, *Topological vector spaces, distributions and kernels*, Dover books on mathematics, Dover Publications, 2006.
77. Ricardo Carrizo Vergara, Denis Allard, and Nicolas Desassis, *A general framework for SPDE-based stationary random fields*, Bernoulli **28** (2022), no. 1, 1–32.
78. G. Vidossich, *Characterization of separability for LF-spaces*, Annales de l’institut Fourier **tome 18** (1968), no. 2, p. 87–90.
79. N. Wahlstrom, M. Kok, T. B. Schön, and F. Gustafsson, *Modeling magnetic fields using Gaussian processes*, 2013 IEEE International Conference on Acoustics, Speech and Signal Processing (2013), 3522–3526.
80. Holger Wendland, *Scattered data approximation*, vol. 17, Cambridge university press, 2004.

INSA TOULOUSE, 135 AVENUE DE RANGUEIL, 31400 TOULOUSE, FRANCE
 Email address: `henderso@insa-toulouse.fr`

INSA TOULOUSE, 135 AVENUE DE RANGUEIL, 31400 TOULOUSE, FRANCE

INSA TOULOUSE, 135 AVENUE DE RANGUEIL, 31400 TOULOUSE, FRANCE